Technische Universität München
Institut für Energietechnik

Professur für Thermofluiddynamik

Scattering and Generation of Acoustic and Entropy Waves across Moving and Fixed Heat Sources

Lin Strobio Chen

Vollständiger Abdruck der von der Fakultät für Maschinenwesen der Technischen Universität München zur Erlangung des akademischen Grades eines

DOKTOR – INGENIEURS

genehmigten Dissertation.

Vorsitzender:
Prof. Dr.-Ing. Oskar J. Haidn
Prüfer der Dissertation:
1. Prof. Wolfgang Polifke, Ph.D.
2. Prof. Maria Heckl, Ph.D.

Die Dissertation wurde am 20.09.2016 bei der Technischen Universität München eingereicht und durch die Fakultät für Maschinenwesen am 09.11.2016 angenommen.

Acknowledgement

Firstly, I would like to express my sincere gratitude to my advisor Prof. Wolfgang Polifke for the continuous support of my Ph.D. study and related research, for his patience, motivation, and for his openness and humor in our discussions. His guidance helped me in all the time of research and writing of this thesis. I could not have imagined having a better advisor and mentor for my Ph.D. study.

My greatest thank goes to Prof. Dr. Maria Heckl, my co-advisor, for her advice and encouragement, especially in the toughest moment of the Ph.D., and for hosting me in her research group at Keele University. My gratitude also goes to Dr. Joan Teerling and Naseh Hosseini from Bekaert Combustion Technologies, for their precious insight and constant support during my secondment.

A special thank you goes to all my collegues from the Professur für Thermofluiddynamik, especially my colleagues Sebastian, Thomas and Camilo for their support and patience in the endless discussions on entropy waves. I am also grateful to Kilian, Armin, Carlo, Malte, Thomas Emmert and Stefan for their precious help and insight in overcoming the difficulties in my research. It was my pleasure to work with all of you. I would also like to thank the supervisors and fellows of the TANGO network. Sharing time with talented researchers from all over the world was a source of inspiration.

Last but not least, a special thank you to my family: to my parents Li and Gian Carlo, for their trust and encouragement.

And finally, thank you Jacopo, for being my "partner in crime" in this long journey. None of this would have been possible, without your encouragement, optimism and humor.

Abstract

Thermoacoustic instabilities are a critical problem in the development of lean premixed combustion systems. Coupling between acoustic perturbation, unsteady heat release rate and temperature inhomogeneities may lead to instabilities, which are detrimental for combustors lifespan and cycle operability. This work focuses on the 1-D network model approach, which is proved to correctly predict the unstable acoustic modes of complex combustion systems.

The thesis first focuses on the analytical aspects of the jump conditions and, in particular, the physical mechanisms to be considered when treating the heat source as a compact discontinuity. Indeed, premixed flames and heat exchangers are based on different heat release mechanisms and need to be treated differently in an acoustic network. Linear 1-D acoustic relations are derived for moving heat sources (e.g. premixed flame) and heat sinks at rest (e.g. heat exchangers). By means of these equations, the relation between upstream velocity, air/fuel ratio perturbations, unsteady heat release rate and downstream acoustics and entropy generation has been clarified.

The second part of this thesis is specifically focused on the acoustic behavior of a real-life heat exchanger. Similarly to flames, heat sinks can also trigger thermoacoustic instability effects, since they exhibit unsteady heat release rate in presence of acoustic perturbations. First, numerical study of a real-life heat exchanger is carried out, in order to analyze the impact of the unsteady heat release rate and the geometry on the total scattering behavior. Finally, a thermoacoustic system featuring a 2D flame and a cold heat exchanger in cross-flow is investigated numerically.

Zusammenfassung

Thermoakustische Instabilitäten sind ein entscheidendes Problem bei der Entwicklung vorgemischter Magerverbrennungssysteme. Die gegenseitige Wechselwirkung zwischen akustischen Störungen, schwankender Wärmefreisetzungsrate und Temperaturinhomogenitäten kann zu Instabilitäten führen, welche abträglich für die Lebensdauer und Funktionsfähigkeit eines Verbrenners sind. Diese Arbeit konzentriert sich auf den Ansatz mittels eines eindimensionalen Netzwerkmodells, wobei bewiesen wird dass dieser die instabilen akustischen Moden komplexer Verbrennungssysteme richtig vorhersagt.

Die Arbeit fokusiert sich zunächst auf die analytischen Aspekte der Sprungstellen und insbesondere auf die physikalischen Vorgänge die in bei der Behandlung der Wärmequelle als kompakte Unstetigkeit in Betracht gezogen werden müssen. Tatsächlich basieren vorgemischte Flammen und Wärmetauscher auf verschiedenen Mechanismen der Wärmefreisetzung und müssen in einem akustischen Netzwerk unterschiedlich behandelt warden. Sowohl für sich bewegende Wärmequellen (z.B. vorgemischte Flammen), als auch für ruhende Wärmeableiter (z.B. Wärmetauscher) werden lineare eindimensionale akustische Relationen hergeleitet. Mit Hilfe dieser Formeln wurde die Beziehung zwischen Austrittsgeschwindigkeit, Schwankungen im Luft/Kraftstoff Verhältnis, schwankender Wärmefreisetzungsrate, rückströmender akustischer Störungen und Entropieerzeugung geklärt.

Der zweite Teil dieser Arbeit fokusiert sich spezifisch auf das akustische Verhalten real existierender Wärmetauscher. Ähnlich wie Flammen können auch Wärmeableiter thermoakustische Instabilitäten herbeiführen, da auch bei diesen die Wärmefreisetzung durch den Einfluss akustischer Störungen schwankt. Zunächst wird ein real existierender Wärmetauscher mit numerischen Methoden studiert. Das Ziel dieser Studie ist den Einfluss einer schwankenden Wärmeausstossrate und der Geometrie auf das gesamte Streuverhalten zu analysieren. Abschließend wird ein thermoakustisches System mit einer zweidimensionalen Flamme und ein kalter Wärmetauscher mit Querströmung numerisch untersucht.

Contents

Nomenclature

Latin Characters

A_D	duct cross-sectional area
A_f	flame surface area
c_p	specific heat capacity at constant pressure
c_v	specific heat capacity at constant volume
c	speed of sound
$C_{acoutic}$	acoustic Courant number
$E(\omega)$	frequency response of entropy
E	total energy
$F(\omega)$	frequency response of heat release rate
f, g	Riemann invariants
E	total entropy
He	Helmholtz number
k	wave number
M	Mach number
p	pressure
$\dot{q}(x.t)$	heat release rate per unit of volume
$\dot{Q}(t)$	total heat release rate
R_{univ}	universal gas constant
R	gas-specific constant
s	entropy
S_f	flame speed
S	acoustic scattering matrix
T	temperature
T_{fg}	transfer matrix formulated according to Riemann invariants
T_{pu}	transfer matrix formulated according to pressure and velocity fluctuations
u	velocity
u_s	velocity of flame front in lab frame of reference
$\dot{V}$	volume consumption rate per duct area
V	control volume in which heat release takes place
x_f	flame axial location
Y	mass fraction

Greek Characters

ϕ	equivalence ratio
γ	ratio of specific heats
δt	time step in CFD simulation
δx	cell size in CFD simulation
λ	mean temperature ratio $\bar{T}_2 / \bar{T}_1$
ρ	density
τ	time delay
ω	angular frequency (in radians)
φ	generic conserved quantity across a discontinuity
$f(\varphi)$	flux function of φ

Sub- and Superscripts

$\bar{a}$	superscript, temporal mean value of a
a'	superscript, fluctuation of a, $(a' = a - \bar{a})$
1	subscript, referring to conditions upstream of the flame
2	subscript, referring to conditions downstream of the flame
c	subscript, referring to cold flow conditions
h	subscript, referring to hot gases conditions

1 Introduction

1.1 Thermoacoustic instabilities

Thermoacoustic instability represents a major challenge in the development of lean combustion systems. It is a highly undesirable effect, since it limits the system operational efficiency and can lead to structural failure in the combustor hardware (see Fig. 1.1). Such instability originates from the coupling between the acoustic disturbances, and the unsteady heat release at the heat source. The presence of acoustic perturbations (i.e fluctuations in pressure and velocity) upstream the heat source leads to unsteady heat release rate, which in return generates further acoustic oscillations. These oscillations propagate away from the heat source, and are reflected back at the outer boundaries of the combustor. This results in a closed feedback loop, which may lead to higher unsteady oscillations at the heat source and generate instabilities in the entire system.

The presence of acoustic perturbations upstream the heat source can also cause the so-called "entropy waves", which are temperature inhomogeneities in the burnt gases propagating downstream at the convective flow speed. Marble and Candel [33] have shown that, when such inhomogeneities are accelerated by a nozzle or turbine blades, acoustic oscillations are produced at the acceleration zone. The component propagating in the direction upstream travels back into the combustor, and contributes to low-frequency oscillations. Acoustic perturbation generated from entropy waves are also know as *indirect combustion noise*. It is a critical problem in the aeroengines and afterburners, in which indirect combustion noise causes the "reheat buzz" phenomenon [17, 21, 22, 32, 42, 42].

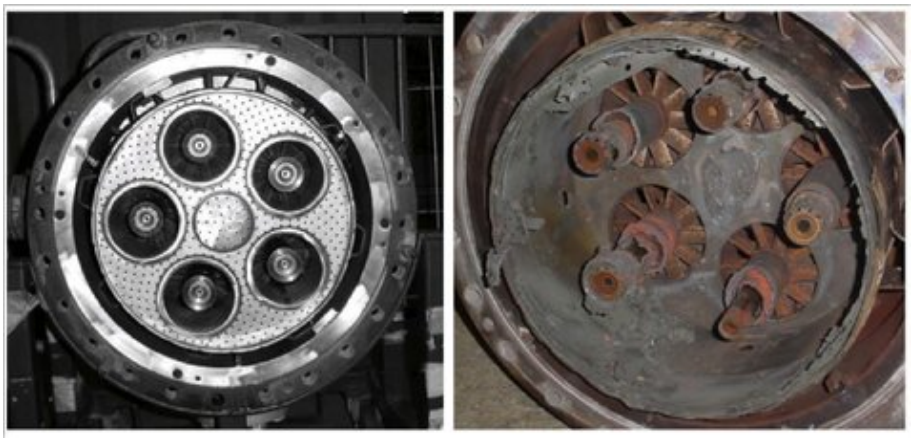

Figure 1.1: Picture of a intact (left) and damaged (right) burner. Source: Limousine Project

A tool which is widely employed for the prediction of the thermoacoustic instabilities is the

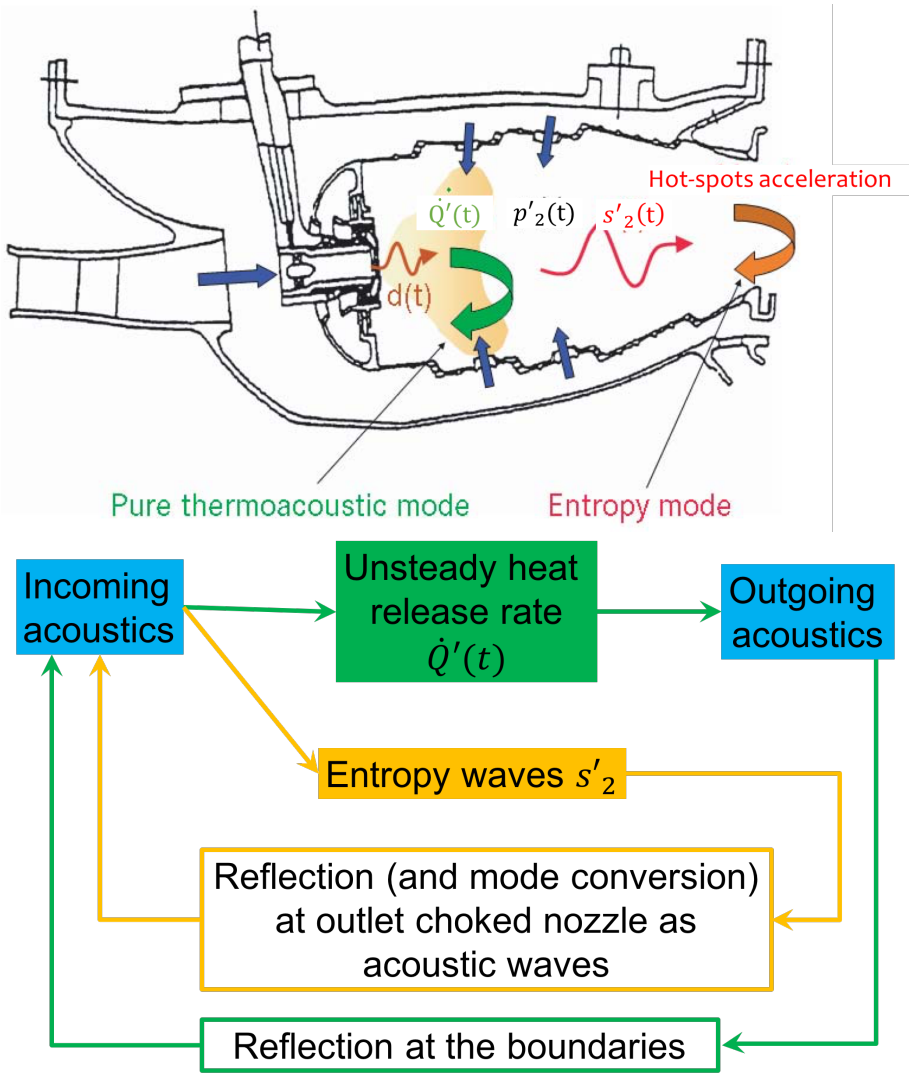

Figure 1.2: Schematic view of the acoustic closed feedback mechanisms. Green arrows represent the direct combustion noise due to the coupling between unsteady heat release rate and acoustics. The orange arrows represent the indirect combustion noise, due to entropy waves accelerated by the downstream chocked nozzle.

acoustic network model [8, 9, 18, 42, 49, 51]. In this approach, each element of the thermoacoustic system (e.g. flame, area changes, ducts) are seen as single subsystems, which are characterized in terms of acoustic scattering properties upstream and downstream. Specifically, the acoustic scattering matrix relates the acoustic waves impinging on the element to the components reflected and transmitted by the element itself. In this approach, the quality of the predictions strictly depends on the modeling of the single elements. Therefore, the correct prediction of the source terms for direct and indirect acoustics is essential, as entropy waves and heat release fluctuations are the driving force for acoustic oscillations, and the main source of instabilities. A correct prediction of instabilities is vital for the application of passive or active control systems on the burner. Passive control consist in damping elements, such as perforated plates, Helmholtz resonators, or modification of the combustor geometry. Active control, instead, consists in imposing varying acoustic signals, which interact destructively with the self-excited

oscillations in the system.

1.2 Thermo-acoustic characterization of heat exchangers

The topic of the present dissertation is part of the TANGO project (Thermo and Aeroacoustic Non-linearities in Green combustors with Orifice structures). TANGO is a Marie Curie Initial Training Network, funded by European Commission and features a consortium of scientific institutions across all Europe and India. The scope of the project is to develop and implement solutions to prevent thermoacoustic instabilities in green combustors.

This work originates from one aspect of the research activities in TANGO. It focuses on the unsteady behavior of heat sinks, such as cold heat exchangers, in a thermoacoustic systems.

Indeed, the most part of thermoacoustics literature has focused on flames, since they represent the main source of thermoacoustic instabilities. Instead, little is known about the thermoacoustic behavior of cooling elements, despite their broad application in combustion systems. This is because heat subtraction has always been associated to damping (i.e. stabilizing) effects. However, this assumption is not always correct. The original work by Rayleigh on the instability criterion reads as follows:

"*If heat be communicated to, and abstracted from, a mass of air vibrating (for example) in a cylinder bounded by a piston, the effect produced will depend upon the phase of the vibration at which the transfer of heat takes place. If heat be given to the air at the moment of greatest condensation, or be taken from it at the moment of greatest rarefaction, the vibration is encouraged. On the other hand, if heat be given at the moment of greatest rarefaction, or abstracted at the moment of greatest condensation, the vibration is discouraged.*"

The well-known Rayleigh criterion [46], which is a consequence of the previous statement, expresses the necessary (but non sufficient) condition for instabilities to arise:

$$G = \int_V \int_T \dot{q}'(x,t)\, p'(x,t)\, dt\, dx > 0, \tag{1.1}$$

where $p'(x,t)$ is the pressure oscillation, $\dot{q}'(x,t)$ is the heat release rate fluctuation, T is the oscillation cycle period and V is the control volume, in which heat release takes place. For the Rayleigh index G to be greater than zero, positive heat release rate oscillations should occur at the moment of highest compression, while negative oscillations should take place at the moment of greatest rarefaction. Such condition may be verified for flames as well as for heat exchangers. Therefore, depending on the phase between pressure and heat release rate fluctuations, a heat exchanger may also trigger or damp instabilities. The first observation of the thermoacoustic effect in heat subtraction was documented by J. Bosscha, who noticed that sound could be produced also when hot air flows over a cold screen [46].

Apart from the unsteady heat release rate, another interesting aspect of heat exchangers is to be found in the geometry. The presence of a several tube bundles in a combustion system certainly introduces a blockage effect with acoustic scattering, which could also contribute to the

thermoacoustic instabilities.

1.3 Flames and heat exchangers

As shown in Fig. 1.2, active elements in a thermoacoustic system are characterized by their unsteady heat release rate $\dot{Q}'$ [1] or their entropy generated downstream s_2'. Across the discontinuity, no information is provided on the mechanism of heat release, or the kind of heat source involved. Indeed, flames and heat exchangers have different heat release (or heat transfer) mechanisms. Does the black-box approach adopted in the previous literature correctly predict the downstream acoustics and entropy? Or should the heat release mechanism be accounted for in the analytical modeling of heat sources?

An answer to these questions was given by Chu [6, 7], who stated that the *"chief difference between a flame and a heat exchanger lies in the fact that, for a flame, the relative velocity between flame front and incoming flow is not known and is related to the flame speed, whereas for a heater, such relative velocity is assumed to be given."* The time-varying "relative velocity between flame front and incoming flow" is the consequence of the kinematic balance, which is present in the combustion process of the premix flames, while heat exchangers are fixed, and not subject to any kinematic balance.

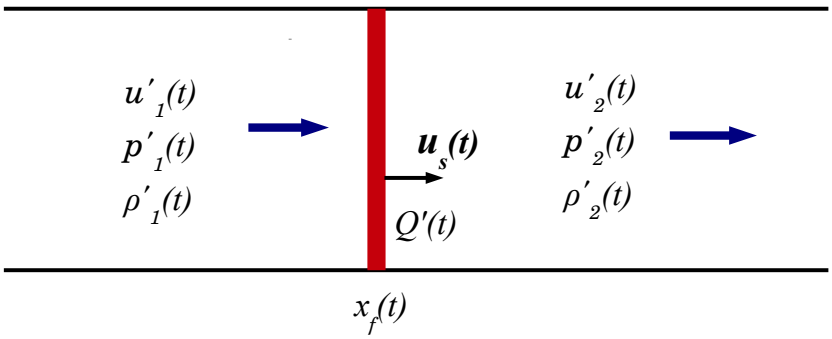

Figure 1.3: A quasi-1D heat source in presence of mean flow. Upstream perturbations u_1', p_1', ρ_1' are amplified across the discontinuity. Downstream perturbations u_2', p_2', ρ_2' are related to the oscillations upstream and to the unsteady heat release rate $\dot{Q}'$. In the case of a moving heat source, the relative velocity of the flame front with respect to the fixed observer is given by $u_s(t)$. In linear regime, the flame oscillates around the mean flame position $\bar{x}_f$. For a heat source at rest, the velocity of the heat source in the laboratory frame is zero $u_s(t) = 0$, thus the location of the source, $\bar{x}_f$, is constant in time.

In the present dissertation, analytical studies of jump conditions for fixed and moving heat sources have been first carried out [54, 55]. The main focus of the analytical work are the para-

[1] $\dot{Q}$ is the volume integral of $\dot{q}(x)$. $\dot{Q} = \int_V \dot{q}(x)dx$

doxical results in terms of entropy production in the jump conditions for a heat source at rest (especially at zero Mach) [1], and the resolution of such apparent contradiction by applying a modified version of the jump equations to premixed flames. The results of the new analytical relations are then validated against unsteady direct numerical simulations [56]. After assessing the differences in modeling between flames and heat exchangers, the analysis focuses on the acoustic scattering properties of a real-life heat exchanger, used in domestic boilers [53]. The goal is to understand the overall scattering properties of a heat exchanger with optimized geometry and heat transfer efficiency, and the validity of the network model approach in predicting the scattering behavior of a non-compact heat exchanger. Finally, the analysis of a thermoacoustic system featuring both heat source (premixed flame) and heat sink in cross-flow has been carried out [52].

Introduction chapters give the theoretical background for the work carried out in the papers. Chapter 2 gives the analytical background for linear acoustic conservation equations across a heat source. It also focuses on the different formulation found in literature for the cases of moving heat sources (e.g. premixed flame) and those at rest (e.g. heat exchangers). Chapter 3, on the other hand, gives an overview of the approaches to unsteady numerical simulation of thermoacoustic systems, and the system identification process.

2 Analytic background

In this chapter, the analytical modeling of acoustic scattering and propagation across heat sources and ducts are introduced. These analytical models describe the single subsystems (e.g. flame, duct, area change) which interact acoustically in a larger network model, which describes the complex systems, such as combustion chambers. The aim of this chapter is to show how systems stability can be determined starting from the acoustic relations in the network model.

2.1 Linear acoustics

Acoustic waves consist in small disturbances in pressure and velocity, which propagate in a gaseous medium. The small amplitude allows for linearization of the quantities of interest:

$$p'(x,t) = p(x,t) - \bar{p}(x); \qquad u'(x,t) = u(x,t) - \bar{u}(x); \qquad \rho'(x,t) = \rho(x,t) - \bar{\rho}(x); \tag{2.1}$$

where the overbar denotes the mean quantity, and the superscript denotes the perturbation quantity. The propagation of such perturbations takes place at the speed of sound c, which is function of the thermophysical properties of the medium and temperature:

$$c = \sqrt{\gamma R T}, \tag{2.2}$$

where γ is the ratio of specific heats ($\gamma = c_p / c_v$) and R is the ratio between the universal gas constant and the molecular weight of the gas ($R = R_{univ}/M$). The propagation of acoustic waves in the medium can be considered as inviscid and non-dissipative [45]. Therefore, the relation between acoustic perturbation p', ρ' and speed of sound is:

$$c^2 = \frac{p'}{\rho'}. \tag{2.3}$$

The propagation of such perturbations in presence of uniform mean flow in x-direction, without source terms, is described by the wave equation [45]:

$$\left(\frac{\partial}{\partial t} + \bar{u}\frac{\partial}{\partial x}\right)^2 p' - c^2 \nabla^2 p' = 0. \tag{2.4}$$

The solution for *plane waves* to the equation above is given by:

$$\begin{aligned} \frac{p'(x,t)}{\bar{\rho}\bar{c}} &= f(x,t) + g(x,t), \\ u'(x,t) &= (f(x,t) - g(x,t)), \end{aligned} \tag{2.5}$$

where f and g are the Riemann invariants, i.e. complex-valued acoustic waves propagating in the positive (f) and negative x-direction (g):

$$\begin{aligned} f &= \hat{F} \cdot \exp\Big(- ik^{+}x + i\omega t \Big) \\ g &= \hat{G} \cdot \exp\Big(- ik^{-}x + i\omega t \Big). \end{aligned} \tag{2.6}$$

In Eq. (2.6), $\hat{F}$ and $\hat{G}$ are the amplitudes of the acoustic waves f and g. k^{+} and k^{-} are the wave numbers in the positive and negative $x-$directions, respectively. The wave number $k\pm$ is related to the angular frequency ω, the speed of sound $c = \sqrt{\gamma RT}$ and Mach number M as:

$$k\pm = \pm \frac{\omega / c}{1 \pm M}. \tag{2.7}$$

In case of zero mean flow, the wave number simplifies to: $k = \omega / c$.

2.2 Network model

As observed in [36, 39], thermoacoustic instabilities are not a local, but a global phenomenon. In fact, acoustic waves travel in the combustor and are reflected at boundaries and discontinuities. Therefore, conditions at the boundaries of a thermoacoustic system (e.g. combustion chamber walls, nozzles) can influence the stability of the heat source, even if the elements involved are far away from each other.

Real thermoacoustic systems feature complex geometries and extensive domains. The use of full-scale CFD tools for determining the thermoacoustic behavior of the total system can be certainly computationally challenging. This is the reason why more efficient low-order network models are used for the prediction of thermoacoustic instability.

The strategy of network modeling is to divide complex geometries found in real combustors in several subsystems. This approach is advantageous, because in simple elements, such as ducts or temperature jump, acoustic waves propagation can be modeled analytically by linearizing the conservation equations. The acoustic waves propagating in the system is assumed as plane waves. Such assumption is valid, since in linear thermoacoustics the frequency range of interest is always lower than the *cut-on* frequency, so all the transversal modes decay exponentially [4, 45]. A simple model featuring a plane flame in a duct can be divided in 3 elements, as represented in Fig. 2.1 and 2.2: an upstream duct (1-2), an active heat source (2-3) and a downstream duct (3-4). The relations between the incoming and outgoing characteristic waves (respectively f_1, g_2 and f_2, g_1 for D1) in each element is given by the specific scattering matrix of the element.

According to [41], the acoustic elements can be classified in three categories :

- One-port element (such as "open end" boundary condition in Fig. 2.2), characterized only by a connection at one side of the element;
- Two-port connecting elements, typically ducts, which feature a certain length in the direction of wave propagation.

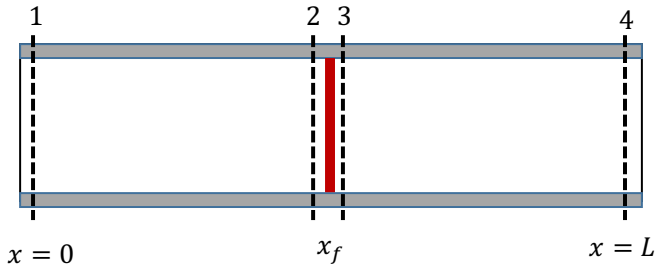

Figure 2.1: Simple thermoacoustic system featuring a plane flame in a duct with open ends

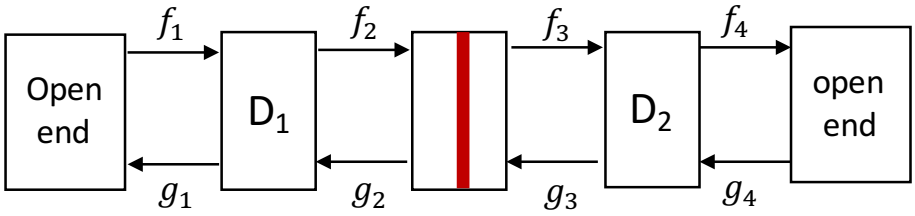

Figure 2.2: Corresponding network modeling of the system in Fig. 2.1. The model is divided into 3 subsystems (upstream duct, flame, downstream duct), which lie between the two open-end acoustic boundary conditions

- Two-port connecting nodes, i.e. discontinuities with negligible axial extension, such as temperature discontinuity or sudden area changes

From a cause-effect perspective, characteristic waves approaching the acoustic element (f_u, g_d) are related to the outgoing waves (f_d, g_u) through the scattering matrix SM. The elements on the matrix diagonal represent the transmission coefficients of the element, while off-diagonal coefficients represent the reflection properties.

$$\begin{pmatrix} \hat{F}_d \\ \hat{G}_u \end{pmatrix} = \underbrace{\begin{pmatrix} T_u & R_d \\ R_u & T_d \end{pmatrix}}_{S} \begin{pmatrix} \hat{F}_u \\ \hat{G}_d \end{pmatrix}. \tag{2.8}$$

The propagation of acoustic plane waves in a lossless duct of length x_f, like element D1 in Fig. 2.2, is expressed as [35, 41]:

$$\begin{pmatrix} \hat{F}_2 \\ \hat{G}_1 \end{pmatrix} = \underbrace{\begin{pmatrix} e^{-ik^+ x_f} & 0 \\ 0 & e^{-ik^-(x_f)} \end{pmatrix}}_{S_{duct}} \begin{pmatrix} \hat{F}_1 \\ \hat{G}_2 \end{pmatrix}, \tag{2.9}$$

where x_f is the length of the duct. In absence of damping effects, the amplitude of the acoustic waves entering the duct remains constant, and outgoing and incoming waves only differ by the acoustic time-delay $\tau = x_f / c(1 \pm M)$.

In addition to Eq. (2.8), the acoustic properties of a two-port element can be also reformulated as transfer matrix. Transfer matrix relates the downstream waves in terms of f and g to the

upstream waves:

$$\begin{pmatrix} \hat{F}_d \\ \hat{G}_u \end{pmatrix} = T_{fg} \cdot \begin{pmatrix} \hat{F}_u \\ \hat{G}_d \end{pmatrix}. \tag{2.10}$$

Recalling Eqs. (2.5) - (2.6), transfer matrix in Eq. (2.10) can also be reformulated in terms of up- and downstream pressure and velocity fluctuations:

$$\begin{pmatrix} p' \\ u' \end{pmatrix}_d = T_{pu} \cdot \begin{pmatrix} p' \\ u' \end{pmatrix}_u. \tag{2.11}$$

The algebraic relations between different formulations of the acoustic scattering/transfer matrix S, T_{fg} and T_{pu} can be found in [16].

2.2.1 Total system matrix and stability criterion

The transfer matrix of the total acoustic system can be obtained by simply multiplying the transfer matrix of the single elements in series: $T_{sys} = T_n \cdot T_{n-1} \cdot ... \cdot T_1$. The total acoustic transfer matrix of the system in Fig. 2.2 would result in:

$$\underbrace{\begin{bmatrix} 1 & -R_{open} & 0 & 0 & 0 & 0 & 0 & 0 \\ T_{11}^{D1} & T_{12}^{D1} & -1 & 0 & 0 & 0 & 0 & 0 \\ T_{21}^{D1} & T_{22}^{D1} & 0 & -1 & 0 & 0 & 0 & 0 \\ 0 & 0 & T_{11}^{f} & T_{12}^{f} & -1 & 0 & 0 & 0 \\ 0 & 0 & T_{21}^{f} & T_{22}^{f} & 0 & -1 & 0 & 0 \\ 0 & 0 & 0 & 0 & T_{11}^{D2} & T_{12}^{D2} & -1 & 0 \\ 0 & 0 & 0 & 0 & T_{21}^{D2} & T_{22}^{D2} & 0 & -1 \\ 0 & 0 & 0 & 0 & 0 & 0 & R_{open} & -1 \end{bmatrix}}_{\mathbf{T}_{sys}} \cdot \underbrace{\begin{pmatrix} \hat{F}_1 \\ \hat{G}_1 \\ \hat{F}_2 \\ \hat{G}_2 \\ \hat{F}_3 \\ \hat{G}_3 \\ \hat{F}_4 \\ \hat{G}_4 \end{pmatrix}}_{\mathbf{V}_{state}} = \underbrace{\begin{pmatrix} 0 \\ 0 \\ 0 \\ 0 \\ 0 \\ 0 \\ 0 \\ 0 \end{pmatrix}}_{\mathbf{V}_{ex}}, \tag{2.12}$$

where T_{sys} is the system matrix, $\mathbf{V}_{state}$ is the system state vector, and $\mathbf{V}_{ex}$ is the excitation vector. The stability of the system is frequency-dependent, and can be established by solving the characteristic equation:

$$\mathbf{det}\,[\ T_{sys}\,(\Omega)] = 0 \tag{2.13}$$

The solutions of the characteristic equation are the complex eigenfrequencies of the system:

$$\Omega_{eig} = \omega_{eig} + i\alpha \tag{2.14}$$

According to the convention adopted in Eq. (2.6) for the time dependency, the system is stable if the imaginary part of the eigenvalues $\alpha > 0$, condition which leads to the exponential decay of the perturbations in the system.

2.2.2 Compactness

As mentioned in Section 2.2, the connecting nodes are discontinuities with negligible axial extension. The ratio between the thickness of the discontinuity and the acoustic wavelength is represented by the dimensionless Helmholtz number He. When the condition:

$$He = \frac{\omega L}{c} = \frac{2\pi}{\lambda} L << 1 \tag{2.15}$$

is verified, the element is defined as acoustically "compact".

Compactness can be defined also w.r.t. the convective velocity. Such criterion is useful in the analysis of entropy waves propagation/generation across discontinuities, since temperature inhomogeneities propagate at flow speed. In this case, the velocity of propagation in Eq. (2.15) is the convective speed $|\bar{u}|$, and not the speed of sound, c. When acoustic *or* convective compactness is satisfied, it is possible to derive the scattering properties of the discontinuity by applying the conservation equations right up- and downstream the jump. Matching conditions can be therefore derived, even without giving a detailed description of the flow through the jump.

2.2.3 Rankine-Hugoniot equations

In the modeling of 1D acoustics, the matching conditions across compact, active heat sources is obtained by applying the "Rankine-Hugoniot" relations to the conservation equations. The "Rankine-Hugoniot" equations are well-known in gasdynamics for describing jump conditions across shock waves. For a shock waves propagating in a medium with velocity u_s, the Rankine-Hugoniot relations for conserved quantities between upstream and downstream the shock is [26, 44]:

$$u_s = \frac{f_2(\varphi) - f_1(\varphi)}{\varphi_2 - \varphi_1}, \tag{2.16}$$

where φ_2 and φ_1 are the conserved quantity before and after the discontinuity and $f_2(\varphi)$ and $f_1(\varphi)$ are the flux functions of φ. The condition above can indeed be applied to the conserved quantities across active acoustic heat sources, which feature an additional source term in the energy conservation equation, $\dot{Q}'$, the unsteady response in heat release rate in presence of acoustic perturbations. Thanks to the compactness hypothesis, the quasi-steady, incompressible conservation equations can be applied. Applying Eq. (2.16) to the Euler equations, it follows for mass, momentum and energy:

$$\begin{aligned} u_s(\rho_d - \rho_u) &= (\rho_d u_d - \rho_u u_u) \\ u_s(\rho_d u_d - \rho_u u_u) &= (\rho_d u_d^2 + p_d - \rho_u u_u^2 - p_u) \\ u_s(\rho_d E_d - \rho_u E_u) &= (\rho_d u_d H_d - \rho_u u_u H_u - \dot{Q}). \end{aligned} \tag{2.17}$$

Subscript -u and -d define the conditions right up- and downstream the discontinuity, respectively; while E is the total energy and H is the total enthalpy [1]. Linear acoustic perturbation

[1] the relation between E and H is expressed as follows:

$$H = E + \frac{p}{\rho} = e + \frac{1}{2}u^2 + \frac{p}{\rho} = h + \frac{1}{2}u^2 \tag{2.18}$$

pertains to small oscillations in pressure and velocity (p', u'). They cause all the relevant variables in the flow to oscillate around their mean value. Therefore, it is possible to decompose any variable in a mean component, which varies only in space, and a fluctuating component, which fluctuates in both space and time:

$$\phi(x,t) = \bar{\phi}(x) + \phi'(x,t). \tag{2.19}$$

2.2.3.1 Jump conditions for a generic heat source at rest

By linearizing the conservation equations in (2.17) and retaining only the fluctuating components, it is possible to derive the matching conditions across an active source (for detailed derivation, see Appendix of [24]). In literature, it is often assumed that the heat source is fixed at an axial position [9] (see x_f in Fig. 2.2), therefore $u_s = 0$. The acoustic conservation equations are written as [1, 9, 25, 42, 49] :

$$\begin{aligned}
&[\rho'\bar{u} + u'\bar{\rho}]_1^2 = 0, \\
&[p' + \rho'\bar{u}^2 + 2\bar{\rho}\bar{u}u']_1^2 = 0, \\
&[c_p\bar{T}(\rho'\bar{u} + u'\bar{\rho}) + \bar{\rho}\bar{u}(c_pT' + \bar{u}u')]_1^2 = \dot{Q}'.
\end{aligned} \tag{2.20}$$

After these consideration, we obtain for the jump conditions across a fixed heat source:

$$\begin{aligned}
u_2' &= u_1' + \bar{u}_1(\lambda - 1)\left(\frac{\dot{Q}'}{\bar{\dot{Q}}} - \frac{p_1'}{\bar{p}_1}\right) + \mathcal{O}(M^2) \\
p_2' &= p_1' + \mathcal{O}(M^2)
\end{aligned} \tag{2.21}$$

As it is implied in the compactness assumption, the dynamics at the flame front are not included in the equations. The only term describing the unsteady response of the heat source is $\dot{Q}'$, the fluctuating heat release rate. As proved by several works in literature [3, 11, 27, 50], the unsteady heat release at heat sources such as flame and heat exchangers is sensitive to velocity. In frequency domain, the unsteady heat release rate $\dot{Q}'$ caused by velocity perturbations(u') is represented by the frequency-dependent flame transfer function:

$$F(\omega) = \frac{\dot{Q}'(\omega)}{\bar{\dot{Q}}} \Big/ \frac{u_1'(\omega)}{\bar{u}_1}. \tag{2.22}$$

In frequency domain, the Eqs. (2.21) above can be therefore formulated as:

$$\begin{aligned}
u_2' &= u_1'(1 + (\lambda - 1)F(\omega)) + \mathcal{O}(M^2) \\
p_2' &= p_1' + \mathcal{O}(M^2).
\end{aligned} \tag{2.23}$$

The term $p_1'/\bar{p}_1$ has been neglected since the normalizes pressure oscillations are much smaller than the velocity perturbations:

$$\frac{p'}{\bar{p}} = \mathcal{O}(\gamma\bar{M})\frac{u'}{\bar{u}}. \tag{2.24}$$

2.2.3.2 Special case of premixed flames

The case of a premixed flame requires some special considerations. In most 1-D models, compact flames are modeled as a sudden discontinuity across which unburnt cold premixture become burnt hot gases (see Fig. 2.1). However, by looking at the Fig. 2.3, which was first proposed in Blackshear's work in 1953 [2], the flame features three separate zones.

The zone A1 (with duct width A_1), is the upstream zone where only cold premixture exists. The zone A2 (with duct width A_2) is where only burnt gases exist. The mass conservation for these two zones can be expressed by the continuity equation in in Eqs. (2.20). Between A1 and A2, however, the premixture and burnt gases coexist in the flame zone. Considering the flow as incompressible, the mass flow conservation for the flame zone can be written as [2]:

$$A_1 u_1(t) = A_f(t) S_f + \frac{\partial V_f(t)}{\partial t}, \tag{2.25}$$

$$A_2 u_2(t) = A_f(t) S_f \frac{\rho_1}{\rho_2} + \frac{\partial V_f(t)}{\partial t}, \tag{2.26}$$

where S_f, A_f , V_f are the flame burning speed, the flame area and flame volume, respectively. The presence of velocity perturbations upstream may lead to flame-stretching (see the dashed white line in Fig. 2.3), due to the instantaneous imbalance between incoming premixture and mass burning rate at the flame surface. As a consequence, both the flame area and the flame volume increase. The increase in flame area, on the other hand, compensates for the higher incoming mass flow, so that a new equilibrium condition can be established. This adaptive behavior of the flame front leads to a balance between up- and downstream as:

$$A_2 u_2(t) - A_1 u_1(t) = A_f(t) S_f \left(\frac{\rho_1}{\rho_2} - 1 \right) \tag{2.27}$$

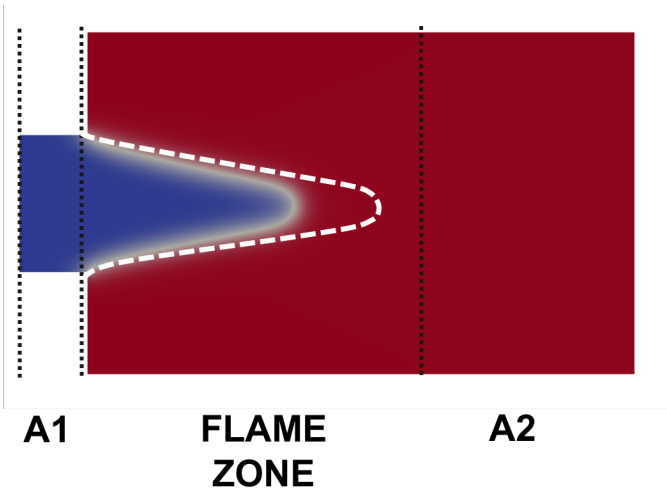

Figure 2.3: A ducted flame can be divided in 3 zones: an upstream zone (with duct cross-section A_1), a downstream zone (with duct cross-section A_2), and a flame zone, in which burnt and unburnt gases co-exist. The white dashed line highlights the profile of the flame when it stretches under velocity perturbations

With respect to Eq. (2.20), the relation above accounts for the movement of the discontinuity itself. This shows that the hypothesis of a discontinuity at rest is not valid for premixed flames. With the movement of the discontinuity, two aspects have to be considered, when analyzing the

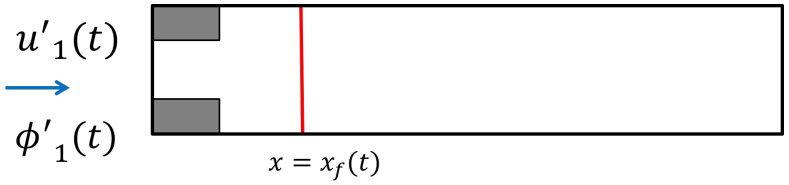

Figure 2.4: 1D modeling of the flame in Fig. 2.3. The space-averaged position of the flame front varies in time ($x_f(t)$)

stability of thermoacoustic systems. First, the position of the source changes in time (see Fig. 2.4). This affects the propagation of acoustic waves and therefore the stability behavior of the system. This aspect in non-linear flames has been analyzed by Luzzato [30, 31], who considered the effects on stability of flame displacement. The other problem pertains the influence of the flame front movement (A'_f,V'_f,$\partial V_f(t)/\partial t$) on the scattering and generation of acoustic and entropy waves. The latter aspect is analyzed in the present work [54–56].

2.2.4 Validity of network model approach

Network models can be a very powerful tool for predicting thermoacoustic instabilities. They are generally applied to systems in which plane waves are involved, but application to higher order modes is also possible (see [13],[5],[48]).

The validity of the acoustic network and the accuracy of the predictions on stability depend mainly on the precision of the single identified elements. Indeed, the scattering matrix of single elements might change, when the distance between the subsystems decrease and elements can mutually influence each other's scattering properties. A good example is found in the case of the premixed flame with a heat exchanger in cross-flow. When the distance between the two active elements (see Fig. 2.5) decreases, the flame tip impinges on the cylindrical shell of the heat exchanger, and mean-flow interactions occur. In such situation, the juxtaposition of the scattering matrix extrapolated from single elements (flame, heat exchanger) do not equal the scattering behavior identified for the joint system.

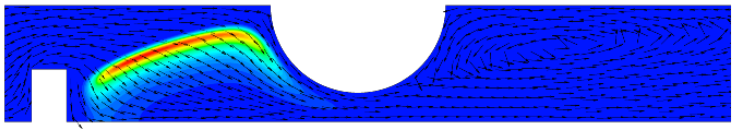

Figure 2.5: Heat release field of the case featuring 2D flame and cylindrical heat exchanger. The flame tip impinges on the cylinder and splits. Published with permission of *Hosseini et. al* [20])

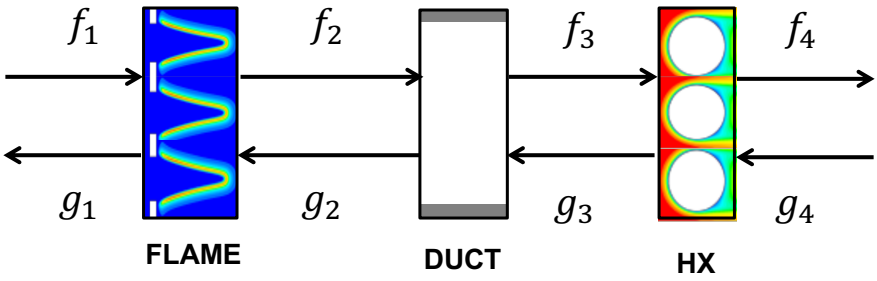

Figure 2.6: Network model of segregated elements, featuring flame, duct, and cold heat exchanger

In the case of the system flame-heat exchanger the mean-flow influence can be found even before the impingement. The presence of a cold cylinder downstream the flame may influence the velocity field and thus the response of the flame to acoustics. On the other hand, close to the flame tip the velocity shows a non-uniform profile, which could also influence the behavior of the heat exchanger. The validity of this specific network model is therefore limited to distances at which such interactions do not take place.

2.2.5 Temperature inhomogeneities in the network models

In the analysis of network models, the presence of temperature inhomogeneities should also be taken into account [12, 19, 23, 47]. This is because perturbations in temperature, which travel at convective speed, may also influence the propagation of the acoustic waves. In fact, the speed of sound depends on temperature, and the deviations from the homogeneous mean temperature field may lead to different stability behavior in the system [17, 57, 58].

The influence of temperature inhomogeneities is even more important, when a chocked nozzle is placed downstream the unsteady heat source. The acceleration of temperature inhomogeneities represents a source for indirect acoustic perturbations. An indirect component of reflected acoustic waves (g_{ind} in Fig. 2.7) may add up to the upstream traveling component of direct acoustic wave (g_d) and lead to changes in system stability [33, 42].

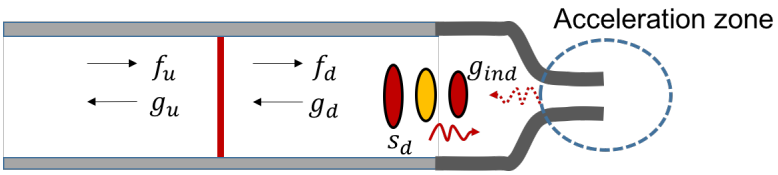

Figure 2.7: "Hot-" and "cold spots" may be generated downstream an unsteady heat source. These entropy waves (s_d) are reflected as acoustic perturbation (g_{ind})at the chocked nozzle

Therefore, in addition to the relations for acoustic variables, the Rankine-Hugoniot equations should also account for entropy variables, such as density or temperature perturbations. Only then, the acoustic source and propagation in the network model are modeled correctly and comprehensively.

3 Unsteady numerical simulation of thermoacoustic systems

In realistic geometries and systems, an analytical formulation which accounts for all the physical mechanisms contributing to the global scattering behavior of the acoustic elements cannot be achieved for every case. Propagation and scattering of acoustic waves are in fact subject to effects such as acoustic damping, vortex shedding, flow inertia. In flames, several effects concur to the unsteady heat release rate (flame area change, flame thickening, wall-flame interaction, etc...) and an analytical model for $\dot{Q}(t)$ cannot be easily found. Therefore, while identifying the scattering behavior of the elements, applying the quasi-steady acoustic conservation equations is not sufficient. Instead, experimental measurements and numerical simulation are more often adopted. In this chapter, we will introduce the existing approaches in identifying the system response in the linear regime, from a "black-box" perspective.

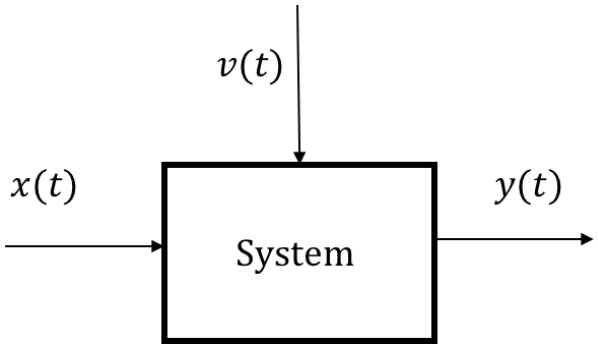

Figure 3.1: A system characterized by its output ($y(t)$), input ($x(t)$) and disturbance signal($v(t)$).

3.1 Analysis approach

In the black-box approach, the physical mechanisms of acoustic scattering are not explicitly accounted for. Instead, the dynamics of the acoustic element is characterized only by the system response (output) to external excitation signals (input).

In the present work, only the linear, causal, time invariant systems are considered. Time-invariance implies that the system's response does not depend explicitly on time. Therefore, if a signal $x(t)$ produces a response $y(t)$, the same input applied at time $t+\tau$ will produce the same response $y(t)$, with a delay of τ. The system behavior can therefore be described by the

impulse response convolution function:

$$y(t) = \int_0^{+\infty} g(\tau)x(t-\tau)d\tau, \tag{3.1}$$

where $g(\tau)$ is the impulse response (or weighting function) of the system.

Causality implies that the response of the system $y(t)$ depends only on present and past excitation signals $x(t-\tau)$, and not on future inputs, so $\tau \geq 0$ [28].

Linearity of the system implies that the relation between input and the output remains constant, and does not depend on the input signal magnitude or frequency. Moreover, the frequency of the system response should correspond to the excitation signal frequency.

Time-invariance implies that the system can be entirely characterized by time delays. This means that the system response to a discrete time series x_t can be expressed as:

$$y_t = b_0 x_t + b_1 x_{t-1} + ... + b_N x_{t-N}, \tag{3.2}$$

and the transfer function $G(q)$ can be written as [38, 40, 50]:

$$G(q) = \sum_{n=0}^{N} b_n q^{-n}, \tag{3.3}$$

where q is the shift operator, so: $q^{-n}x_t = x_{t-n}$. Here, a finite integer is used (N), instead of ∞, because we assume that the response of the systems becomes negligible for $n > N$. $G(q)$ is the transfer operator of the system, since:

$$y(t) = G(q)x(t). \tag{3.4}$$

Similarly, when disturbance is present, a transfer operator can be defined for $v(t)$:

$$v(t) = H(q)e(t) \qquad H(q) = \sum_{n=0}^{N} h_n q^{-n}, \tag{3.5}$$

where $e(t)$ is white noise, characterized by a specific PDF, and $H(q)$ is the transfer operator of the disturbances. The global description of a system with superimposed disturbance will be:

$$y(t) = G(q)u(t) + H(q)e(t). \tag{3.6}$$

3.1.1 Flame transfer function: Single Input-Single Output approach

Linear acoustic perturbations consist of small fluctuations of velocity and pressure in a steady state system. With reference to the numerical setup in Fig. 3.2, at time $t = t^*$, a small perturbation in velocity (and pressure) is imposed to the inlet conditions:

$$u_1(t^*) = \bar{u}_1 + u_1'(t^*); \qquad \rightarrow \qquad \dot{Q}(t^*) = \bar{\dot{Q}} + \dot{Q}'(t^*); \tag{3.7}$$

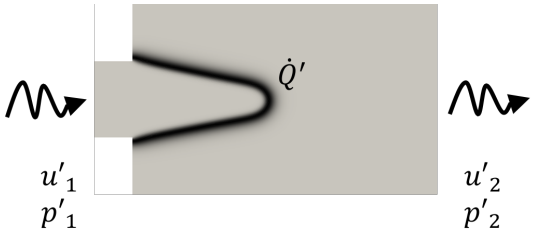

Figure 3.2: Unsteady upstream perturbation as input signal imposed to a 2D slit flame.

Figure 3.3: Single-Input, Single-Output approach

For the characterization of a heat source transfer function $F(\omega)$, the corresponding input and output coincide with the velocity fluctuation $u'(t)$ and the heat release rate fluctuations $\dot{Q}'(t)$, respectively. The model which characterizes the heat release response of the heat source is then:

$$F(\omega) = \frac{\dot{Q}'(\omega)}{\bar{\dot{Q}}} \Big/ \frac{u'_1(\omega)}{\bar{u}_1}. \tag{3.8}$$

For discrete time series, the transfer function corresponds to the Z-transform of the impulse response function $G(q)$:

$$F(\omega) = \sum_{n=0}^{N} b_n e^{-i\,\omega\,n\,\Delta t}, \tag{3.9}$$

where Δt is the sampling interval and ω is the angular frequency.

The identification of the transfer function is possible only if the system remains in the linear regime. The classic open and closed end conditions lead to a reflection coefficient of magnitude unity and are not suitable for the identification. Instead, the Navier-Stokes Characteristic Boundary Conditions (NSCBC) [37, 43] are often used, since they ensure a quasi non-reflective condition at the boundaries, so an open-loop system is achieved, and the perturbations remain in the linear regime.

3.1.2 Identification of LTI models

As pointed out in Section 3.1, the assumption of linearity implies that a model, when excited by a signal at a certain frequency f^*, shall give a response, which is also at frequency f^*. It follows that the most straightforward approach in analyzing system's response is to excite the system with a monofrequent sinusoidal signal and register the response. In Fig. 3.4 the dots represent respectively the magnitude and the phase of the flame transfer function $F(\omega)$. The system of

reference is the laminar 2D flame in Fig. 3.2 and 3.5. The transfer function is the ratio between the response $\hat{\dot{Q}}'(\omega)/\bar{\dot{Q}}$ (normalized unsteady heat release rate oscillations) and the input signal $\hat{u}'(\omega)/\bar{u}$ (normalized velocity perturbations at inlet) in frequency domain, according to Eq. (3.8) and (3.1). The transfer function $F|_u(\omega)$ is the solution to the "closure problem" in the Rankine-Hugoniot equations, and the input needed for the flame subsystem in the network model.

The monofrequent excitation shows some obvious drawback: for a range of frequencies (e.g. from 0 to 1000 [Hz]) it is necessary to perform n simulations, when n points are needed in the range of interest. This can be computationally expensive, especially when many parameters studies are needed.

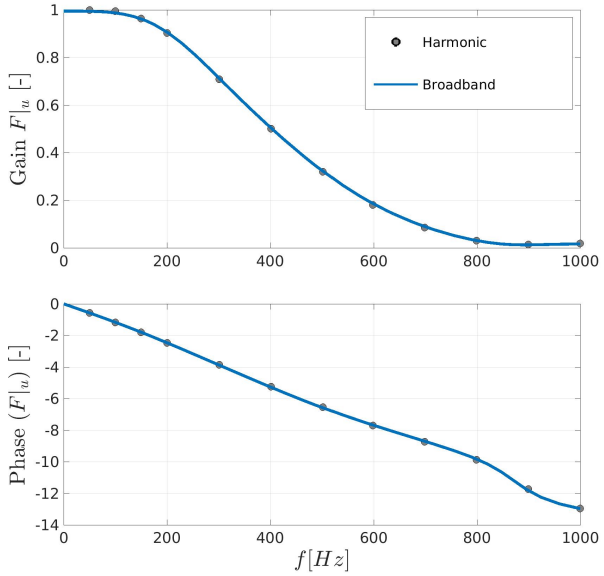

Figure 3.4: Identified gain and phase of a perfectly premixed flame transfer function F. The transfer function shows a typical low-pass behaviour, which means that the response in terms of heat release rate fluctuations are higher when then upstream acoustic excitation have low frequencies. In this case, the function is identified by using monofrequent (dots) and broadband (line) signals as excitation.

For laminar flow fields, it is possible to apply the same approach by using a multi-sinusoidal, or a step-function, as input signal. However, the step-function needs higher computational efforts to be well resolved [38]. Moreover, most flows and flames found in real combustors are turbulent and may show small random oscillations which cannot be attributed to acoustic perturbations. In these cases, a simple Fourier transform of the input signal and system response may give incorrect predictions for the system transfer function. It is then necessary to account for the presence of the additional disturbances in the model.

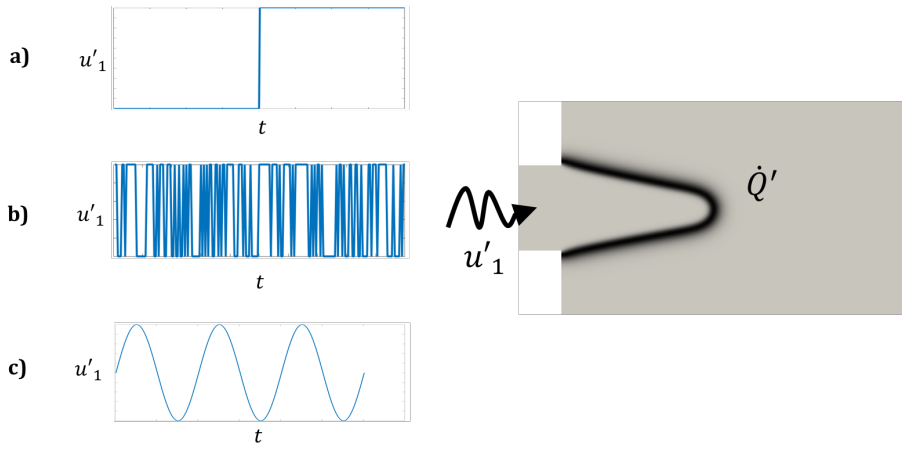

Figure 3.5: Excitation signals as input: step function (a), random binary broadband signal (b), monofrequent signal (c).

3.1.2.1 An example of model parametrization

A very generic description of the system in terms of input and output can be given by the linear difference equation:

$$y(t) + a_1\, y(t-1) + \cdots + a_{n_a}\, y(t-n_a) = b_1\, x(t-1) + \cdots + b_{n_b}\, x(t-n_b) + e(t), \quad (3.10)$$

where $\theta = [a_1, ..., a_{n_a}, b_1, ..., b_{n_b}]$ are the model parameters to be estimated. Defining the functions $A(q)$ and $B(q)$:

$$A(q) = 1 + a_1 q^{-1} + ... + a_{n_a} q^{-n_a} \qquad B(q) = 1 + b_1 q^{-1} + ... + b_{n_b} q^{-n_b}. \quad (3.11)$$

According to Eq. (3.6) and (3.10), the time series can be defined as:

$$y(t) = \frac{B(q)}{A(q)} x(t) + \frac{1}{A(q)} e(t) = G(q,\theta)x(t) + H(q,\theta)e(t). \quad (3.12)$$

The model described above is called "Autoregressive Exogeneous" (ARX) model. Note that for the case $n_a = 0$, the model reduces to the Finite Impulse Response (see Eq. (3.3)).

The ARX model is only one of the many models available for the identification of LTI systems, and its description is given here as an example of parametrization for G and H. The most common models such as ARMAX, Output-Error and Box-Jenkins belong to the same family of bloack-box models and are well described in [29].

3.1.3 Acoustic scattering matrix: Single Input-Multi Output and Multi Input-Multi Output approach

For the identification of acoustic scattering behavior, the Single Input-Multi Output or the Multi Input-Multi Output approach is used. With reference to the flame in Fig. 3.2 and to the scheme in

Fig. 3.6, the system is excited by a signal at the inlet f_u, and the outputs are measured in terms of reflected wave g_u and transmitted wave f_d. The upstream reflection R_u and transmission coefficient T_u can be identified.

$$\begin{pmatrix} f_d \\ g_u \end{pmatrix} = \underbrace{\begin{pmatrix} T_u & R_d \\ R_u & T_d \end{pmatrix}}_{S} \begin{pmatrix} f_u \\ g_d \end{pmatrix}. \tag{3.13}$$

A SISO approach in the determination of the scattering matrix implies two separate unsteady

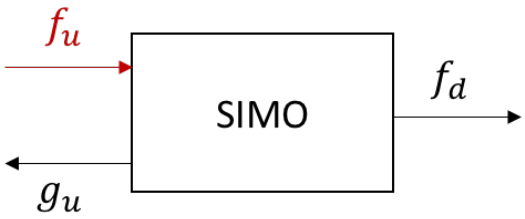

Figure 3.6: Single-Input, Multi-Output approach

simulations, with broadband excitations imposed separately at the inlet and outlet. A Multi Input-Multi Output allows for the identification of the scattering matrix in only one simulation. In this case, the signals imposed at the boundaries should be statistically uncorrelated [15].

Figure 3.7: Multi-Input, Multi-Output approach

3.2 Unsteady time series: implicit and explicit time scheme

The unsteady time series are obtained from unsteady simulations starting from a converged solution. In the present work, two different solvers (AVBP [1] and rhoPimpleFOAM from OpenFOAM) are used to perform the simulations. We will not focus here on the details of the solvers, since several numerical setups are described in the papers. Instead, we will make some considerations on the use of implicit and explicit method in the solution of unsteady transport equations.

In the solution of the time-dependent discretized partial and ordinary differential equations, both explicit and implicit methods can be used. In the **explicit** method, the variable $\Phi(t+1)$

[1] http://www.cerfacs.fr/ avbp/AVBP_V6.X/AVBPHELP/avbphelp.php

is an explicit function of the same variable at time t: $\Phi(t+1) = F(\Phi(t))$. The **implicit** method expresses the variable $\Phi(t+1)$ as: $F(\Phi(t), \Phi(t+1)) = 0$. An example applied to 1-D conservation equations can be found in [14].

In the numerical simulation of thermoacoustic systems, an explicit method is useful for resolving the acoustic waves propagation, and the interaction between acoustics, vorticity and entropy. Computationally it may be expensive, since the stability of the computation is limited by the acoustic Courant number [36]:

$$C_{acoustic} = \frac{c\,\Delta t}{\Delta x} < 1, \tag{3.14}$$

where c ist the speed of sound, Δt is the time step and Δx is the cell size. The condition on Courant number should be satisfied for every time step, in the whole numerical domain. For the solver AVBP, the value of 0.7 for $C_{acoustic}$ is found to be a good compromise between stability and numerical effort. Implicit schemes can as well be adopted for thermoacoustic numerical simulations. Compared to the explicit methods, the implicit methods are more stable [14], and do not diverge for Courant numbers higher than unity. However, some information on acoustic propagation through the numerical domain might be lost, and the time delay is not accurate.

4 Summary of papers

The work carried out in the course of the dissertation research has been published in five journal and conference papers (including 3 peer-reviewed papers) published in the years 2014-2016.

4.1 ICSV21: *On the jump conditions for flow perturbations across a moving heat source*

Summary

In this paper, we present the analytical framework of 1-D conservation equations for acoustic perturbations across a moving and fixed heat source. In these equations, an additional term, u'_s, has been introduced. u'_s represents the movements of the flame front, which adapts to the incoming velocity fluctuations by changing its surface area. We explain why the kinematic balance and the flame front movement are essential to the prediction of the acoustic scattering behavior. In fact, for a passive flame front ($\dot{Q}' = 0$) which moves *with* the incoming velocity perturbations, the velocity jump across the discontinuity is: $u'_2 = u'_1$. In the case of a heat source at rest (e.g. heat exchanger, heated wire) and no heat release rate fluctuations ($\dot{Q}' = 0$), the jump condition is $u'_2 = (\bar{T}_2/\bar{T}_1)\,u'_1$.

Contribution

I conceived the outline of this paper together with S. Bomberg and Prof. W. Polifke. I contributed to the theoretical work with the derivation of the linearized conservation equations up to first order in Mach and analyzed the application of the equations to moving heat sources and sources at rest. As the first author, I prepared the first draft of the paper and submitted the final version to the conference.

Reference

L. Strobio Chen, S. Bomberg, W. Polifke, *"On the jump conditions for flow perturbations across a moving heat source"*, 21st International Congress on Sound and Vibration (ICSV21), Beijing, China, 13 – 17 July 2014.

4.2 Combust. Flame 2016: *Propagation and generation of acoustic and entropy waves across a moving flame front*

Summary

As the previous work [54], this paper also discusses the linear acoustic conservation equations across a moving heat source. However, in this paper, a deeper insight is given to the consequences of the flame front movement. It is first shown how the analytic model of the flame at rest cannot be applied to premixed flames, since leads to unphysical prediction on entropy waves generation, and to apparent contradictions in the case of $M = 0$. Instead, by applying the *moving* flame front model, it is possible to give a physically sound prediction of the leading order entropy waves generation across the flame front. Indeed, in the moving model, temperature inhomogeneities are *only* related to the upstream fluctuations in equivalence ratio. In absence of equivalence ratio fluctuations, the total heat release rate is governed by the unsteady volume consumption at the flame front, and no fluctuations in temperature is found in burnt gases. The appendix, finally, elucidates how first order entropy terms are generated, even in absence of equivalence ratio perturbations. In this case, the entropy waves (which are negligible for small Mach regimes) are produced from the coupling of upstream acoustic fluctuations p_1', u_1', T_1' and the *mean heat release rate* $\bar{\dot{Q}}$.

Contribution

I conceived the outline of this paper together with S. Bomberg and Prof. W. Polifke. I contributed to the theoretical work with the interpretation of the entropy source in the linearized acoustic conservation equations. Moreover, I did an extensive literature research in order to compare the formulation used in previous analytical works to the formulation presented in the paper and analyzed the interconnections among the different formulations.

As the first author, I wrote the draft of the paper and, in quality of corresponding author, I implemented the suggestions made by the reviewers, prepared the rebuttals and submitted the final version.

Reference

L. Strobio Chen, S. Bomberg, W. Polifke, *Propagation and generation of acoustic and entropy waves across a moving flame front*, Combust. Flame, Vol 166, 170-180, Apr. 2016

4.3 ASME Turbo Expo 2016: *On generation of entropy waves by a premixed flame*

Summary

This paper is the numerical counterpart of the two previous publications [54, 55]. Here, it has been proved numerically that the fixed flame front model is not suitable for predicting entropy waves generation. The results from fully compressible CFD simulations show that only negligible temperature inhomogeneities are produced downstream a perfectly premixed flame. It follows that the formulation given in previous work in literature [9, 10] are misleading, since they predicted leading order entropy generation even for perfectly homogeneous premixture.

Indeed, leading order entropy waves are produced downstream a premixed flame, only when equivalence ratio changes upstream. Following the analytical results in [55], the entropy waves s_2'/c_p in presence of ϕ' have been evaluated numerically . The order of magnitude entropy waves evaluated at the outlet of the computational domain validates the analytical predictions. However, for an accurate prediction of the low-frequency limit of the entropy transfer function ($E_\phi(\omega) = (s_2'/c_p)/(\phi'/\bar{\phi})$), it is necessary to account for the thermophysical properties of real gases before and after combustion.

Contribution

I conceived the outline of this paper together with T. Steinbacher, Prof. W. Polifke and Dr. C. Silva. I performed the compressible simulations in AVBP of the adiabatic flame, and carried out the post-processing of the unsteady time series and the identification of the entropy transfer function.

Reference

Lin Strobio Chen, Thomas Steinbacher, Camilo Silva, Wolfgang Polifke, *"On generation of entropy waves by a premixed flame"*, ASME Turbo Expo, Seoul, South Korea, 13–17 June 2016

Erratum

Fig. 7 in the paper contains a scaling error: the low-frequency limit of the entropy transfer function gain $|E|_\phi(\omega)$ is lower than the prediction given by Eq. (25). The correct values are given below, in Fig 4.1, even if the general conclusions do not change: the low-pass filter behavior is conserved. The difference in the low-frequency limit value is due to the variation in specific heat at constant pressure with temperature, which should not be neglected. This can be also evinced from Fig. 4.2 (Fig. 8 in the paper), in which the magnitude of entropy waves evaluated at the outlet from CFD is about 3/4 the prediction given by Eq. (10). The correct graphic is as follows:

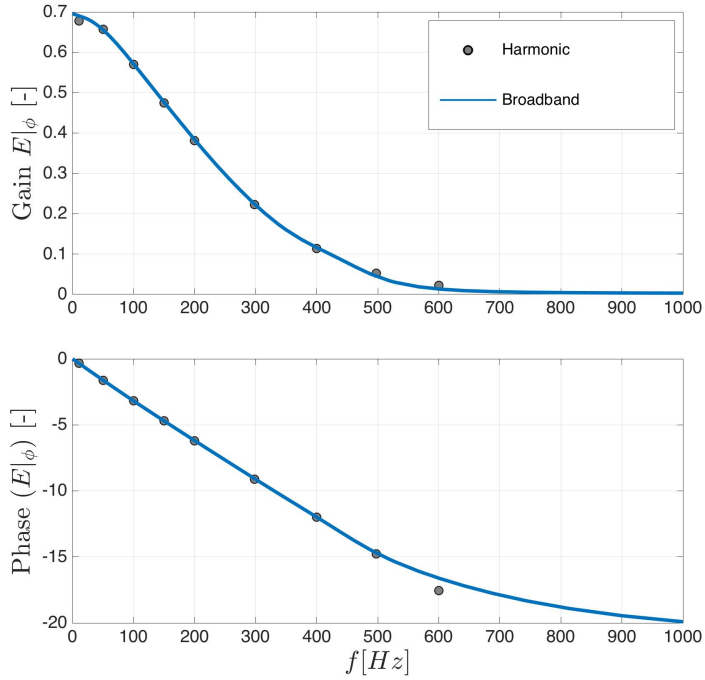

Figure 4.1: Entropy transfer function $E|_\phi$. The low-frequency limit of the gain is ~ 0.67, not ~ 0.8 as given in the paper.

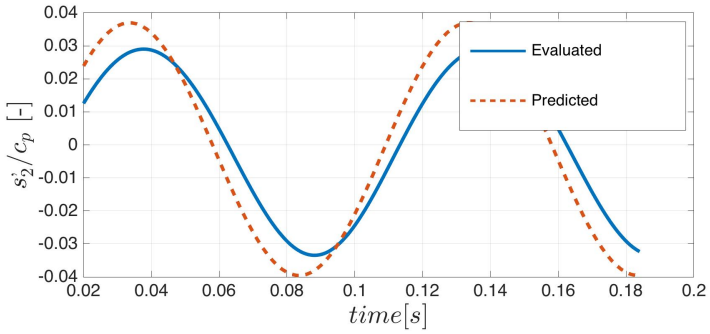

Figure 4.2: The comparison between predicted entropy ~ $\left(1-\frac{1}{\lambda}\right)$ and entropy probed at the outlet for the case $f = 10[Hz]$. The ratio between the magnitudes is ~ 0.785. It can be easily proved that: $0.785 \cdot \left(1-\frac{1}{\lambda}\right) \approx 0.67$

4.4 ICSV22: *Thermo-acoustic characterization of a heat exchanger in cross flow using compressible and weakly compressible numerical simulation*

Summary

In the present work, a heat exchanger as used for hot water supply in domestic boilers is investigated numerically. The objective of the study is to identify the frequency response of the heat transfer rate with respect to perturbations of flow velocity, and the acoustic scattering matrix of the heat exchanger. Compressible and weakly compressible simulations have been carried out for the identification of the heat exchanger transfer function ($\mathrm{HXTF}(\omega) = (\dot{Q}'/\bar{\dot{Q}})/(u_1'/\bar{u}_1)$) in a real-life *non-compact* heat exchanger. Good agreement is found between the weakly and the fully compressible simulation results. Considerations on the relation between unsteady heat transfer rate and entropy production in heat exchangers (fixed heat sources) at low frequencies have been carried out.

In order to find the role of the geometry and the unsteady heat transfer rate on the acoustic scattering, he authors developed a Grey-box model of the heat exchanger scattering matrix, combining the geometric properties of the tube array and the HXTF. Good qualitative agreement is found in the comparison with scattering matrix identified from fully compressible simulations. However, some discrepancies are found at low frequencies.

Contribution

I conceived the outline of this paper together with A. Witte and Prof. Polifke. I performed the compressible simulations in OpenFOAM of the heat exchanger, the post-processing of the unsteady acoustic signals and implemented the network model of the system. As the first author, I wrote the first draft of the paper and submitted the final version to the conference.

Reference

L. Strobio Chen, A. Witte, W. Polifke, *"Thermo-acoustic characterization of a heat exchanger in cross flow using compressible and weakly compressible numerical simulation"*,
22nd International Congress on Sound and Vibration (ICSV22), Florence, Italy, 12 – 16 July 2015

4.5 ICSV23: *Acoustic scattering behavior of a 2D flame with heat exchanger in cross-flow*

Summary

In this work, a thermoacoustic system featuring a 2D flame and a cold heat exchanger in cross-flow has been analyzed numerically. Analysis shows that the heat exchanger scattering properties can have a significant impact on the total system acoustic scattering properties, especially in presence of resonance peaks due to the flame intrinsic feedback. Such influence may not be readily apparent. However, results in the paper show that, close to resonance peaks, the total scattering behavior can be very sensitive to small changes in the reflection properties of the heat exchanger.

The study has also focused on the validity of the network approach at varying distance between flame and heat exchanger. As pointed out in the section 2.2.4, the acoustic network approach is valid, provided that the elements in the network interact only acoustically and no changes in the mean flow field occurs. It has been found that, in the case analyzed, such limit occurs at a distance of about 10 mm between the flame holder and the cylinder. At 10 mm the mean flow field is changed with respect to the segregated case, since the velocity profile upstream the heat exchanger is not uniform, but is influenced by the flame flow field.

Contribution

I conceived the outline of this paper together with N. Hosseini, Prof. Polifke and Dr. J. Teerling. I personally performed the compressible simulations in AVBP of flame, heat exchanger and the joint system, the network model of the systems and the post-processing in Matlab. To support the numerical results, I also carried out the analytical derivations of the scattering matrix for the joint system (flame+HX). As the first author, I wrote the first draft of the paper and, in quality of corresponding author, I implemented the suggestions made by the reviewers, prepared the rebuttal and submitted the final version.

Reference

L. Strobio Chen, N. Hosseini, W. Polifke, J. Teerling, V. Kornilov, I. Lopez Arteaga, P. de Goey, *"Acoustic scattering behavior of a 2D flame with heat exchanger in cross-flow"*, 23rd International Congress on Sound and Vibration (ICSV23), Athens, Greece, 10 – 14 July 2016.

5 Conclusions

5.1 Analytic modeling of jump conditions across moving and fixed heat sources

In the first analytical studies, the differences between flames and heat exchangers have been explored. The analysis has shown that, up to first order in Mach number, the difference in analytic modeling between a moving heat source (premixed flame) and a heat source at rest (heat exchanger) lies primarily in the prediction of entropy production and the correct formulation for the linearized continuity equation for acoustic perturbations [1].

With the analytical model used in the publications [54–56], it was possible to identify the dominant source for entropy wave generation in premixed flames, which consists in fluctuations of equivalence ratio upstream of the flame. It was also possible to explain the origin of first order entropy waves produced downstream a perfectly premixed flame, which originate from the interaction between the upstream acoustics and the *mean* heat release rate at the flame. The model presented and discussed in this work also allows to explain and solve the paradox mentioned by Bauerheim in [1] for conservation of acoustic mass flow rate at zero Mach.

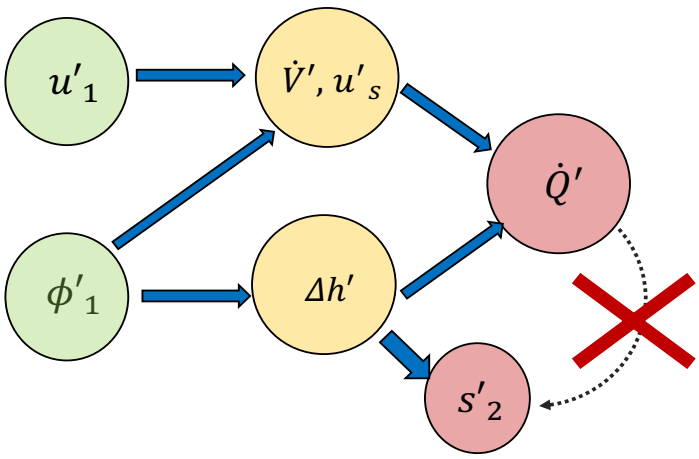

Figure 5.1: The schematic picture shows the interconnection between upstream acoustic perturbations (u', ϕ'), flame front kinematics $(u'_s, \dot{V}'_f)$ and mass specific changes $\Delta h'$, and the production of acoustic and entropy source terms. No direct relation can be established between the unsteady heat release rate (per unit of volume) and entropy waves production.

The analytical works have also clarified the interdependency between the unsteady heat release rate $\dot{Q}'$ (i.e. flame transfer function) and entropy wave generation (see Fig. 5.1). Is has been proved that entropy wave generation does not univoquely relate to the unsteady heat release rate at the flame front.

On the other hand, heat sources at rest cannot adapt to the incoming flow perturbations, as it happens in premixed flames. Therefore, an increase in incoming mass flow always generates downstream temperature fluctuations. This also happens at the low-frequency limit, since the HXTF of real heat exchangers never equal unity, unless the heat exchanger has infinite surface.

5.2 Influence of a cold heat exchanger on the scattering behavior of the thermoacoustic system

System featuring fixed heat sources such as cold heat exchangers may produce more entropy waves downstream. In addition to this, analyses in [52, 53] have shown that the presence of a cold heat exchanger may strongly impact on the acoustic scattering behavior (therefore, on the stability) of a thermoacoustic system, when placed downstream a flame or an active heat source. Even nearly acoustically transparent elements (i.e. low reflection coefficients, transmission coefficients close to unity) can greatly enhance the acoustic amplification of the system. For the test case analyzed in [52] we quantified the impact of the heat exchanger on the thermoacoustic stability. Stability maps obtained for the network models pictured in Figs. 5.2 - 5.3 suggest that, for the configuration explored in [52], in presence of a weak reflection coefficient at the boundaries, the presence of a single tube row enhances system instability (The blue area, which indicates stability, is reduced in Fig. 5.3). To explore the effect of multiple tube bundles downstream the heat source, a third network model is created, with a fictitious heat exchanger tube row, which has the same acoustic scattering property as the first tube bundle, and the same temperature ratio between upstream and downstream. The destabilizing effect is enhanced in this third case.

The eigenfrequencies (f_{eig1} = 260 Hz, f_{eig2} = 255 Hz, f_{eig3} = 230 Hz) decrease when multiple heat exchangers are placed downstream the flame, since the temperature of the downstream flow (and the speed of sound) are lower.

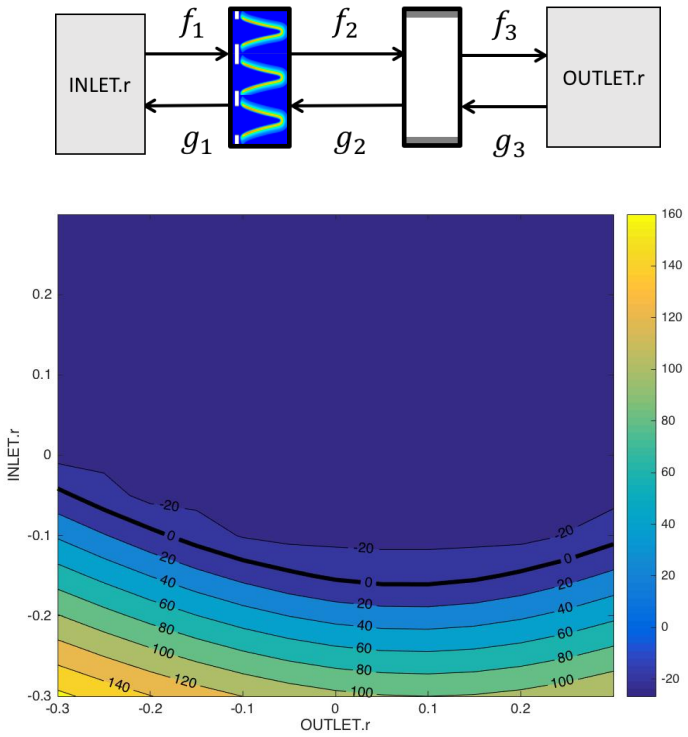

Figure 5.2: Stability map of a system featuring a ducted premixed flame as in [52]. Positive Growth rate indicate unstable system. The duct before the outlet is 0.5 m long. INLET.r and OUTLET.r are the reflection coefficients at the inlet and outlet, respectively.

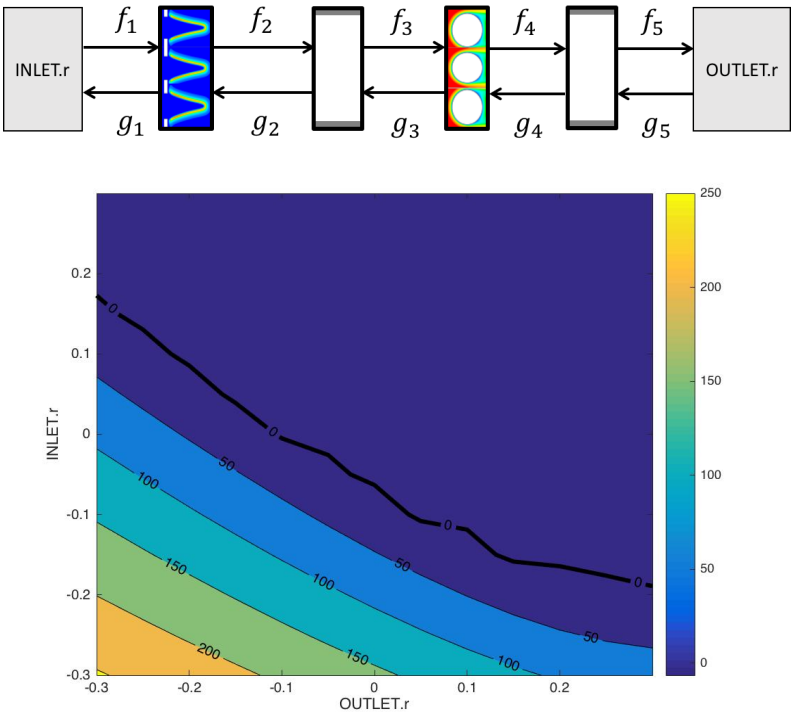

Figure 5.3: Stability map of a system featuring a ducted premixed flame and a single row of heat exchanger tube as in [52]. Positive Growth rate indicate unstable system. The duct before the outlet is 0.5 m long, while the ducts between sources and sinks are 0.01 m long. INLET.r and OUTLET.r are the reflection coefficients at the inlet and outlet, respectively.

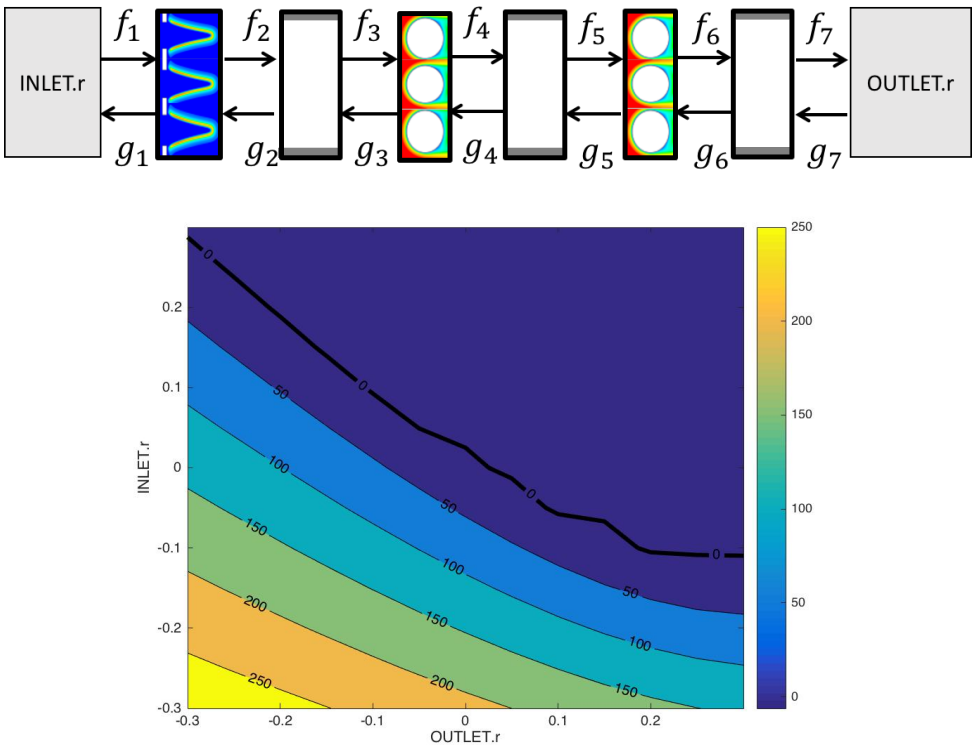

Figure 5.4: Stability map of a system featuring a ducted premixed flame and double row of heat exchanger tube as in [52]. Positive Growth rate indicate unstable system. The duct before the outlet is 0.5 m long, while the ducts between sources and sinks are 0.01 m long. INLET.r and OUTLET.r are the reflection coefficients at the inlet and outlet, respectively.

6 Outlook

In the present work, we focused on the acoustic scattering and entropy generation across moving premixed flames and fixed heat sources, such as heat exchangers. It has been found that moving sources and sources at rest have different entropy generation mechanisms. Compared to premixed flames, heat exchangers are more prone to generation of temperature inhomogeneities. From a network model perspective, such inhomogeneities should be taken into account, not only downstream of heat exchangers, but also close to the so-called "secondary entropy sources", such as non-adiabatic walls, cold flow injection (see temperature inhomogeneities due to cold flow injection in the afterburner in Fig. 6.1), cooled turbine blades or acoustic dampers. Close to these parts, the temperature field has a 2-D or 3-D distribution, which should be accounted for in the propagation of acoustic waves.

As shown in the conclusions (Sec. 5), the presence of heat exchanger tube bundles greatly influences the system stability. The effect of the cooling element cannot be determined a priori. Instead, it depends on the geometry (area blockage), temperature jump and unsteady heat transfer rate. In real systems, several tube bundles are found downstream of the flame, in order to optimize the heat exchange and the environmental restrictions on emissions temperature. A more detailed study should be carried out, in order to extend the thermoacoustic stability analysis to more complex geometries.

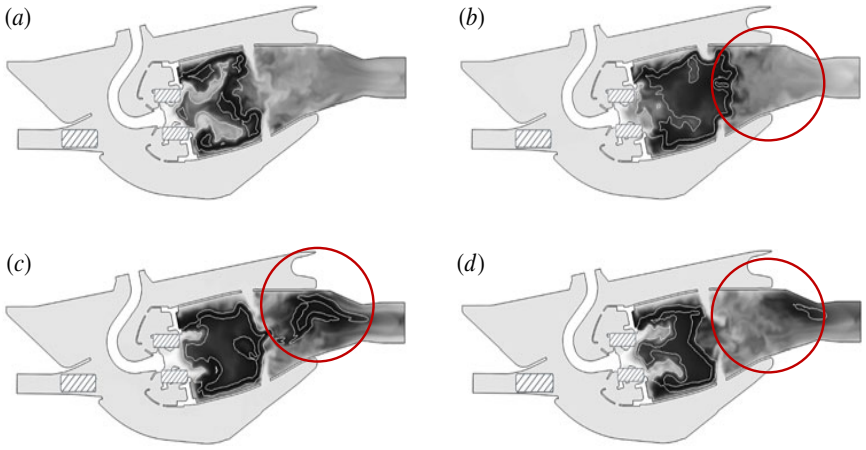

Figure 6.1: Cold flow injection downstream the combustion zone creates inhomogeneities in temperature field. [34]

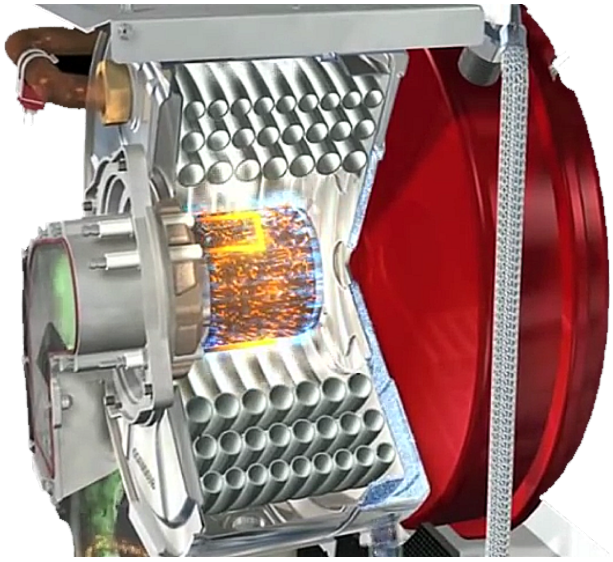

Figure 6.2: Example of real burner geometry. Image courtesy of Slant/Fin and Bekaert Combustion Technology B.V.

List of Figures

Bibliography

[1] M. Bauerheim, F. Nicoud, and T. Poinsot. Theoretical analysis of the mass balance equation through a flame at zero and non-zero Mach numbers. *Combustion and Flame*, 162: 60–67, 2014. ISSN 0010-2180. doi: 10.1016/j.combustflame.2014.06.017.

[2] P. L. Blackshear. Driving standing waves by heat addition. In *Symposium (International) on Combustion*, volume 4, pages 553–566. Elsevier, 1953.

[3] R. S. Blumenthal, P. Subramanian, R. Sujith, and W. Polifke. Novel Perspectives on the Dynamics of Premixed Flames. *Combustion and Flame*, 160:1215–1224, Mar. 2013. doi: 10.1016/j.combustflame.2013.02.005.

[4] A. Cárdenas Miranda. *Influence of Enhanced Heat Transfer in Pulsating Flow on the Damping Characteristics of Resonator Rings*. Phd thesis, TU München, 2014.

[5] A. Cárdenas Miranda and W. Polifke. Combustion Stability Analysis of Rocket Engines with Resonators Based on Nyquist Plots. *Journal of Propulsion and Power*, 30(4):962–977, 2014. doi: 10.2514/1.B35149.

[6] B. T. Chu. On the generation of pressure waves at a plane flame front. *4th Symposium on Combustion*, 1953.

[7] B. T. Chu. Stability of Systems Containing a Heat Source - The Rayleigh Criterion. Technical report, 1956.

[8] A. Dowling and G. Bloxsidge. Reheat buzz- An acoustically driven combustion instability. In *American Institute of Aeronautics and Astronautics and NASA, Aeroacoustics Conference, 9 Th, Williamsburg, VA*, page 1984, 1984.

[9] A. P. Dowling. The calculation of thermoacoustic oscillation. *J. of Sound and Vibration*, 180:557–581, 1995.

[10] A. P. Dowling and S. R. Stow. Acoustic Analysis of Gas Turbine Combustors. *Journal of Propulsion and Power*, 19(5), 2003. doi: 10.2514/2.6192.

[11] S. Ducruix, D. Durox, and S. Candel. Theoretical and Experimental Determinations of the Transfer Function of a Premixed Laminar Flame. *Proc. Comb. Inst.*, 28:765–773, 2000.

[12] J. Eckstein, E. Freitag, C. Hirsch, T. Sattelmayer, R. von der Bank, and T. Schilling. Forced Low-Frequency Spray Characteristics of a Generic Airblast Swirl Diffusion Burner. In *Proc. of ASME Turbo Expo 2003 Power for Land, Sea and Air*, GT-2003-38646, pages 1–8, Atlanta, Georgia, USA, 2003. ASME.

[13] S. Evesque and W. Polifke. Low-order acoustic modelling for annular combustors: Validation and inclusion of modal coupling. In *ASME Turbo Expo 2002: Power for Land, Sea, and Air*, pages 321–331. American Society of Mechanical Engineers, 2002.

[14] J. H. Ferziger and M. Perić. *Computational Methods for Fluid Dynamics*. Springer Berlin Heidelberg, Berlin, Heidelberg, 3 edition, 2002. ISBN 978-3-540-42074-3 978-3-642-56026-2.

[15] S. Föller and W. Polifke. Advances in Identification Techniques for Aero-Acoustic Scattering Coefficients from Large Eddy Simulation. In *18th International Congress on Sound and Vibration (ICSV18)*, Rio de Janeiro, Brazil, 2011.

[16] A. M. G. Gentemann. *Identifikation von Akustischen Transfermatrizen Und Flammenfrequenzgängen Mittels Strömungssimulation*. Phd thesis, TU-München, 2006.

[17] C. S. Goh and A. S. Morgans. The Influence of Entropy Waves on the Thermoacoustic Stability of a Model Combustor. *Combustion Science and Technology*, 2012. doi: 10.1080/00102202.2012.715828.

[18] M. A. Heckl. Active control of the noise from a Rijke tube. In *Aero-and Hydro-Acoustics*, pages 211–216. Springer, 1985.

[19] S. Hochgreb, D. Dennis, I. Ayranci, W. Bainbridge, and S. Cant. Forced and Self-Excited Instabilities From Lean Premixed, Liquid-Fuelled Aeroengine Injectors at High Pressures and Temperatures. In *ASME Turbo Expo 2013: Turbine Technical Conference and Exposition*, volume GT2013-95311, page V01BT04A023, San Antonio, Texas, USA, June 2013. ASME. doi: 10.1115/GT2013-95311.

[20] N. Hosseini, V. Kornilov, O. Teerling, I. L. Arteaga, and L. P. H. de Goey. Development of a Numerical Model for Obtaining Flame Transfer Function in a Simplified Slit Burner with Heat Exchanger. In *The 21st International Congress on Sound and Vibration*, 2014.

[21] J. Humphrey and F. Culick. Pressure oscillations and acoustic-entropy interactions in ramjet combustion chambers. in: AIAA/SAE/ASME/ASEE 23rd Joint Propulsion Conference, 1987.

[22] J. Keller, W. Egli, and J. Hellat. Thermally induced flow frequency oscillations. *J. of Appl. Math. Physics*, 1985.

[23] K. Kim and S. Hochgreb. Effects of Nonuniform Reactant Stoichiometry of Thermoacoustic Instability in a Lean-Premixed Gas Turbine Combustor. *Combust. Sci. Technol*, 184:1–21, 2012.

[24] J. Kopitz. *Kombinierte Anwendung von Strömungssimulation, Netzwerkmodellierung Und Regelungstechnik Zur Vorhersage Thermoakustischer Instabilitäten*. PhD thesis, Technical University Munich, 2007.

[25] J. Kopitz and W. Polifke. CFD-based Application of the Nyquist Criterion to Thermo-Acoustic Instabilities. *J. Comp. Phys*, 227:6754–6778, 2008. doi: doi:10.1016/j.jcp.2008.03.022.

[26] R. LeVeque. *Finite Volume Methods for Hyperbolic Problems*. Cambridge Texts in Applied Mathematics. Cambridge University Press, 2002. ISBN 978-1-139-43418-8.

[27] T. Lieuwen. Modeling premixed combustion-acoustic wave interactions: A review. *Journal of Propulsion and Power*, 19(5):765–781, 2003.

[28] L. Ljung. *System Identification*. Springer, 1998.

[29] L. Ljung. *System Identification*. Springer, 1998.

[30] C. M. Luzzato and A. S. Morgans. The effect of a laminar moving flame front on thermoacoustic oscillations of an anchored ducted V-flame. *Combustion Science and Technology*, (just-accepted), 2014.

[31] Luzzato, Charles M. *Modelling and Control of Combustion Instabilities with Anchored Laminar Ducted Flames*. Phd thesis, Imperial College, London, 2015.

[32] M. Macquisten and A. Dowling. Low-frequency combustion oscillations in a model afterburner. *Combustion and Flame*, 94(3):253–264, 1993. ISSN 0010-2180.

[33] F. Marble and S. Candel. Acoustic disturbance from gas non-uniformities convected through a nozzle. *Journal of Sound and Vibration*, Vol 55, n. 2:225–243, 1977.

[34] E. Motheau, F. Nicoud, and T. Poinsot. Mixed acoustic–entropy combustion instabilities in gas turbines. *Journal of Fluid Mechanics*, 749:542–576, 2014.

[35] M. L. Munjal. *Acoustics of Ducts and Mufflers*. John Wiley & Sons, 1987.

[36] Poinsot and D. Veynante. *Theoretical and Numerical Combustion*. Edwards, R. T. Incorporated, Philadelphia, 2 edition, 2005. ISBN 1-930217-10-2.

[37] T. Poinsot and S. Lele. Boundary Conditions for Direct Simulation of Compressible Viscous Flows. *Journal of Compuational Physics*, 101:104–129, 1992.

[38] W. Polifke. Divide et Impera – Combining CFD, system identification and system modelling to analyse thermo-acoustic combustion instabilities. In *3. NAFEMS CFD-Seminar: "Simulation Gekoppelter Strömungsvorgänge (Multifield FSI)"*, Wiesbaden, Germany, 2006. NAFEMS.

[39] W. Polifke. Low-Order Analysis Tools for Aero- and Thermo-Acoustic Instabilities. In C. Schram, editor, *Advances in Aero-Acoustics and Thermo-Acoustics*, VKI LS 2011-01. Van Karman Institute for Fluid Dynamics., Rhode-St-Genèse, Belgium, Rhode-St-Genèse, BE, 2010. ISBN 978-2-87516-012-6.

[40] W. Polifke. Black-box system identification for reduced order model construction. *Annals of Nuclear Energy*, 67:109–128, 2014.

[41] W. Polifke, J. van der Hoek, and B. Verhaar. Everything you always wanted to know about f and g. Technical report, Technical Report of ABB Corporate Research, Baden, Switzerland, 1997.

[42] W. Polifke, C. O. Paschereit, and K. Döbbeling. Constructive and Destructive Interference of Acoustic and Entropy Waves in a Premixed Combustor with a Choked Exit. *Int. J. of Acoustics and Vibration*, 6(3):1–38, 2001.

[43] W. Polifke, C. Wall, and P. Moin. Partially reflecting and non-reflecting boundary conditions for simulation of compressible viscous flow. *J. of Comp. Physics*, 213:437–449, 2006.

[44] W. J. M. Rankine. On the Thermodynamic Theory of Waves of Finite Longitudinal Disturbance. 160:277–288, Jan. 1870. doi: 10.1098/rstl.1870.0015.

[45] S. Rienstra and A. Hirschberg. An Introduction to Acoustics. Technical report, Eindhoven University of Technology, 2014.

[46] P. L. Rijke. Notiz über eine neue Art, die in einer an beiden Enden offenen Röhre enthaltene Luft in Schwingungen zu versetzen. *Annalen der Physik*, 183(6):339–343, 1859.

[47] T. Sattelmayer. Influence of the combustor aerodynamics on combustion instabilities from equivalence ratio fluctuations. *Journal of Engineering for Gas Turbines and Power(Transactions of the ASME)*, 125(1):11–19, 2003.

[48] B. Schuermans. *Modeling and Control of Thermoacoustic Instabilities*. PhD thesis, EPFL, Lausanne, 2003.

[49] B. B. H. Schuermans, W. Polifke, and C. O. Paschereit. Modeling Transfer Matrices of Premixed Flames and Comparison with Experimental Results: ASME 99-GT-132. Int. Gas Turbine & Aeroengine Congress & Exhibition, Indianapolis, Indiana, USA, 1999. ASME.

[50] C. F. Silva, T. Emmert, S. Jaensch, and W. Polifke. Numerical study on intrinsic thermoacoustic instability of a laminar premixed flame. *Combustion and Flame*, 162(9):3370 – 3378, 2015. ISSN 0010-2180. doi: 10.1016/j.combustflame.2015.06.003.

[51] S. R. Stow and A. P. Dowling. A time-domain network model for nonlinear thermoacoustic oscillations. In *ASME Turbo Expo 2008: Power for Land, Sea, and Air*, pages 539–551. American Society of Mechanical Engineers, 2008.

[52] L. Strobio Chen, N. Hosseini, W. Polifke, J. Teerling, V. Kornilov, I. Lopez Arteaga, and P. de Goey. Acoustic Scattering Behaviour of a 2D Flame with Heat Exchanger in Cross-Flow. In *23rd International Congress on Sound and Vibration (ICSV23)*, Athens, Greece, 10 – 14 July 2016. ICSV.

[53] L. Strobio Chen, A. Witte, and W. Polifke. Thermo-acoustic characterization of a heat exchanger in cross flow using compressible and weakly compressible numerical simulation. In *The 22nd International Congress of Sound and Vibration*, Florence, Italy, 12-16 July 2015.

[54] L. Strobio Chen, S. Bomberg, and W. Polifke. On the Jump Conditions for Flow Perturbations Across a Moving Heat Source. In *21st International Congress on Sound and Vibration (ICSV21)*, volume 5, pages 3902–3909, Beijing, China, July 2014. ICSV. ISBN 978-1-63439-238-9.

[55] L. Strobio Chen, S. Bomberg, and W. Polifke. Propagation and Generation of Acoustic and Entropy Waves Across a Moving Flame Front. *Comb. and Flame*, 166:170–180, Apr. 2016. doi: 10.1016/j.combustflame.2016.01.015.

[56] L. Strobio Chen, T. Steinbacher, C. Silva, and W. Polifke. On Entropy Waves Production Across a Premixed Flame. In *Proceedings of ASME 2016 Turbo Expo: Turbomachinery Technical Conference & Exposition*, GT2016-57026, Seoul, Korea, 2016. ASME.

[57] D. Wassmer, B. Schuermans, O. Paschereit, and J. Moeck. An Acoustic Time-of-Flight Approach for Unsteady Temperature Measurements: Characterization of Entropy Waves in a Model Gas Turbine Combustor. *Journal of Engineering for Gas Turbines and Power(Transactions of the ASME)*, 2016.

[58] D. Yang and A. Morgans. Helmholtz resonators for damping combustor thermoacoustics. In *22nd International Congress on Sound and Vibration (ICSV22)*, Florence, Italy, July 2015. ICSV.

Reprints of original articles

ICSV21: *On the jump conditions for flow perturbations across a moving heat source*

As required by the International Institute of Acoustics and Vibration (IIAV), which owns the reproduction rights of the papers published in the ICSV Conference Proceedings, we include the following statements for the reproduction of the ICSV papers in the present work:

The paper ICSV21: "On the jump conditions for flow perturbations across a moving heat source", by Lin Strobio Chen, Sebastian Bomberg, Wolfgang Polifke was submitted to and was presented at the 21st International Congress on Sound and Vibration (ICSV21) held in Beijing, China, from 13 to 17 July 2014. It was published in the ICSV21 Conference Proceedings under the copyright of the International Institute of Acoustics and Vibration (IIAV.)

ICSV 21
13-17 July, 2014, Beijing/China

The 21st International Congress on Sound and Vibration

13-17 July, 2014, Beijing/China

ON THE JUMP CONDITIONS FOR FLOW PERTURBATIONS ACROSS A MOVING HEAT SOURCE

Lin Strobio Chen, Sebastian Bomberg, Wolfgang Polifke

Lehrstuhl für Thermodynamik, TU München, D-85747, Garching, Germany,
e-mail: strobio@td.mw.tum.de

In linear acoustics, the acoustic scattering properties across a compact heat source are described by the well-known Rankine-Hugoniot equations. These equations relate the downstream fluctuations of pressure and velocity to upstream perturbations and fluctuations of the heat release. However, if the heat source considered is a moving premixed flame, the Rankine-Hugoniot equations can give seemingly contradictory results. The overall objective of this paper is to shed light on the apparent inconsistencies which may arise from the Rankine-Hugoniot relations in the case of moving premixed flames, by analyzing the influence of the flame front movement with respect to acoustic and entropy waves propagation across the discontinuity. In addition, two limit-cases are examined: the first case consists in a fluctuating flame front, which is purely convected by upstream velocity fluctuations; the latter is a perfectly fixed flame front. Finally, accounting for the two limit cases, the validity of the Rankine-Hugoniot equations is discussed.

1. Introduction

The modeling of acoustic scattering properties of a heat source is a fundamental step in the study of every thermoacoustic system. The interaction between a thin flame front and acoustic disturbances was first analyzed by Chu [1]. In his analysis, Chu not only tried to analytically quantify the amplification of acoustic disturbances across the flame, but also gave insight on the relation between the flame front movement and acoustics. In the linear regime, the Rankine-Hugoniot relations are a widely employed analytical model to assess results from simulations and experiments [10] [3]. These equations are derived from the linearized conservation equations for fluctuating mass, momentum and energy across the heat source. However, the Rankine-Hugoniot relations do not take explicitly into account any information concerning the unsteady position of the heat source. The objective of this paper is to investigate the influence of the dynamics of the heat source on the overall system acoustics, and to assess the validity of the Rankine-Hugoniot equations.
For this purpose, a set of equations describing the conservation of mass, momentum and energy across a temperature discontinuity is derived (Section 3); then, the influence of the heat source movement is analyzed with respect to entropy and acoustic waves (Section 4); next, a model for a quasi 1-dimensional premixed flame is taken into account as source term (Section 5); finally, with reference to the case of premixed flame, the case of a fluctuating flame front is compared against the case of a fixed flame front (Section 6).

2. Apparent contradictions in Rankine-Hugoniot relations

The Rankine-Hugoniot relations consist of a system of two equations (see derivation in [3]):

$$u_2' = u_1' + \bar{u}_1 \left(\frac{\bar{T}_2}{\bar{T}_1} - 1 \right) \left(\frac{\dot{Q}'}{\bar{\dot{Q}}} - \frac{p_1'}{\bar{p}_1} \right) + \mathcal{O}(M^2) \tag{1}$$

$$p_2' = p_1' + \mathcal{O}(M^2) \tag{2}$$

The subscript '1' denotes variables upstream and '2' denotes quantities downstream the heat source. The downstream acoustic quantities are related to the upstream fluctuations through mean flow quantities ($\bar{T}_1, \bar{T}_2, \bar{u}_1$) and heat release fluctuations ($\dot{Q}'$). Now, considering the case in which the heat release of the source is constant ($\dot{Q}' = 0$), and pointing out the fact that the pressure fluctuations ($p_1'/\bar{p}_1$) are negligible with respect to velocity fluctuations, the system reduces simply to:

$$u_2' = u_1' \tag{3}$$

$$p_2' = p_1' \tag{4}$$

This solution seems to contradict the fluctuating mass conservation equation:

$$\frac{\rho_2'}{\rho_2} + \frac{u_2'}{u_2} = \frac{\rho_1'}{\rho_1} + \frac{u_1'}{u_1}, \tag{5}$$

which suggests that downstream velocity fluctuations should be higher than upstream[1], as a result of the temperature and density discontinuity.
However, the result $u_1' = u_2'$ suggests that the discontinuity is being 'convected' by the upstream velocity fluctuations u_1'. In fact, the fluid particle, which is accelerated by the fluctuations in upstream velocity, cannot penetrate the discontinuity, in case the latter is accelerated to the same extent, as an effect of u_1'. Therefore, the velocity fluctuation u_1' associated to the flow particle cannot undergo any amplification, and the discontinuity can be regarded as an impermeable moving membrane between the cold mixture and the hot burnt gases. In view of these considerations, a formalism which accounts for the movement of the heat source is needed, so as to assess the influence of the heat source movement on the system acoustics.

3. Conservation equations across a moving heat source

3.1 Derivation

The Rankine-Hugoniot equations in thermoacoustics are essentially conservation equations expressed in integral form. The relations describe discontinuities over infinitesimally thin surfaces, such as flame fronts or shock waves, for which the integration volume tends to zero. Across a shock wave propagating with velocity u_s, the **Rankine-Hugoniot jump condition** for an arbitrary flux function $f(\phi)$ is expressed as [6]:

$$u_s \left(\boldsymbol{\phi_2} - \boldsymbol{\phi_1} \right) = \boldsymbol{f}(\phi)_2 - \boldsymbol{f}(\phi)_1, \tag{6}$$

In 1-D thermoacoustic systems, the governing equations for acoustics are the non-homogeneous Euler equations, in which viscous effects and gravity are neglected:

$$\frac{\partial \boldsymbol{\phi}}{\partial t} + \frac{\partial \boldsymbol{f}(\phi)}{\partial x} = \boldsymbol{S}, \tag{7}$$

where $\boldsymbol{\phi}$, $\boldsymbol{f}(\phi)$ and the source term vector $\boldsymbol{S}$ are of the form:

[1] the density fluctuations are negligible with respect to the velocity fluctuations

$$\boldsymbol{\phi} = \begin{pmatrix} \rho \\ \rho u \\ \rho E \end{pmatrix} \qquad \boldsymbol{f}(\phi) = \begin{pmatrix} \rho u \\ \rho u^2 + p \\ u(E+p) \end{pmatrix} \qquad \boldsymbol{S} = \begin{pmatrix} 0 \\ 0 \\ \dot{q} \end{pmatrix}. \tag{8}$$

The non-homogeneity is determined by the presence of the heat source in the energy equation. For an ideal gas, the total specific energy and enthalpy of the fluid are expressed as:

$$E = e + \frac{1}{2}u^2, \tag{9}$$

$$H = h + \frac{1}{2}u^2 = E + \frac{p}{\rho}, \tag{10}$$

$$e = c_v T = \frac{p}{(\gamma - 1)\rho}, \tag{11}$$

where $\gamma = c_p/c_v$.
Applying the jump condition (6) to the Euler equations (7), the conservation equations for mass, momentum and energy are given as follows:

$$u_s(\rho_2 - \rho_1) = \rho_2 u_2 - \rho_1 u_1, \tag{12}$$

$$u_s(\rho_2 u_2 - \rho_1 u_1) = \rho_2 u_2^2 - \rho_1 u_1^2 + p_2 - p_1, \tag{13}$$

$$u_s(\rho_2 E_2 - \rho_1 E_1) = \rho_2 u_2 H_2 - \rho_1 u_1 H_1 - \dot{Q}, \tag{14}$$

where $\dot{Q} = \int_1^2 \dot{q} dx$. Considering the eqs. (9), the energy and enthalpy of the flow can be rewritten in terms of u, p and ρ. In addition, under the hypothesis of constant specific heats, $c_{p1} = c_{p2}$, $c_{v1} = c_{v2}$ the energy equation reduces to:

$$u_s\left(\frac{p_2}{\gamma - 1} - \frac{p_1}{\gamma - 1} + \frac{1}{2}\rho_2 u_2^2 - \frac{1}{2}\rho_1 u_1^2\right) = \frac{\gamma}{\gamma - 1}u_2 p_2 - \frac{\gamma}{\gamma - 1}u_1 p_1 + \frac{1}{2}\rho_2 u_2^3 - \frac{1}{2}\rho_1 u_1^3 - \dot{Q}. \tag{15}$$

3.2 Linearization

Acoustics pertain to the small perturbations to a steady base flow. Therefore, in order to focus on acoustic conservation equations, all variables (u, p, ρ, u_s) are decomposed into a mean part, which is constant in time but spatially varying, and a fluctuating component, which is varying both in time and space:

$$u(x,t) = \bar{u}(x) + u'(x,t). \tag{16}$$

The decomposition for the heat source speed is:

$$u_s(x,t) = 0 + u_s'(x,t). \tag{17}$$

In the lab reference frame, the heat source oscillates around a fixed mean position. Thus, its mean velocity equals zero, while its oscillation is represented by u_s'. After linearization and retaining only first order fluctuating terms, the linear conservation equations for fluctuating quantities are obtained. Since the flow regimes of interest are all in low-Mach number range, only terms up to 1^{st} order in Mach number are retained in the derivation. Omitting algebraic manipulations, the equations reduce to:
Mass:

$$\rho_2' u_2 - \rho_1' u_1 + \rho_2 u_2' - \rho_1 u_1' = (\rho_2 - \rho_1)u_s', \tag{18}$$

Momentum:

$$p_2' = p_1', \tag{19}$$

Energy:

$$\frac{\gamma}{\gamma-1}(p_2'u_2 - p_1'u_1 + p_2u_2' - p_1u_1') = \dot{Q}'. \tag{20}$$

The linearized equation of state for perfect gas was taken into account during the derivation:

$$p' = \rho'\mathcal{R}T + \rho\mathcal{R}T' \tag{21}$$

It is interesting to underline the fact that, by neglecting terms of higher order in Mach number, the momentum equation simply reduces to: $\bar{p}_1 = \bar{p}_2$ (see [1]) and upstream pressure fluctuation can be considered equal to the pressure fluctuation downstream. As a consequence of this, terms depending on the heat source movement (u_s') vanish from the energy equation. Therefore, only the mass conservation equation is influenced by the movement of the heat source.

3.3 Normalized equations

In order to simplify the analysis, the eqs. (18) to (20) are non-dimensionalized by mean flow quantities. The normalized equations relate the upstream and downstream quantities only through $\lambda = \bar{T}_2/\bar{T}_1$.

Mass:

$$\frac{\rho_2'}{\bar{\rho}_2} - \frac{\rho_1'}{\bar{\rho}_1} + \frac{u_2'}{\bar{u}_2} - \frac{u_1'}{\bar{u}_1} = \frac{u_s'}{\bar{u}_1}\left(\frac{1}{\lambda} - 1\right) \tag{22}$$

Momentum:

$$\frac{p_1'}{\bar{p}_1} = \frac{p_2'}{\bar{p}_2} \tag{23}$$

Energy:

$$\frac{\dot{Q}'}{\dot{Q}} = \frac{p_1'}{\bar{p}_1} + \frac{u_2'}{\bar{u}_2}\left(\frac{\lambda}{\lambda-1}\right) - \frac{u_1'}{\bar{u}_1}\left(\frac{1}{\lambda-1}\right) \tag{24}$$

The normalized conservation equations were derived considering the normalized equation of state for perfect gases:

$$\frac{\rho_2'}{\bar{\rho}_2} + \frac{T_2'}{\bar{T}_2} = \frac{\rho_1'}{\bar{\rho}_1} + \frac{T_1'}{\bar{T}_1} \tag{25}$$

Equations (22) to (24) were first derived by Chu [1] and later by Schuermans [4]. Both employed these equations in premixed flame front modeling. However, the set of acoustic equations above can be used to describe any discontinuity in which heat transfer in involved. This is possible, provided that the extension of the heat source is much smaller than the acoustic wavelength (i.e. hypothesis of *compactness* is verified) and the heat release fluctuation is expressed in the integral form ($\dot{Q}'$), with a 'black-box' approach. Here, this formalism will be used to address the apparent inconsistency expressed by eq. (3), by shedding light on the relation amongst acoustics, heat release fluctuations and motion of the heat source.

4. Scattering and generation of acoustic and entropy waves

The equations (22) - (24) are a system of 3 equations in 3 unknowns. These unknowns consist of: acoustic fluctuations ($u_2'/\bar{u}_2, p_2'/\bar{p}_2$) and fluctuations of density $\rho_2'/\bar{\rho}_2$. Since density fluctuations are a function of both pressure and entropy oscillations [8], it is convenient to replace density with entropy fluctuations:

$$\frac{\rho'}{\bar{\rho}} = \frac{p'}{\gamma\bar{p}} - \frac{s'}{c_p}, \tag{26}$$

so as to segregate the interplay between entropy and acoustic waves across the discontinuity. The solution of the system is:

$$\begin{pmatrix} \frac{u_2'}{\bar{u}_2} \\ \frac{p_2'}{\bar{p}_2} \\ \frac{s_2'}{c_p} \end{pmatrix} = \underbrace{\begin{bmatrix} \frac{1}{\lambda} & \left(\frac{1}{\lambda}-1\right) & 0 \\ 0 & 1 & 0 \\ \left(\frac{1}{\lambda}-1\right) & \left(\frac{1}{\lambda}-1\right) & 1 \end{bmatrix}}_{\mathbf{M}} \begin{pmatrix} \frac{u_1'}{\bar{u}_1} \\ \frac{p_1'}{\bar{p}_1} \\ \frac{s_1'}{c_p} \end{pmatrix} + \underbrace{\begin{bmatrix} \left(1-\frac{1}{\lambda}\right) \\ 0 \\ \left(1-\frac{1}{\lambda}\right) \end{bmatrix}}_{\mathbf{N}} \cdot \frac{\dot{Q}'}{\bar{\dot{Q}}} + \underbrace{\begin{bmatrix} 0 \\ 0 \\ \left(1-\frac{1}{\lambda}\right) \end{bmatrix}}_{\mathbf{U}} \cdot \frac{u_s'}{\bar{u}_1} \tag{27}$$

A matrix form is used, in order to highlight the contribution of every variable to the overall flow oscillations. The matrix M contains the correlations between upstream and downstream acoustic and entropy oscillations; matrix N expresses the contribution of the heat release fluctuations to the downstream oscillations, while matrix U expresses the influence of the heat source movement.
The terms M_{11}, M_{12}, M_{21}, M_{22} represent the acoustic matrix, since they express the relation between upstream and downstream acoustic quantities exclusively. The terms M_{31} and M_{32} express the part of entropy fluctuations related to acoustics. Terms M_{13} and M_{23}, conversely, express the contribution of entropy oscillations to acoustics. However, the latter terms equal zero. Consequently, across a discontinuity, acoustics waves propagation is independent of entropy waves, while entropy fluctuations are strictly related to pressure and velocity oscillations. The term M_{33} suggests that incoming entropy fluctuations are merely convected through the discontinuity, without any amplification.
The derivation up to 1^{st} order in Mach number leads to the identity between upstream and downstream mean and fluctuating pressures. This is shown by the independence of pressure oscillations of both $\dot{Q}'$ and u_s'. On the other hand, the heat release fluctuations influence the velocity and entropy fluctuations to the same extent.
Looking at vector U, there seems to be no influence of the heat source movement on the acoustics downstream. In fact, the velocity fluctuations of the heat source seems to be influencing only the entropy fluctuations downstream. However, before drawing conclusions on the overall influence of the heat source movement on the acoustics, it is necessary to solve the 'closure problem', by relating the heat release fluctuations $\dot{Q}'$ to upstream fluctuations.

5. Quasi 1-D modeling of a perfectly premixed flame

In the present analysis, a ducted, perfectly premixed flame will be taken into account as heat source (see fig.1). The heat release per unit of flame area for a premixed flame is:

$$\dot{Q} = S_f A_f \rho_1 \phi q \tag{28}$$

where S_f is the mean flame front speed, averaged on the flame surface, $A_f(t)$ is the flame area, q is the mass specific enthalpy of the fuel and ϕ is the equivalence ratio of the mixture. Here, q and ϕ are considered constant, since the flame under analysis is *perfectly* premixed.
In the steady case, the total mass flow upstream equals the mass being burnt by the flame front. At the flame front, continuity imposes:

$$u_1 A_d = S_f A_f \tag{29}$$

where A_d is the area of the duct section. Whilst A_d is constant, the flame area change as an effect of flame stretching and wrinkling, contributing to the mass burning rate of the flame front. In quasi 1-dimensional modeling, the effects of flame area change (A_f') and flame speed fluctuations(S_f') are taken into account in one variable: S_{FB}', also called 'flame brush' speed. Given (28), the normalized heat release fluctuations is expressed as:

$$\frac{\dot{Q}'}{\bar{\dot{Q}}} = \frac{S_f'}{\bar{S}_f} + \frac{A_f'}{\bar{A}_f} + \frac{\rho_1'}{\bar{\rho}_1} = \frac{S_{FB}'}{\bar{S}_{FB}} + \frac{\rho_1'}{\bar{\rho}_1} \tag{30}$$

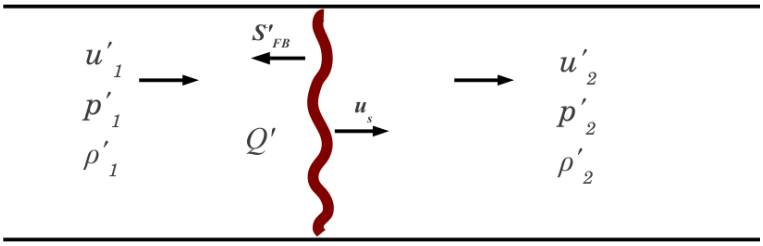

Figure 1. Quasi 1-D moving flame front

According to Chu [1], the flame front movement with respect to the fixed frame of reference is given by the so-called 'flame condition':

$$\frac{u_s'}{\bar{u}_1} = \frac{u_1'}{\bar{u}_1} - \frac{S_{FB}'}{\bar{S}_{FB}} \tag{31}$$

where $\bar{S}_{FB} = \bar{u}_1$. Eq. (31) states that the movement of the flame front in a premixed flame is non-zero when the perturbations of u_1 and S_{FB} are not equal. So, considering eq. (31) and (26), the heat release fluctuation of a perfectly premixed flame can be expressed as:

$$\frac{\dot{Q}'}{\bar{\dot{Q}}} = \frac{u_1'}{\bar{u}_1} - \frac{u_s'}{\bar{u}_1} + \frac{1}{\gamma}\frac{p_1'}{\bar{p}_1} - \frac{s_1'}{c_p} \tag{32}$$

Replacing $\frac{\dot{Q}'}{\bar{\dot{Q}}}$ in eq. (33) with eq. (32), the resulting system matrix reduces to:

$$\begin{pmatrix} \frac{u_2'}{\bar{u}_2} \\ \frac{p_2'}{\bar{p}_2} \\ \frac{s_2'}{c_p} \end{pmatrix} = \underbrace{\begin{bmatrix} 1 & \left(1-\frac{1}{\gamma}\right)\left(\frac{1}{\lambda}-1\right) & \frac{1}{\lambda}-1 \\ 0 & 1 & 0 \\ 0 & \left(1-\frac{1}{\gamma}\right)\left(\frac{1}{\lambda}-1\right) & \frac{1}{\lambda} \end{bmatrix}}_{\mathbf{M}} \begin{pmatrix} \frac{u_1'}{\bar{u}_1} \\ \frac{p_1'}{\bar{p}_1} \\ \frac{s_1'}{c_p} \end{pmatrix} + \underbrace{\begin{bmatrix} \frac{1}{\lambda}-1 \\ 0 \\ 0 \end{bmatrix}}_{\mathbf{U}} \cdot \frac{u_s'}{\bar{u}_1} \tag{33}$$

From the system matrix above, it clearly results that the flame front movement influences the acoustics of the system (see vector U). However, the influence is indirect, because the effects of the flame front movement impact on the system through the heat release fluctuations. As a consequence of this, the heat release fluctuations modeling becomes of crucial importance in characterizing the scattering properties of thermoacoustic systems, not only because it relates $\dot{Q}'$ to upstream perturbations, but also because it clarifies the relation between $\dot{Q}'$ and the motion of the heat source itself.

6. Analysis of limit cases

In this section, two limit-cases are analyzed, in order to clarify the effects of the flame front movement on velocity fluctuations. The solutions for downstream pressure and entropy will not be evaluated, since in the case of a premixed flame those quantities are not influenced by the flame front movement.

6.1 Moving flame front acoustics

The first limit case considers the hypothesis in which the flame front movement equals the upstream velocity perturbations ($\frac{u_1'}{\bar{u}_1} = \frac{u_s'}{\bar{u}_1}$). According to eq. (32), the flame model reduces to:

$$\left(\frac{\dot{Q}'}{\bar{\dot{Q}}}\right)_{moving} = \left(\frac{1}{\gamma}\frac{p_1'}{\bar{p}_1}\right) - \left(\frac{s_1'}{c_p}\right) \tag{34}$$

it follows from eq. (33) that the solution for downstream velocity fluctuations is:

$$\frac{u_2'}{\bar{u}_2} = \frac{u_1'}{\bar{u}_1}\frac{1}{\lambda} + \frac{p_1'}{\bar{p}_1}\left(1-\frac{1}{\gamma}\right)\left(\frac{1}{\lambda}-1\right) + \frac{s_1'}{c_p}\left(\frac{1}{\lambda}-1\right) \tag{35}$$

The solution (35) shows that $\frac{u_2'}{\bar{u}_2}$ is influenced by both acoustic and entropy perturbations. However, for acoustic waves, the impact of $\frac{p_1'}{\bar{p}_1}$ is much smaller than the contribution of velocity perturbations. Some considerations on the order of magnitude yield [9]:

$$\frac{p'}{\bar{p}} = \mathcal{O}\left(\gamma \bar{M}\right)\frac{u'}{\bar{u}} \qquad\qquad \frac{p'}{\bar{p}} \sim \mathcal{O}\left(\frac{\rho'}{\bar{\rho}}\right) \tag{36}$$

For low-Mach number flow regimes, the normalized pressure fluctuations are much smaller than than the velocity fluctuations. Moreover, considering the upstream flow as isentropic ($s_1' = 0$), the downstream velocity is expressed as:

$$u_2' = u_1' \tag{37}$$

The result in eq. (37) can be explained by the fact that, in the case considered, the flame front movement $\frac{u_s'}{\bar{u}_1}$ counterbalances perfectly $\frac{u_1'}{\bar{u}_1}$, so that the flame sheet is merely convected back and forth by the velocity perturbations.

6.2 Fixed flame front acoustics

The second limit-case deals with the hypothesis of a fixed flame front, i. e. $u_s' = 0$. According to eq. (32), the flame model is in this case:

$$\frac{\dot{Q}'}{\bar{\dot{Q}}} = \frac{u_1'}{\bar{u}_1} + \frac{1}{\gamma}\frac{p_1'}{\bar{p}_1} - \frac{s_1'}{c_p} \tag{38}$$

making the same considerations as in the previous case (eq. (36)), and considering the upstream flow as isentropic, the flame model reduces to:

$$\frac{\dot{Q}'}{\bar{\dot{Q}}} = \frac{u_1'}{\bar{u}_1} \tag{39}$$

which states that, for a fixed perfectly premixed flame, the normalized heat release fluctuation is mainly a function of the upstream velocity perturbation. With reference to eq. (33), the solution for downstream velocity fluctuations is:

$$u_2' = u_1'\frac{\bar{T}_2}{\bar{T}_1} \tag{40}$$

This is the solution expected if the 'naive' continuity equation were applied. In fact, the velocity fluctuations downstream exceed those upstream as an effect of the temperature jump. For the flame to be fixed, according to eq. (31), the flame brush speed should compensate the fluctuations of upstream velocity.

7. Conclusions

In the present work, some apparent contradictions arising from the Rankine-Hugoniot relations in the case of a moving heat source are considered. In order to address these inconsistencies, mass, momentum and energy conservation equations are derived for flow disturbances across a moving discontinuity. The results show a direct influence of the source movement on entropy waves downstream the discontinuity (see eq. (27)), and an indirect influence on acoustics, through heat release rate $\dot{Q}'$

(see eq. (32)). With reference to the quasi 1-D perfectly premixed flame model, two limit cases are taken into account, so as to highlight the differences in downstream acoustics between a moving and a fixed flame, *ceteris paribus*. The comparison shows that velocity fluctuations downstream are heavily influenced by the flame front movement, and that apparently not reasonable results (as $u'_1 = u'_2$) can be explained by considering the unsteady position of the flame front.
Finally, by analyzing the solution in matrix (33), it is possible to state that the Rankine-Hugoniot relations describe the acoustics across heat sources correctly, provided that the conservation equations are developed up to 1^{st} order in Mach number. In addition, both upstream perturbation and heat source dynamics have to be taken into account in the identification of the heat release fluctuations $\dot{Q}'$.

8. Acknowledgements

The presented work is part of the Marie Curie Initial Training Network Thermo-acoustic and aero-acoustic nonlinearities in green combustors with orifice structures (TANGO). We gratefully acknowledge the financial support from the European Commission under call FP7-PEOPLE-ITN-2012. Financial support for Sebastian Bomberg by the German Research Foundation DFG, project PO 710/12-1 and the Technische Universität München / Institute for Advanced Study, funded by the German Excellence Initiative, is gratefully acknowledged.

REFERENCES

[1] Chu, B. T. *On the generation of pressure waves at a plane flame front*, 4th Symp. Int. on Comb. (1953), 603-612

[2] Chu, B. T. *Mechanism of generation of pressure waves at flame fronts*, Technical Note, 1956

[3] Kopitz, J. *Kombinierte Anwendung von Strömungssimulation, Netzwerkmodellierung und Regelungstechnik zur Vorhersage thermoakustischer Instabilitaten*, PhD Thesis (2007), Technical University Munich

[4] Schuermans, B. B. H., Bellucci V., Guethe, F. and Paschereit, C. O. *A detailed analysis of thermoacoustic interaction mechanism in a turbulent premixed flame*, Proceedings of ASME Turbo Expo 2004, Power of Land, Sea, and Air, June 14-17, 2004, Vienna, Austria

[5] Schuermans, B. B. H. and Polifke, W. and Paschereit, C. O. *Modeling transfer matrices of premixed flames and comparison with experimental results*, Int'l Gas Turbine and Aeroengine Congress & Exposition, 1999, Indianapolis, Indiana, USA

[6] LeVeque, R. J. *Numerical methods for conservation laws*, 2nd ed., Basel, Birkhäuser, 1992

[7] Poinsot, T., & Veynante, D. *Theoretical and numerical combustion*, RT Edwards, Inc.

[8] Dowling, A. *The calculation of thermoacoustic oscillations*, Journal of Sound and Vibration (1995) 180(4), 557-581

[9] Dowling, A. *Nonlinear self excited oscillations of a ducted flame*, Journal of Fluid Mechanics (1997), vol. 346, 271-290

[10] Keller, J. J. *Thermoacoustic Oscillations in Combustion Chambers of Gas Turbines*, AIAA Journal (1995), vol. 33, 2280-2287

Combust. Flame 2016: ***Propagation and generation of acoustic and entropy waves across a moving flame front***

Combustion and Flame 000 (2016) 1–11

Contents lists available at ScienceDirect

Combustion and Flame

journal homepage: www.elsevier.com/locate/combustflame

Propagation and generation of acoustic and entropy waves across a moving flame front

Lin Strobio Chen*, Sebastian Bomberg, Wolfgang Polifke

Professur für Thermofluiddynamik, Technische Universität München, D-85747 Garching, Germany

ARTICLE INFO

Article history:
Received 17 April 2015
Revised 14 January 2016
Accepted 16 January 2016
Available online xxx

Keywords:
Kinematic balance
Premixed flame
Acoustic scattering
Entropy generation
Mass flow conservation
Mach number

ABSTRACT

In analytical models of the propagation and generation of acoustic and entropy waves across a premixed flame, the relations that couple upstream and downstream flow variables often consider the flame as a discontinuity at rest. This work shows how the model of a flame at rest can misrepresent the generation of entropy waves, and how it leads to paradoxical results concerning the conservation of mass and volume flow rates across the flame. Such inconsistencies can be resolved by taking into account the movement of the flame in the coupling relations for flow perturbations. Analysis in a quasi-1D framework shows that in the absence of perturbations in equivalence ratio, the magnitude of the entropy waves generated across the flame are *first order* in Mach number and derive from interactions between the upstream acoustics and the *mean* heat release rate. For non-perfectly premixed flames, fluctuations in equivalence ratio may generate perturbations in entropy of *leading order* in Mach number. Furthermore, for the moving flame model conservation of volume flow rate across a passive, perfectly premixed flame appears as a natural consequence of mass and energy conservation.

1. Introduction

In lean combustion systems, one of the major challenges to technological progress is thermo-acoustic instability. Such instabilities may be caused by fluctuations in pressure or velocity, i.e. acoustic disturbances, which impinge on the flame, causing the heat release rate to become unsteady. Fluctuations in heat release rate will in turn generate more acoustic disturbances, so that a feedback-loop is established, which may result in self-excited instability.

Acoustic perturbations at a flame can also cause so-called "entropy waves", i.e. temperature inhomogeneities in the burnt gases that are transported convectively. As Marble and Candel [1] have explained, when such inhomogeneities experience acceleration downstream of the flame (e.g. through a nozzle), acoustic waves are generated in both upstream and downstream directions from the zone of acceleration. The upstream propagating component travels back into the combustion chamber, contributing to the acoustic oscillations in the system. This mechanism can also trigger thermo-acoustic instabilities, see [2–5].

According to Rayleigh [6], instabilities in a thermo-acoustic system can occur, when thermal and acoustic disturbances interact constructively. Therefore, understanding the mechanisms of acoustic and entropy waves generation across the flame, and their propagation in the system is crucial for prediction and control of the thermo-acoustic instabilities.

To predict system instabilities, the framework of low-order network models is widely employed [5,7–13]. In this framework, a one-dimensional thermo-acoustic system is represented as a network of acoustic elements, each one characterized by its transfer matrix, which expresses the relations between the flow perturbations in velocity u', pressure p' and entropy s' upstream of the element to the perturbations downstream, see [14].

In an idealized treatment, such relations may be derived analytically from the linearized conservation equations for mass, momentum and energy. The effect of a heat source on the acoustic field may also be deduced from these conservation equations. In this case, the analysis should describe the scattering of acoustic waves by the temperature and density gradients that result from mean heat release rate $\bar{\dot{Q}}$, as well as account for the coupling between the fluctuations of heat release $\dot{Q}'$ and the acoustic perturbations.[1]

* Corresponding author. Fax: +49 8928916218.
E-mail address: strobio@tfd.mw.tum.de, linstrobiochen@gmail.com (L. Strobio Chen).

[1] Here and in the following, overbars $\bar{\ldots}$ denote mean values, while primed quantities $\ldots'$ refer to fluctuations around the mean.

http://dx.doi.org/10.1016/j.combustflame.2016.01.015
0010-2180/

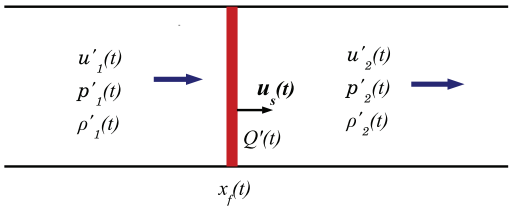

Fig. 1. A compact heat source in quasi-1D flow with flow perturbations u', p', ρ' at upstream ("1") and downstream ("2") locations, respectively. For a heat source at rest, the velocity of the heat source in the laboratory frame $u_s(t) = 0$, thus the location of the source, $\bar{x}_f$, is constant in time.

The configuration considered in the present paper is depicted in Fig. 1. The heat source is regarded as a one-dimensional discontinuity. This is appropriate if the heat source is *compact*, i.e. if both acoustic and entropy wavelengths are much larger than the axial extent of the heat source. Moreover, it is often assumed that the heat source is *fixed at position* $\bar{x}_f$. A derivation of thermo-acoustic coupling relations by analysis of the conservation laws for mass, momentum and energy as they apply for a compact heat source at rest can be found in several prior studies, see e.g., [10,15–17].

However, paradoxical conclusions may result from the thermo-acoustic coupling relations for a heat source at rest. The first contradiction concerns the production of entropy waves by a heat source. The coupling relations for a heat source at rest imply that in general unsteady heat release $\dot{Q}' \neq 0$ should result in the generation of entropy waves, i.e. $s' \neq 0$ downstream of the heat source, see [10,18,19]. However, in the case of a perfectly premixed flame with homogeneous fuel/air premixture, the presence of significant entropy waves (i.e. temperature inhomogeneities) downstream of the combustion zone is difficult to justify physically, because in the case of adiabatic and complete combustion, the temperature increase across the flame and thus also the temperature downstream of the flame should be constant.

The second issue has been raised by Bauerheim et al. [17] for the case of a passive flame ($\dot{Q}' = 0$) at rest, in the limit of vanishing mean flow Mach number. In the absence of mean flow, the energy conservation equation is reduced to conservation of volume flux, which implies that fluctuations of upstream ("1") and downstream ("2") velocities be equal, $u'_1 = u'_2$. However, this is in apparent contradiction with mass conservation, which for $M = 0$ would seem to impose $u'_1\bar{\rho}_1 = u'_2\bar{\rho}_2$. Bauerheim et al. [17] reexamined the quasi-1D conservation equations and observed that acoustic and entropy perturbations are coupled. At zero Mach number, a singularity in entropy is produced, which acts as an additional source term in the mass balance equation, which "explains why mass conservation of fluctuations is satisfied at non-zero Mach number while volume flow rate is conserved at zero Mach number" [17]. Thus the paradox is resolved, but the conclusions that result from the mathematical arguments are not easily reconciled with physical intuition.

For the two cases mentioned above, conclusions developed from linearized conservation equations for mass and energy are either apparently contradictory, or non-intuitive. This is rather unsatisfactory, since mathematical models should represent and clarify the actual physical problem. The physical meaning of the interdependency among entropy waves generation, unsteady heat release and mass flow conservation needs to be re-examined and contextualized by revisiting the coupling relations and the underlying assumptions.

In this work, it will be shown how the issues described can be resolved by relaxing the assumption that the heat source is at rest. Instead, the flame front will be considered as a moving discontinuity, which implies that movement of the heat source must be taken into account in the conservation equations. Equations which describe the propagation of small flow disturbances across a moving heat source were first derived by Chu [20,21]. Although the moving flame model has been used since in many studies, see e.g., [7,12,22–29], its consequences on acoustic scattering and generation of entropy wave have not been fully explored. The present paper will analyze these consequences, by verifying the validity of the equations with physical arguments and examples.

In Section 2, we will introduce the difference between a moving heat source and a heat source at rest and explicate some consequences of movement of the heat source. In particular, the linearized conservation equations for perturbations of velocity, pressure and entropy across a moving heat source are analyzed (Section 3). Section 4 turns to the particular case of a moving premixed flame front, with fluctuations in heat release rate, flame speed and flame surface area in response to upstream velocity perturbations. Next, the consequences of the flame front movement on entropy generation and acoustic scattering are examined for both perfectly and non-perfectly premixed flame (Sections 5 and 6). Finally, after terminology is established and the main results of this study are presented, Section 7 discusses and contextualizes previous publications on the model of a moving flame [7,12,22–29] and a flame at rest [10,15–17,30–32], respectively.

2. Motivation

In this section, we state the problems discussed in the previous section in mathematical terms and discuss some of the limitations that are implied with the application of the conservation equations of mass, momentum and energy to a heat source at rest. For the sake of simplicity, the case of a "passive source", i.e. a heat source without fluctuations of the heat release rate, $\dot{Q}' = 0$, will be considered.

In presence of perturbations, relevant variables are divided into a mean component, which varies spatially, and a fluctuating component, which in general is a function of both time and space:

$$\varphi(x,t) = \bar{\varphi}(x) + \varphi'(x,t). \tag{1}$$

For analysis of the perturbations across a compact heat source, a commonly adopted approach is to consider the linearized conservation equations just upstream and downstream of a discontinuity. The equations for conservation of mass, momentum and energy read (cf. [5,10,15–17,32,33]):

$$\begin{aligned} &[\rho'\bar{u} + u'\bar{\rho}]_1^2 = 0, \\ &[p' + \rho'\bar{u}^2 + 2\bar{\rho}\bar{u}u']_1^2 = 0, \\ &[c_p\bar{T}(\rho'\bar{u} + u'\bar{\rho}) + \bar{\rho}\bar{u}(c_pT' + \bar{u}u')]_1^2 = \dot{Q}'. \end{aligned} \tag{2}$$

Angular brackets $[\varphi]_1^2$ with sub-/super-scripts denote the difference between values of a flow variable φ upstream ("1") and downstream ("2") of the jump, i.e. $[\varphi]_1^2 = \varphi_2 - \varphi_1$. As mentioned in the previous section, the source region is considered as infinitesimally thin (i.e. compact with respect to acoustic and, in presence of mean flow, to entropy waves [10]) and fixed at position $\bar{x}_f$ in the stream-wise direction (see Fig. 1). The discontinuity is regarded as a "black-box", and its dynamic response to upstream perturbations is only represented by the source term $\dot{Q}'$.

In order to simplify the analysis, the fluctuating terms may be normalized by their respective mean values. Additionally, since flow regimes of interest are typically characterized by $M \ll 1$, terms of second or higher order in Mach number may be

Please cite this article as: L. Strobio Chen et al., Propagation and generation of acoustic and entropy waves across a moving flame front, Combustion and Flame (2016), http://dx.doi.org/10.1016/j.combustflame.2016.01.015

neglected. Therefore, Eqs. (2) reduce to [12,15,27,34]:

$$\begin{aligned}
&\frac{\rho_2'}{\bar{\rho}_2}+\frac{u_2'}{\bar{u}_2}=\frac{\rho_1'}{\bar{\rho}_1}+\frac{u_1'}{\bar{u}_1},\\
&\frac{p_2'}{\bar{p}_2}=\frac{p_1'}{\bar{p}_1}+\mathcal{O}(M^2),\\
&\frac{u_2'}{\bar{u}_2}\left(\frac{\bar{T}_2}{\bar{T}_2-\bar{T}_1}\right)=\frac{\dot{Q}'}{\bar{\dot{Q}}}+\frac{u_1'}{\bar{u}_1}\left(\frac{\bar{T}_1}{\bar{T}_2-\bar{T}_1}\right)-\frac{p_1'}{\bar{p}_1}+\mathcal{O}(M^2).
\end{aligned} \tag{3}$$

Considering the simplest case of a passive heat source ($\dot{Q}'=0$) and recalling the relation between entropy waves and fluctuations in pressure and density:

$$\frac{s'}{c_p}=\frac{p'}{\gamma\bar{p}}-\frac{\rho'}{\bar{\rho}}, \tag{4}$$

Eqs. (3) give for the entropy waves produced downstream:

$$\frac{s_2'}{c_p}=\left(\frac{\bar{T}_1}{\bar{T}_2}-1\right)\left(\frac{u_1'}{\bar{u}_1}+\frac{p_1'}{\bar{p}_1}\right)+\frac{s_1'}{c_p}+\mathcal{O}(M^2). \tag{5}$$

Now, assuming that the upstream flow is isentropic $s_1'=0$, and considering that for linear perturbations and small Mach numbers pressure fluctuations are negligible compared to velocity fluctuations,

$$\frac{p_1'}{\bar{p}_1}=\mathcal{O}(\gamma M)\frac{u_1'}{\bar{u}_1}\ll\frac{u_1'}{\bar{u}_1}, \tag{6}$$

it is reasonable to state that entropy production across the passive source is mainly due to the velocity perturbations:

$$\frac{s_2'}{c_p}\approx\left(\frac{\bar{T}_1}{\bar{T}_2}-1\right)\frac{u_1'}{\bar{u}_1}. \tag{7}$$

Such dependency is easily explained for a compact heater. In fact, in presence of constant total heat transfer rate ($\dot{Q}=\dot{m}c_p\Delta T=const$), as the mass flow rate through the heater changes, the specific enthalpy jump will also change, generating temperature fluctuations. This is confirmed by Eq. (7), which shows that in response to a positive fluctuation in velocity u_1' (i.e. to an increase in mass flow), a drop in downstream specific entropy s_2' must take place.

However, for the case of a *perfectly premixed* flame, where the equivalence ratio is constant and cannot be affected by flow perturbations, the dependency expressed in Eq. (7) seems unphysical. In fact, in this case, the specific enthalpy jump is constant by definition and does not depend on the changes in mass flow rate.

Why do the coupling relations in Eqs. (2) and (3) fail to represent the physics of a perfectly premixed flame? The answer was given by Chu (see [21]), who pointed out that, acoustically speaking, the "chief difference between a flame and a heater" lies in the fact that the flame front has a dynamic behavior and can move from its mean position in response to upstream perturbations. Such movement, however, is not known a priori and is related to the local flame speed, "whereas for a heater, such movement is assumed to be given".

Indeed, the flame is not a fixed discontinuity, but can move, wrinkle or stretch in response to velocity perturbations. The presence of a moving discontinuity, instead of one at rest, impacts directly on the acoustic scattering and entropy generation across the heat source.

In fact, in presence of a moving discontinuity, the instantaneous mass flow crossing the flame front does no longer depend exclusively on the incoming flow conditions (ρ_1, u_1), but also on the unsteady movement of the flame front itself. Considering a quasi-1D configuration – see Fig. 1 – the instantaneous mass flow crossing the discontinuity becomes:

$$\dot{m}(t)=(u_1(t)-u_s(t))\rho_1(t), \tag{8}$$

where $u_s(t)$ is the velocity of the flame front in the laboratory frame of reference, determined by kinematic balance between flame propagation and convection. This balance may be disturbed by flow perturbations, resulting in $u_s'(t)\neq 0$. Eq. (8) shows that, depending on the response of the flame to acoustics in terms of $u_s(t)$, very different results for the mass conservation equation may be obtained.

Furthermore, mass-specific entropy s is – just like temperature T – an intensive quantity, related to the total heat release $\dot{Q}(t)$ through the mass consumption at the flame front. Therefore, entropy and temperature fluctuations downstream of the flame can be correctly predicted *if and only if* the fluctuations in mass consumption are also quantified correctly.

The second issue mentioned in the introduction concerns the specific case of combustion in the limiting case of zero Mach number [17]. In absence of mean flow, $M=0$, Eqs. (2) for a passive flame $\dot{Q}'=0$ are simplified to:

$$\bar{\rho}_1u_1'=\bar{\rho}_2u_2', \tag{9}$$

$$p_1'=p_2', \tag{10}$$

$$\bar{T}_1\bar{\rho}_1u_1'=\bar{T}_2\bar{\rho}_2u_2'. \tag{11}$$

At zero Mach, the combustion is perfectly isobaric, $p_1=p_2$. With the ideal gas law, $\rho_1T_1=\rho_2T_2$. It follows that the energy conservation Eq. (11) is reduced to

$$u_1'=u_2', \tag{12}$$

which may be interpreted as conservation of volume flow rate (per duct cross-sectional area) across the flame.

The validity of volume flow rate conservation at zero Mach is in agreement with the results of many thermoacoustic studies. It can be easily verified with the linearized Rankine–Hugoniot equations (see [2,15,34]):

$$\begin{aligned}
&u_2'=u_1'+\bar{u}_1\left(\frac{\bar{T}_2}{\bar{T}_1}-1\right)\left(\frac{\dot{Q}'}{\bar{\dot{Q}}}-\frac{p_1'}{\bar{p}_1}\right)+\mathcal{O}(M^2),\\
&p_2'=p_1'+\mathcal{O}(M^2).
\end{aligned} \tag{13}$$

With reference to Eq. (13), in absence of mean flow, the upstream and downstream velocity perturbations coincide; thus agreement with Eq. (12) is established.

However, the result in Eq. (12) does not agree with the mass conservation expressed by Eq. (9), which implies that the velocity fluctuations are amplified across the flame front as an effect of the temperature jump. Bauerheim et al. [17] proved the consistency of volume flow conservation at $M=0$ with mass flow conservation at $M\neq 0$. In their analysis, the entropy wave source terms were crucial to the solution of the problem. However, as mentioned previously, the generation of entropy waves downstream a premixed flame front should be a function of the enthalpy of the premixture, and, in principle, independent from mass flow conservation. Is there a solution to the inconsistency between volume and mass flow at $M=0$, which does not depend on entropy generation, in the specific case of a premixed flame?

Although the question of mass vs. volume flow rate conservation might seem to be completely unrelated to the problem of generation of entropy waves, we argue that its resolution can be found in the flame front movement as well. In fact, Eq. (9) expresses the continuity equation across a heat source at rest, while the shape and position of a flame front are usually not fixed, as mentioned

Please cite this article as: L. Strobio Chen et al., Propagation and generation of acoustic and entropy waves across a moving flame front, Combustion and Flame (2016), http://dx.doi.org/10.1016/j.combustflame.2016.01.015

previously (see Eq. (8)). Therefore, the mass conservation equation should be formulated for the case of a *moving* heat source. This formulation allows for the decoupling of entropy generation from the mass conservation equation, in the case of a moving flame front. Moreover, we shall demonstrate (see Chapter 6) that the condition expressed by Eq. (12) indeed implies for a passive flame that the flame front is moved back and forth by the velocity perturbations (see Fig. 1), such that the velocity u_s' of the discontinuity itself equals the fluctuations in velocity u_1', which in turn equal the downstream fluctuations u_2'.

The considerations presented for the two cases suggests that the flame front movement should be taken into account when analyzing the coupling of acoustic waves across a flame front and the generation of entropy waves by the flame. The next section will review the formalism introduced by Chu [20,21] to analyze the perturbations across a moving premixed flame front. The analysis is extended up to 1st order in Mach.

3. Coupling relations for acoustics and entropy across a moving heat source

3.1. Derivation

In gas dynamics, the Rankine–Hugoniot conditions express the relation between the flow variables upstream and downstream of an infinitesimally thin discontinuity, typically a shock wave. Across a moving shock wave that is propagating with velocity u_s, the Rankine–Hugoniot conditions for the vector $\boldsymbol{\varphi}$ of flow variables are expressed as (see [35]):

$$u_s(\varphi_2 - \varphi_1) = f(\varphi)_2 - f(\varphi)_1. \tag{14}$$

In a system of conservation equations associated to the vector $\boldsymbol{\varphi}$, $\boldsymbol{f}(\varphi)$ is the vector of flux functions of the conserved variables.

In the present study the Rankine–Hugoniot conditions for a moving discontinuity will be applied to a plane, infinitesimally thin heat source in one dimensional flow, see Fig. 1. For the moment, we make no further assumptions on the nature of the heat source. The application that we have in mind is, of course, a compact premixed flame in a quasi-1D flow configuration. Pertinent consequences for the acoustic/entropy coupling relations will be explored in the next section.

The relevant governing equations are the non-homogeneous Euler equations:

$$\frac{\partial \boldsymbol{\varphi}}{\partial t} + \frac{\partial \boldsymbol{f}(\varphi)}{\partial x} = \boldsymbol{S}, \tag{15}$$

where $\boldsymbol{\varphi}, \boldsymbol{f}(\varphi)$ and the source term $\boldsymbol{S}$ are of the form:

$$\boldsymbol{\varphi} = \begin{pmatrix} \rho \\ \rho u \\ \rho E \end{pmatrix}, \quad \boldsymbol{f}(\varphi) = \begin{pmatrix} \rho u \\ \rho u^2 + p \\ u(E+p) \end{pmatrix}, \quad \boldsymbol{S} = \begin{pmatrix} 0 \\ 0 \\ \dot{q} \end{pmatrix}. \tag{16}$$

The conserved flow variables are mass, momentum and energy, while the inhomogeneity of the equations is due to the heat source term in the energy equation.

Applying the jump condition in Eq. (14) to the variables in Eq. (16), the conservation equations across a moving heat source (first presented by Chu [21]) read:

$$\rho_2 u_2 - \rho_1 u_1 = u_s(\rho_2 - \rho_1), \tag{17}$$

$$\rho_2 u_2^2 - \rho_1 u_1^2 + p_2 - p_1 = u_s(\rho_2 u_2 - \rho_1 u_1), \tag{18}$$

$$\rho_2 u_2 H_2 - \rho_1 u_1 H_1 - \dot{Q} = u_s(\rho_2 E_2 - \rho_1 E_1), \tag{19}$$

As already mentioned, $u_s(t)$ is the velocity of the heat source in the laboratory frame of reference. As an extension of the original formulation in [35], which is frequently used in gas dynamics, here we have included a source term in the energy equation, $\dot{Q}$, which is the total heat release rate per cross-sectional area, $\dot{Q} = \int_{\bar{x}_f^-}^{\bar{x}_f^+} \dot{q}\, dx$. Recalling the relations between the total energy E and total enthalpy H for an ideal gas:

$$H = h + \frac{1}{2}|u|^2 = e + \frac{p}{\rho} + \frac{1}{2}|u|^2 = E + \frac{p}{\rho}, \tag{20}$$

$$\rho e = \frac{p}{\gamma - 1}, \tag{21}$$

and under the hypothesis of constant γ and c_p, it is possible to reformulate the energy conservation Eq. (19) in terms of primitive variables ρ, u and p:

$$\frac{\gamma}{\gamma-1}(u_2 p_2 - u_1 p_1) + \frac{1}{2}\left(\rho_2 u_2^3 - \rho_1 u_1^3\right) - \dot{Q} = u_s\left(\frac{1}{\gamma-1}(p_2 - p_1) + \frac{1}{2}\left(\rho_2 u_2^2 - \rho_1 u_1^2\right)\right). \tag{22}$$

Assuming flow in the low Mach regime, terms of second or higher order in Mach are neglected. This is appropriate for many combustion systems, as discussed below. The conservation equations reduce to (see [20,27]):

$$[\rho u]_1^2 - u_s[\rho]_1^2 = 0, \tag{23}$$

$$[p]_1^2 = \mathcal{O}(M^2), \tag{24}$$

$$\frac{\gamma}{\gamma-1}[up]_1^2 = \dot{Q} + \mathcal{O}(M^2). \tag{25}$$

3.2. Linearized, non-dimensional conservation equations

In the present analysis, we consider a thin planar heat source oscillating around a fixed mean position $\bar{x}_f$, see Fig. 1. The decomposition for $u_s(t)$ is thus:

$$u_s(t) = 0 + u_s'(t). \tag{26}$$

The equations for the mean quantities developed up to $\mathcal{O}(M^2)$ are:

$$[\bar{\rho}\bar{u}]_1^2 = 0, \tag{27}$$

$$[\bar{p}]_1^2 = \mathcal{O}(M^2), \tag{28}$$

$$\frac{\gamma}{\gamma-1}[\bar{u}\bar{p}]_1^2 = \bar{\dot{Q}} + \mathcal{O}(M^2). \tag{29}$$

Subtracting Eqs. (27)–(29) from Eqs. (23)–(25), the conservation equations for perturbation quantities are obtained. Retaining only the fluctuations of first order and normalizing by the corresponding mean quantities yields for mass:

$$\frac{\rho_2'}{\bar{\rho}_2} - \frac{\rho_1'}{\bar{\rho}_1} + \frac{u_2'}{\bar{u}_2} - \frac{u_1'}{\bar{u}_1} = \frac{u_s'}{\bar{u}_1}\left(\frac{1}{\lambda} - 1\right), \tag{30}$$

momentum:

$$\frac{p_1'}{\bar{p}_1} = \frac{p_2'}{\bar{p}_2} + \mathcal{O}(M^2), \tag{31}$$

and energy:

$$\frac{\dot{Q}'}{\bar{\dot{Q}}} = \frac{p_1'}{\bar{p}_1} + \frac{u_2'}{\bar{u}_2}\left(\frac{\lambda}{\lambda-1}\right) - \frac{u_1'}{\bar{u}_1}\left(\frac{1}{\lambda-1}\right) + \mathcal{O}(M^2), \tag{32}$$

Please cite this article as: L. Strobio Chen et al., Propagation and generation of acoustic and entropy waves across a moving flame front, Combustion and Flame (2016), http://dx.doi.org/10.1016/j.combustflame.2016.01.015

where $\lambda \equiv \bar{T}_2/\bar{T}_1$ is the ratio between downstream and upstream mean temperatures. The normalized conservation equations were derived considering the normalized equation of state for perfect gases:

$$\frac{\rho_2'}{\bar{\rho}_2} + \frac{T_2'}{\bar{T}_2} = \frac{\rho_1'}{\bar{\rho}_1} + \frac{T_1'}{\bar{T}_1}. \tag{33}$$

Eqs. (30)–(32) are formulated for the case $\bar{M}_1 \neq 0$. In absence of mean flow, the linearized conservation equations cannot be expressed in the non-dimensional form $(u_2'/\bar{u}_2, p_2'/\bar{p}_2, \rho_2'/\bar{\rho}_2)$, but in terms of absolute fluctuating quantities (u_2', p_2', ρ_2').

3.3. Scattering and generation of acoustic and entropy waves

Eqs. (30)–(32) are a system of three equations in three unknowns. Two of them, u_2' and p_2', are acoustic quantities, while the third, ρ_2', is a function of both acoustic and entropy fluctuations, see Eq. (4). By substituting the density fluctuations it is possible to separate the acoustic scattering, i.e. the transmission and reflection of acoustic waves, from entropy generation. Omitting the algebraic manipulations and neglecting terms of 2*nd* order and higher order in Mach number, Eqs. (30)–(32) are re-written in terms of acoustic and entropy perturbations as follows:

$$\begin{pmatrix} \frac{u_2'}{\bar{u}_2} \\ \frac{p_2'}{\bar{p}_2} \\ \frac{s_2'}{c_p} \end{pmatrix} = \underbrace{\begin{bmatrix} \frac{1}{\lambda} & \left(\frac{1}{\lambda}-1\right) & 0 \\ 0 & 1 & 0 \\ \left(\frac{1}{\lambda}-1\right) & \left(\frac{1}{\lambda}-1\right) & 1 \end{bmatrix}}_{\mathbf{M}} \begin{pmatrix} \frac{u_1'}{\bar{u}_1} \\ \frac{p_1'}{\bar{p}_1} \\ \frac{s_1'}{c_p} \end{pmatrix} + \underbrace{\begin{bmatrix} \left(1-\frac{1}{\lambda}\right) \\ 0 \\ \left(1-\frac{1}{\lambda}\right) \end{bmatrix}}_{\mathbf{N}} \frac{\dot{Q}'}{\bar{\dot{Q}}} + \underbrace{\begin{bmatrix} 0 \\ 0 \\ \left(1-\frac{1}{\lambda}\right) \end{bmatrix}}_{\mathbf{U}} \frac{u_s'}{\bar{u}_1} \tag{34}$$

The matrix **M** and the vectors **N** and **U** express the respective influence of upstream perturbations, fluctuations of heat release rate and velocity of the heat source on the downstream perturbations.

The terms M_{11} , M_{12}, M_{21} and M_{22} represent the acoustic transfer matrix, since they relate exclusively acoustic fluctuations p', u' at upstream and downstream positions to each other. The matrix coefficients M_{21} and M_{22} show that the pressure does not exhibit a discontinuity at the heat source. This is a direct consequence of the low Mach number approximation, valid up to first order in Mach number (M).

The matrix coefficients M_{31} and M_{32} will be non-zero if the mean heat release rate is non-zero, such that $T_2 \neq T_1$ and thus $\lambda \neq 1$. In this case, entropy is coupled to the acoustics, i.e. upstream acoustic fluctuations can generate downstream entropy waves. Conversely, the scattering of acoustic waves is independent from upstream entropy perturbations, as $M_{13} = M_{23} = 0$.

The vector **U** shows that the immediate influence of heat source movement is restricted to the production of entropy waves. Such a results is very interesting, since it confirms the idea expressed above (see Section 2) that flame front movement plays a fundamental role in the correct prediction of entropy generation across a premixed flame.

On the other hand, it appears that there is no direct influence of the velocity u_s' on the acoustic coupling relations (see U_1 and U_2). This suggests that the Rankine–Hugoniot relations (13) derived from the conservation equations for a generic heat source at rest (see e.g., [2,5,12,15,34]) are also valid for the case of a moving heat source, at least for perturbations up to first order in Mach number. However, before drawing conclusions on the *absolute* independence of the acoustic coupling relations from flame front movement, it is necessary to take into account interdependencies between fluctuations of the rate of heat release and the velocity of a heat source that result from its physical nature. Such interdependencies or constraints will be different for a heater, or a premixed flame, or a non-premixed flame, say, and need to be taken into account when trying to achieve closure for the system of Eqs. (34) by relating the heat release fluctuations to the upstream perturbations, $\dot{Q}' = \dot{Q}'(p_1', u_1', s_1')$. This will be done in the next section for the case of a premixed flame in a quasi-1D flow configuration.

4. Coupling relations for acoustics and entropy across a moving premixed flame

The thermoacoustic closure problem referred to at the end of the previous section is usually concerned with the quantification of heat release fluctuation $\dot{Q}'$ in response to acoustic perturbations. This may be achieved, e.g., by determining a flame transfer function [12,36–39]. In the present paper, we pursue a different goal and concentrate on the interdependencies between flame speed, flame movement, flame surface area and heat release rate that result from the "physics" of the particular flame configuration at hand. This allows to describe and analyze the role of flame movement in acoustic scattering and entropy generation at a premixed flame. The analysis is carried out in a quasi-1D framework.

4.1. Kinematic balance at a premixed flame front

For a ducted premixed flame one may define a specific (per duct cross-sectional area, units m/s) rate of volume consumption,

$$\dot{V} \equiv \frac{1}{A_d}\int_{A_f} S_f \, dA = \frac{S_f A_f}{A_d}, \tag{35}$$

where A_d is the cross-sectional area of the duct, which is assumed constant, S_f the flame speed and A_f the flame surface area. The second identity holds if the flame speed S_f is constant along the surface of the flame, which is assumed in the following without essential loss of generality.

The following kinematic condition links the velocity u_1 of premixture upstream of the flame with the velocity u_s of the flame in the laboratory frame and the volume consumption rate $\dot{V}$:

$$u_1(t) = \dot{V}(t) + u_s(t). \tag{36}$$

For an anchored flame in steady state, kinematic balance between flow and flame propagation implies (see also Fig. 1)

$$\bar{u}_1 = \bar{\dot{V}}, \tag{37}$$

with $\bar{u}_s = 0$. On the other hand, if the flow is perturbed, the flame will respond with changes in shape and position, such that

$$u_1'(t) = \dot{V}'(t) + u_s'(t). \tag{38}$$

Evidently, the volume consumption rate $\dot{V}$ may be interpreted as an *effective flame speed*, akin to the *flame brush speed* in turbulent combustion modelling, which describes summarily the effect of flame shape on the consumption rate of premixture: elongated or wrinkled flames have a flame surface area A_f larger than the duct cross-sectional area A_d and thus consume more premixture than flat flames.

4.2. Heat release and volume consumption for a premixed flame

In a premixed flame, heat release takes place when premixture is consumed at the flame front. It follows that the heat release rate for a lean premixed flame may be expressed in terms of the volume consumption rate $\dot{V}$ as follows:

$$\dot{Q} = \rho_1 \dot{V} \phi \, q, \tag{39}$$

Please cite this article as: L. Strobio Chen et al., Propagation and generation of acoustic and entropy waves across a moving flame front, Combustion and Flame (2016), http://dx.doi.org/10.1016/j.combustflame.2016.01.015

where $\dot{Q}$ is the heat release rate per cross-sectional area of the duct (units W/m^2), ϕ the equivalence ratio of the premixture (which equals unity for stoichiometric conditions) and q the mass specific enthalpy of the premixture in stoichiometric conditions (units J/kg).

For small perturbations, one formulates

$$\frac{\dot{Q}'}{\bar{\dot{Q}}} = \frac{\rho_1'}{\bar{\rho}_1} + \frac{\dot{V}'}{\bar{\dot{V}}} + \frac{\phi'}{\bar{\phi}}. \tag{40}$$

Combining expression (40) with the kinematic conditions Eqs. (36), (38) and (4), which relates perturbations in density to those of pressure and entropy, gives the following expression for the heat release fluctuations of a premixed flame:

$$\frac{\dot{Q}'}{\bar{\dot{Q}}} = \frac{u_1'}{\bar{u}_1} - \frac{u_s'}{\bar{u}_1} + \frac{\phi'}{\bar{\phi}} + \frac{1}{\gamma}\frac{p_1'}{\bar{p}_1} - \frac{s_1'}{c_p}. \tag{41}$$

How to interpret this result? It is obviously not an alternative formulation of the energy balance Eq. (32) across a compact heat source, as it does not involve any downstream quantities (index "2"). Also, it should not be interpreted as a flame transfer function. Premixed flames respond predominantly to perturbations of upstream flow velocity, $\dot{Q}' \sim F_u(u')$, or equivalence ratio, $\dot{Q}' \sim F_\phi(\phi')$. The corresponding flame transfer functions F_u and F_ϕ (see Huber and Polifke [40]) depend in a non-trivial manner on detailed flow-flame interactions, which are not the subject of the present study. Instead, Eq. (41) should be regarded as an expression of interdependencies among flow perturbations, flame movement and rate of heat release. These constraints result from the physical effects that govern a lean, premixed flame front, see Eqs. (36) and (39).

In the previous section, we have presented a general expression of the coupling relations for mass, momentum and energy across a compact, moving heat source, i.e. Eq. (34). The corresponding relations for the specific case of a premixed flame are obtained by substituting the result (41) for relative fluctuations in heat release $\dot{Q}'/\bar{\dot{Q}}$ in Eq. (34), resulting in:

$$\begin{pmatrix} \frac{u_2'}{\bar{u}_2} \\ \frac{p_2'}{\bar{p}_2} \\ \frac{s_2'}{c_p} \end{pmatrix} = \underbrace{\begin{bmatrix} 1 & \left(1-\frac{1}{\gamma}\right)\left(\frac{1}{\lambda}-1\right) & \frac{1}{\lambda}-1 \\ 0 & 1 & 0 \\ 0 & \left(1-\frac{1}{\gamma}\right)\left(\frac{1}{\lambda}-1\right) & \frac{1}{\lambda} \end{bmatrix}}_{\mathbf{M}} \begin{pmatrix} \frac{u_1'}{\bar{u}_1} \\ \frac{p_1'}{\bar{p}_1} \\ \frac{s_1'}{c_p} \end{pmatrix} + \underbrace{\begin{bmatrix} \left(1-\frac{1}{\lambda}\right) \\ 0 \\ \left(1-\frac{1}{\lambda}\right) \end{bmatrix}}_{\mathbf{F}} \frac{\phi'}{\bar{\phi}} + \underbrace{\begin{bmatrix} \frac{1}{\lambda}-1 \\ 0 \\ 0 \end{bmatrix}}_{\mathbf{U}} \frac{u_s'}{\bar{u}_1} \tag{42}$$

Here we have chosen to represent the interactions in terms of three groups of key variables: upstream flow perturbations u_1', p_1', s_1', equivalence ratio perturbations ϕ' and flame movement u_s'.

Note that upstream entropy fluctuations are often negligible, $s_1' \to 0$. Also, it was shown in Section 2 that the pressure term $p_1'/(\gamma\bar{p}_1)$ in Eq. (41) is of first order in Mach number. On the other hand, as mentioned above, there is no a priori justification for assuming that the order of magnitude of the flame front movement u_s' is small, since it depends in a non-trivial manner on the response of the flame to acoustic perturbations. Similarly, equivalence ratio perturbation are in general a leading order term in Eq. (41), as they result from fluctuations in air and fuel flow rates [12,29]. It is worth noting that in the present quasi 1-D analysis we only consider fluctuations in time and not in space, and that therefore fuel inhomogeneities in the normal direction are not accounted for.

For the special case of a perfectly premixed flame, where fluctuations of equivalence ratio are absent, at low-Mach number and for isentropic upstream conditions, Eq. (41) reduces to:

$$\frac{\dot{Q}'}{\bar{\dot{Q}}} = \frac{u_1'}{\bar{u}_1} - \frac{u_s'}{\bar{u}_1} + \mathcal{O}(M) \tag{43}$$

Correspondingly, the 2nd term on the r.h.s. of Eq. (42) drops out and we see that in this case the downstream flow perturbations (u_2', p_2', s_2') are determined entirely by upstream flow perturbations (u_1', p_1', s_1') and flame movement u_s'.

It should be noted that, even for $\phi' = 0$, the system described in Eq. (42) is still under-determined. In fact, the kinematic response of the flame front u_s' to upstream velocity perturbations is not known a priori. However, according to Eq. (43), such closure problem can be solved, with good approximation, by quantifying the heat release rate response to upstream perturbations in velocity, i.e. by determining the flame transfer function F_u [40] of the perfectly premixed flame.

4.3. Kinematic balance in time and frequency domains

Re-writing the kinematic balance Eq. (38) as

$$u_s'(t) = u_1'(t) - \dot{V}'(t) \tag{44}$$

it becomes evident that the position of the flame front is subject two competing effects: on the one hand, perturbations in the oncoming flow $u_1' > 0$ convect the flame front downstream. On the other hand, perturbations in volume consumption rate $\dot{V}' > 0$ cause the flame front to propagate in the upstream direction.

This additional constraint was combined with Eq. (40) to derive Eq. (42) from (34) by elimination of the heat release $\dot{Q}'$. Alternatively, the equations may be written in terms of heat release $\dot{Q}'$ instead of flame front velocity in the laboratory frame u_s'. Fundamentally, both descriptions are equivalent – but in the present context, the formulation that makes explicit use of the flame velocity u_s' is more convenient. Either way, the system of equations is not closed and a suitable closure model that relates either $\dot{Q}'$ or u_s' to flow perturbations is needed.

Frequently, equations are transformed to the frequency domain and closure is achieved by relating the heat release $\dot{Q}'$ to upstream velocity perturbations u_1' via a flame transfer function $F_u(\omega)$ [38,39]. If one formulates the governing equations with u_s' instead of $\dot{Q}'$, see Eq. (42), a "flame velocity transfer function" $G_u(\omega)$ is required, such that

$$\frac{u_s'}{\bar{u}_1} = G_u(\omega)\frac{u_1'}{\bar{u}_1}. \tag{45}$$

Such a velocity transfer function $G_u(\omega)$ allows to develop interesting conclusions on the relation between heat release rate and the movement of a perfectly premixed flame. Under the assumptions made in the previous section, the expression for the heat release rate Eq. (43) implies that

$$F_u(\omega) = 1 - G_u(\omega). \tag{46}$$

Consequently, at the low frequency limit $\omega \to 0$, where the transfer function for the heat release rate F_u of a perfectly premixed flame approaches unity [41], G_u vanishes and the flame front must remain at rest. Indeed, in this quasi-stationary limit any non-zero flame front velocity $u_s' \neq 0$ would imply flash back or extinction.

On the other hand, the typical low-pass character of premixed flames causes the gain of $|F_u|$ to vanish at high frequencies, indicating that the motion of the flame front is dominated by rapid convective displacement by impinging velocity perturbations. The comparatively slow processes modulating the volume consumption rate, on the other hand, have negligible influence at high frequencies.

Please cite this article as: L. Strobio Chen et al., Propagation and generation of acoustic and entropy waves across a moving flame front, Combustion and Flame (2016), http://dx.doi.org/10.1016/j.combustflame.2016.01.015

In the next two sections, we shall discuss further consequences of the interdependencies between flow and flame perturbations. In particular, the implications of Eqs. (41) and (43) for the generation of entropy waves and the scattering of acoustic waves at a premixed flame will be analyzed in detail.

5. Generation of entropy waves at a premixed flame

In the previous section, coupling relations for flow perturbations across a compact, moving premixed flame have been obtained. Consequences for the generation of entropy waves due to acoustic-flame interactions will be discussed in the following. Both perfectly as well as non-perfectly premixed flames will be considered. The analysis concentrates on the *generation* of entropy waves, thus it will be assumed in the following that there are no perturbations of entropy upstream of the flame ($s_1' = 0$).

In the literature on low-order modeling of flow-flame interactions it has been stated repeatedly (see e.g., [10,18]) that the leading order term in downstream entropy fluctuation is different from zero whenever the normalized fluctuations in heat release rate do not equal the fluctuations in upstream velocity:

$$\frac{s_2'}{c_p} \neq 0 \qquad \Leftrightarrow \qquad \frac{\dot{Q}'}{\bar{\dot{Q}}} \neq \frac{u_1'}{\bar{u}_1}. \tag{47}$$

This result indeed is inevitable if the flame is considered as a heat source at rest, its paradoxical consequences for the prediction of downstream entropy have been discussed in the Introduction.

On the other hand, according to Eq. (42), which describes a flame that may change its position in response to flow perturbations, downstream entropy perturbations evaluate to

$$\frac{s_2'}{c_p} = \underbrace{\left(1-\frac{1}{\lambda}\right)\frac{\phi'}{\bar{\phi}}}_{\mathcal{O}(1)} + \underbrace{\left(1-\frac{1}{\gamma}\right)\left(\frac{1}{\lambda}-1\right)\frac{p_1'}{\bar{p}_1}}_{\mathcal{O}(M)} + \underbrace{\frac{s_1'}{c_p}}_{0}. \tag{48}$$

The last term on the r.h.s. is zero by assumption (see above). The second term, which results from an interaction of acoustic perturbations with the mean temperature jump, is of first order in Mach number. A detailed analysis of this mechanism of entropy wave generation is given in the Appendix of this paper. The only term on the r.h.s. of Eq. (48) that is not negligible at vanishing Mach number is the first term, which describes the result of equivalence ratio fluctuations.

Eq. (48) may be written as follows:

$$s_2' = c_p\left(1-\frac{T_c}{T_h}\right)\frac{\phi'}{\bar{\phi}} + \mathcal{O}(M). \tag{49}$$

The interpretation of this result, which was already developed by Keller [34] and Polifke et al. [5], is rather straightforward: inhomogeneities in the fuel concentration of the premixture modulate the specific heat of combustion and thus result in fluctuations of downstream temperature and density.

For a *perfectly* premixed flame $\phi' = 0$ and $s_2' = \mathcal{O}(M)$, i.e. leading order entropy waves cannot be generated by this type of flame. This does not imply – as Eq. (47) for a flame at rest would suggest – that fluctuations of velocity cause a proportional and immediate perturbation of the heat release rate. Instead, referring to Eq. (40), we find that for a perfectly premixed moving flame

$$\frac{\dot{Q}'}{\bar{\dot{Q}}} = \frac{\dot{V}'}{\bar{\dot{V}}} + \mathcal{O}(M) \tag{50}$$

and conclude that fluctuations in heat release rate vary according to the kinematic response of the flame, which determines e.g. the shape and surface area of the flame and thus its volume consumption rate. However, perturbations of this kind do not generate entropy waves, as they only modulate the rate at which premixture is consumed by the flame, but they do not modulate the heat released per unit mass of premixture and thus do not generate – to leading order – inhomogeneities of entropy.

The analysis in this section has shown that for a premixed flame, the generation of entropy waves is neither a direct nor a necessary consequence of unsteady heat release rate. Instead, entropy waves are generated to leading order in Mach number only from inhomogeneities in the equivalence ratio of the premixture. Additional entropy source terms, which are of first order in Mach number, result from the interaction of acoustic fluctuations with the mean heat release (see the Appendix A). The contradiction discussed in the introduction of this paper is thereby resolved.

The problem of the correct estimation of entropy waves is strictly connected to the correct formulation of mass flow conservation equation. Indeed, across a perfectly premixed flame, no leading order temperature inhomogeneities can be produced, therefore $\rho_2'/\bar{\rho}_2 \sim \mathcal{O}(M)$. In the model of a *flame at rest* (Eqs. (3)), energy conservation gives for a passive source ($\dot{Q}' = 0$): $u_1' = u_2' + \mathcal{O}(M)$, while, in absence of leading order entropy, mass flow conservation gives: $u_2' = (\bar{T}_2/\bar{T}_1)u_1' + \mathcal{O}(M)$. This result shows that inconsistencies indeed arise in the model of the flame at rest, when entropy generation is taken into account. The next section, on the other hand, will show how the *moving flame* model ($u_s' \neq 0$) solves the inconsistency above at both zero and non-zero Mach number.

6. Coupling of velocity perturbations across a perfectly premixed flame

With reference to Eq. (42), we see that velocity perturbations downstream of a premixed flame may result from several contributions: upstream acoustic and entropy perturbations u_1', p_1', s_1', flame movement u_s' and equivalence ratio fluctuations ϕ'. The influences of ϕ' and p_1' are easily explained: as discussed in the previous section, the fluctuations in equivalence ratio and pressure have, respectively, an impact of leading and first order on the downstream entropy fluctuations. A change in downstream entropy (thus, density) implies a modulation of the downstream velocity u_2', due to mass conservation.

On the other hand, the influence of flame movement u_s' cannot be determined a priori in the general case. Eq. (38) shows that flame movement u_s' will result from an imbalance between upstream flow velocity u_1' and specific volume consumption rate $\dot{V}'$ of the flame. The latter depends – see Eq. (35) – on the response of flame area and flame speed to upstream flow perturbations. These effects are non-trivial, and require advanced analytical treatments and detailed experimental or numerical studies.

Nonetheless, it is possible to make simplistic assumptions on the flame response and explore the consequences, in order to highlight the role of the flame movement on the acoustic coupling across the flame. In this section, two limiting cases are analyzed: The first case concerns a passive, moving flame, which is convected around its mean position by velocity perturbations The other case, on the contrary, is a flame at rest.

On both cases, perfect premixture ($\phi' = 0$) will be considered, and we assume the upstream flow to the isentropic, $s_1' = 0$. Only the consequences for downstream velocity u_2' will be discussed, since to leading order pressure and entropy are not influenced by the flame front movement in the case of a premixed flame (see Eq. (42)).

6.1. Limit case I: passive moving flame

According to Eq. (43), the interdependencies between flow perturbations, flame movement and heat release imply for a passive flame with $\dot{Q}' = 0$ that

$$u_1' = u_s' + \mathcal{O}(M). \tag{51}$$

Please cite this article as: L. Strobio Chen et al., Propagation and generation of acoustic and entropy waves across a moving flame front, Combustion and Flame (2016), http://dx.doi.org/10.1016/j.combustflame.2016.01.015

The coupling relations across the flame – see the first line of Eq. (42) – imply in this case that

$$\frac{u_2'}{\bar{u}_2} = \frac{u_1'}{\bar{u}_1}\frac{1}{\lambda} + \mathcal{O}(M). \tag{52}$$

Due to mass conservation Eq. (17), $\bar{u}_1\lambda = \bar{u}_2$, and we conclude that for a passive, perfectly premixed flame

$$u_1' = u_s' + \mathcal{O}(M) = u_2' + \mathcal{O}(M). \tag{53}$$

The physical interpretation of this result is very simple: the flame as a whole is convected back and forth by the velocity perturbations, such that flame movement u_s' corresponds perfectly to u_1' at every instant. There are – by assumption – no fluctuations of heat release rate, $\dot{Q}' = 0$, such that the condition $u_2' = u_1'$ appears obvious. In the limiting case of vanishing Mach number, $M = 0$, there is no transport of premixture towards the flame, such that heat release rate $\bar{\dot{Q}}$ and flame speed S_f must also vanish. This limiting case then corresponds to a temperature discontinuity, which is convected back and forth by the velocity perturbations.

The analysis of this limiting case of a *passive, moving* flame resolves the paradox of mass vs. volume flow rate conservation that was discussed in the Introduction and Section 2. It is gratifying to see that volume flow rate conservation follows in a very straightforward manner from the conservation laws for mass, momentum and energy plus the kinematic conditions at the flame. The latter must be invoked, because it is not assumed that the flame is at rest.

6.2. Limit case II: flame at rest

The second limit-case considers a flame at rest, such that $u_s' = 0$ even in the presence of flow perturbation, $u_1' \neq 0$. The interdependencies in Eq. (41) resulting from the physics of the flame require in this case that

$$\frac{\dot{Q}'}{\bar{\dot{Q}}} = \frac{u_1'}{\bar{u}_1} + \mathcal{O}(M). \tag{54}$$

Furthermore, the coupling relations (42) across a premix flame demand that

$$\frac{u_2'}{\bar{u}_2} = \frac{u_1'}{\bar{u}_1} + \mathcal{O}(M), \tag{55}$$

which may be re-written as

$$u_2' = \frac{\bar{T}_2}{\bar{T}_1}u_1' + \mathcal{O}(M). \tag{56}$$

This result is in agreement with the linearized Rankine–Hugoniot relations (13) and corresponds to "naive" application of the continuity equation to flow across a heat source: the velocity fluctuations downstream exceed those upstream as an effect of the temperature jump.

Returning to the physics of the problem, we realize with Eq. (38) that the flame can only be at rest if the specific volume consumption of the flame is always equal to the upstream velocity, $\dot{V}' = u_1'$. This condition results from the constraint that for a perfectly premixed flame, each fluid element passing through the flame experiences the same increase of temperature.[2] In other words, the flame would have to respond to a modulation of upstream velocity u_1' by adjusting the flame area or flame speed in such a manner, that the volume consumption rate is at each instant in time equal to the upstream velocity. This scenario might be a valid description of realistic flame behavior in the limit of low frequencies. However, the response of a premix flame to flow perturbations is characterized by convective time lags. Thus one must conclude that in order to describe flame–acoustic coupling, the model of a heat source that is free to change its position in response to flow perturbations should be used in the general case ($u_s' \neq 0$).

[2] This constraint would be violated in the case of incomplete combustion or heat loss, but such effects are not considered here.

7. Discussion of previous works

Chu formulated the relations which describe the coupling of acoustic disturbances across a moving, compact flame front [20]. The present study adopted Chu's moving flame model to a quasi-1D framework, and explored consequences for coupling relations and generation of entropy waves. In the following, previous works related to these issues shall be re-visited, in order to further clarify the interdependencies among unsteady heat release rate, flame kinematic response, acoustics and entropy generation.

7.1. Survey of other moving flame front jump conditions

Blackshear [22] proposed matching conditions for velocity and density across a flame front that involve a "flame volume" V_f,

$$A_D u_1(t) = A_f(t)S_f + \frac{\partial V_f(t)}{\partial t}, \tag{57}$$

$$A_D u_2(t) = A_f(t)S_f\frac{\rho_1}{\rho_2} + \frac{\partial V_f(t)}{\partial t}, \tag{58}$$

where A_D is the area of the duct and A_f the area of the flame front. The variation in time of the flame volume $V_f(t)$ decouples the rate of incoming volume flow from the volume consumption rate of premixture at the flame front. This introduces an additional degree of freedom into the model of Blackshear, equivalent to the relaxation of the condition that the flame be at rest.

The flame front velocity in the laboratory flame u_s does not appear explicitly in Blackshear's analysis. But the relation to the ideas discussed in the present paper can be elucidated quite easily. Combining the above equations, one obtains:

$$\rho_2 u_2(t) - \rho_1 u_1(t) = \frac{(\rho_2 - \rho_1)}{A_D}\frac{\partial V_f(t)}{\partial t} \tag{59}$$

In steady state, the partial derivative in time in Eq. (59) is zero, incoming and outgoing volume flow and volume consumption at the flame front are equal to each other. In the unsteady case, the rate of change of the flame volume $\partial V_f(t)/\partial t = A_f(t)S_f - A_D u_1(t)$, see Eq. (57). Substituting this result in Eq. (59) yields

$$\rho_2 u_2(t) - \rho_1 u_1(t) = (\rho_2 - \rho_1)\left(\frac{A_f(t)S_f}{A_D} - u_1(t)\right), \tag{60}$$

which should be interpreted as a combination of the mass conservation across a moving flame front Eq. (17) and the kinematic balance at the flame front Eq. (35).

Dowling [7] adopted the formalism of Blackshear [22] for the analytical study of a premixed flame anchored on a flame holder. Presuming a V-shaped flame front, it was possible to relate fluctuations in flame volume V_f to those of flame surface area A_f and heat release rate $\dot{Q}$. Compare this to the formalism developed in the present study, which does not presume a certain flame shape, but instead requires a transfer function for the heat release rate F_u or the flame velocity G_u to achieve closure, see Section 4.3. One may conclude that the formulations of Chu [20] and Blackshear [22] both share an important feature, i.e. they decouple the rates of incoming flow and volume consumption by introducing an additional degree of freedom, i.e. flame movement u_s and flame volume V_f, respectively. However, the conceptual differences between the two formulations resulted in further development of the models in different directions.

Please cite this article as: L. Strobio Chen et al., Propagation and generation of acoustic and entropy waves across a moving flame front, Combustion and Flame (2016), http://dx.doi.org/10.1016/j.combustflame.2016.01.015

The matching conditions expressed by Eqs. (39) and (40) can be also found in the work by Merk [23,24]. Note, however, that Merk considers only perfectly premixed flames, and mainly focused on the contributions of flame area (or volume) and upstream density.

Pelcé and Rochwerger [25,26] adopted the moving flame model for the description of vibratory instability in cellular flames. Their analysis recovers the quasi 1-D formulation used in the present paper, the kinematic balance at the flame front (see Eqs. (6)–(9) in [26]) is given in the same form as in Eq. (38).

In the more recent literature on 1-D analysis of thermoacoustic systems, see e.g., [10,15,16], the moving flame model (i.e. the kinematic balance at the flame front) has not found extensive application. The reason lies perhaps in the fact that the flame front movement u'_s only appears in the mass conservation equation, while in the energy conservation equation it is found only in terms of higher order in Mach number (see Eq. (22)). Thus the differences between the energy conservation equation in the moving model and the model of the heat source at rest are not readily apparent. As noted in Section 3, the Rankine–Hugoniot relations for u' and p' are exact for fluctuations up to first order in Mach and the flame kinematics can be accounted for implicitly in the fluctuating heat release rate $\dot{Q}'$. Inconsistencies between the two models arise as soon as entropy generation is taken into consideration.

7.2. Flame kinematics and unsteady heat release

Schuermans [12] in the analysis of a premixed, turbulent, swirl stabilized flame, proposed two different closures for a simplistic flame model, featuring only acoustic and equivalence ratio fluctuations. In one model the flame is at rest at an axial position (refer to Eq. (17) in [12]), while the other model regarded the flame as a discontinuity fluctuating around a mean position(refer to Eq. (30) in [12]). The system transfer matrix featuring the moving flame model gave a better agreement with experiments. The model of flame at rest can be recovered in our analysis from Eq. (40), assuming that $u'_s = 0$ and $\dot{V}' = u'_1$ in every instant. The moving flame model can be recovered from Eq. (40), considering that the flame speed and the flame area are both constant, i.e. $u'_s = u'_1$ and $\dot{V}' = 0$. The unsteady heat release rate in the moving flame model is mainly due to equivalence ratio fluctuations. The flame area, however, was considered as constant in this work.

In his review on the modeling of premixed combustion, Lieuwen (see [28, Eqs. (34)–(39)]) made an explicit distinction between the heat release rate due to changes in flame area $\dot{Q}'/\bar{\dot{Q}}|_{u'}$ and the share due to changes in equivalence ratio $\dot{Q}'/\bar{\dot{Q}}|_{\phi'}$. In the context of Lieuwen's analysis, the flame can be modeled as:[3]

$$\frac{\dot{Q}'}{\bar{\dot{Q}}} = \frac{\dot{Q}'}{\bar{\dot{Q}}}\bigg|_{u'} + \frac{\dot{Q}'}{\bar{\dot{Q}}}\bigg|_{\phi'} = \frac{A'_f}{\bar{A}_f} + \frac{\int \Delta h'_R d\bar{A}_f}{\int \Delta \bar{h}_R d\bar{A}_f}, \tag{61}$$

where Δh_R is the heat of reaction, which is function of the equivalence ratio. Eq. (61) is the same formulation as Eq. (40) up to leading order. The former quantity $\dot{Q}'/\bar{\dot{Q}}|_{u'}$ depends on the response of the flame surface $A'_f/\bar{A}_f$ to upstream velocity fluctuations. In our analysis, $\dot{Q}'/\bar{\dot{Q}}|_{u'}$ corresponds to the change in total volume consumption rate $\dot{V}'/\bar{\dot{V}}$ in Eq. (36). On the other hand, $\dot{Q}'/\bar{\dot{Q}}|_{\phi'}$ is related exclusively to the generation of the temperature inhomogeneities downstream. In the quantification of the downstream entropy waves, it is useful to separate the unsteady heat release rate associated to inhomogeneities in the premixture, from the unsteady heat release rate due to modulations in mass flow rate. Such distinction is useful because the area change only governs the amount of the premixture being burnt instantaneously, while the temperature jump is a function of the enthalpy of the premixture only. When determining generation of entropy waves by a premix flame, only the unsteady heat release per unit of mass should be taken into account. According to the formalism above, this corresponds to $\dot{Q}'/\bar{\dot{Q}}|_{\phi'}$. Accounting explicitly for the flame front movement u'_s in the jump relations allows to decouple the entropy production s'_2 from $\dot{Q}'/\bar{\dot{Q}}|_{u'}$, as shown in Eqs. (34) and (42). On the other hand, the model of a heat source at rest does not allow for such decoupling.

[3] The sensitivity of the local flame speed S_f to equivalence ratio fluctuations is not discussed here.

7.3. Models of entropy production by a compact heat source

Dowling [10,31] analyzed the entropy production across a compact heat source at rest. Her analysis yields for the downstream entropy:

$$\frac{s'_2}{c_p} = \left(1 - \frac{1}{\lambda}\right)\left(\frac{\dot{Q}'}{\bar{\dot{Q}}} - \frac{u'_1}{\bar{u}_1} - \frac{p'_1}{\bar{p}_1}\right), \tag{62}$$

where $\dot{Q}(t)$ is the total heat release rate per unit of volume. Eq. (62) shows that, in the case of a heat source at rest (e.g. a heated wire or a heat exchanger) entropy waves are determined predominantly by the unsteady heat release rate (or heat transfer rate) and upstream velocity fluctuations, given that pressure perturbations are of higher order in Mach number. Note that Dowling also distinguishes between the total heat release per unit of volume and per unit of mass, respectively, which is crucial for the correct prediction of entropy generation. These conclusions are in agreement with the analysis presented in Section 5.

However, the reader is cautioned that Eq. (62) is not applicable for perfectly premixed flames, unless $\dot{Q}'/\bar{\dot{Q}} = u'_1/\bar{u}_1$, i.e. if $|FTF| = 1$, which is in general not the case. Eq. (50) may be satisfied in general only if the flame front to is allowed to move (i.e. $u'_s \neq 0$).

Cumpsty [30] presented results in terms of downstream entropy production as a function of Mach number and non-dimensional frequency. The kinematic balance at the flame front was not considered. However, Cumpsty made a reasonable prediction of the entropy waves, because he considered the mass-specific energy equation, instead of the total energy conservation equation. The entropy fluctuations downstream are formulated as: $s'_2/c_p = q'/c_p\bar{T}_1$, where q' corresponds to the mass-specific heat release. This treatment is in line with the arguments put forward in Section 5. Cumpsty's results for downstream entropy fluctuations in function of frequency are mainly constant, and not frequency-dependent, as Eq. (62) would suggest.

In the work of Polifke et al. [5] on the coupling between entropy and acoustic waves at a chocked exit, only fluctuations in heat release rate that are due to changes in fuel mass fraction ($\dot{Q}'_{Y_F}$) were accounted for in the determination of the strength of downstream entropy waves. Fluctuations in the momentary consumption rate due to coherent vortices contribute to perturbations in heat release rate, but do not contribute to the generation of entropy waves. Again, this treatment is in complete agreement with the arguments developed above.

Finally, it is noted that in case the flow through the heated region is not subject to a kinematic balance as would be the case heat exchangers or hot wires, the previous works on discontinuities at rest (Dowling [10]) and the considerations on the limit of vanishing Mach number by Nicoud and Wieczorek [32] and Bauerheim et al. [17] represent a complete and solid analysis of the mechanisms of acoustic scattering and entropy generation.

Please cite this article as: L. Strobio Chen et al., Propagation and generation of acoustic and entropy waves across a moving flame front, Combustion and Flame (2016), http://dx.doi.org/10.1016/j.combustflame.2016.01.015

8. Conclusions

In this paper, a detailed analysis of the conservation equations for acoustic and entropy perturbations across a moving heat source has been carried out. The analysis allows to develop a deeper understanding of the influence of the flame front movement on the acoustic scattering and entropy generation. At the same time, it resolves paradoxical conclusions that result from the assumption of a flame front at rest in a physically intuitive manner.

Important consequences on the substantial generation of entropy waves by a premixed flame were elucidated. Removing the hypothesis of the fixed position of the heat source and invoking instead kinematic balance at the flame front, it has been demonstrated that to leading order in Mach number temperature inhomogeneities downstream of a premixed flame are associated exclusively with inhomogeneities in the mass-specific heat of reaction of the premixture, i.e. the fuel concentration. In the absence of equivalence ratio perturbations, and assuming complete combustion without significant heat loss due to convection or radiation, only a small amount of entropy fluctuations may be generated. These terms are of first order in Mach number, and result from interactions between upstream acoustics and the mean heat release rate.

In addition, the conservation laws for mass, momentum and energy at vanishing Mach number plus the kinematic matching conditions at a moving flame imply that the conservation of volume flow rate across a passive heat source follows in a very straightforward manner from mass conservation.

Acknowledgments

The presented work is part of the Marie Curie Initial Training Network Thermo-acoustic and Aero-acoustic Nonlinearities in Green combustors with Orifice structures (TANGO). We gratefully acknowledge the financial support from the European Commission under call FP7-PEOPLE-ITN-2012. Financial support for Sebastian Bomberg by the German Research Foundation DFG, project PO 710/12-1 and the Technische Universität München/Institute for Advanced Study, funded by the German Excellence Initiative, is gratefully acknowledged.

Appendix A. Analysis of terms of first order in entropy generation

In Section 5 it was shown that to leading order entropy fluctuations downstream of a premixed flame are exclusively due to inhomogeneities in the equivalence ratio of the upstream premixture ϕ'. In the absence of equivalence ratio fluctuations, entropy waves are of first order in Mach number,

$$\frac{s_2'}{c_p} = \underbrace{\left(1-\frac{1}{\gamma}\right)\left(\frac{1}{\lambda}-1\right)\frac{p_1'}{\bar{p}_1}}_{\mathcal{O}(M)}. \tag{A.1}$$

The physical mechanism that leads to these terms is unclear. How are entropy waves generated in absence of inhomogeneities in the premixture? In this section, we will give a detailed explanation of such interaction.

The jump across the flame, at very low Mach numbers, can be regarded as an isobaric process at first order of approximation, see Eq. (31), with mass-specific heat addition

$$q_{1\to 2} = \int_1^2 dq = \int_1^2 T ds = \int_1^2 c_p dT = c_p(T_2 - T_1). \tag{A.2}$$

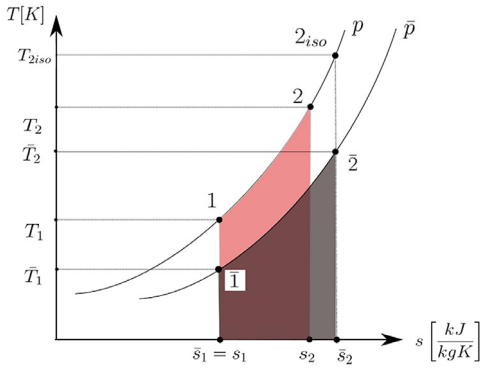

Fig. A.2. The steady and unsteady heat transfer process represented in the T–s plane. It should be noted that the isobaric curves in the T–s plane are not drawn to scale, but serve only to give a qualitative description of the unsteady heat release process. In fact, in the real scale the two curves are much closer, therefore also the change in temperature (T_1) is very small.

The corresponding change in specific entropy equals

$$s_2 - s_1 = \int_1^2 ds = \int_1^2 c_p \frac{dT}{T} = c_p \log\frac{T_2}{T_1}. \tag{A.3}$$

Combining these two results, which are an expression of the 1st and 2nd Law of Thermodynamics, one formulates for mean quantities

$$(\bar{s}_2 - \bar{s}_1) = \frac{\bar{q}}{\bar{T}_{ex}} \tag{A.4}$$

where

$$T_{ex} \equiv \frac{T_2 - T_1}{\log(T_2/T_1)} \tag{A.5}$$

is the logarithmic mean temperature of the heat release process and $\bar{q}$, for a premixed flame, is equal to the specific heat of reaction of the premixture.

For a perfect premixture, the heat of reaction is constant, and so is the associated temperature jump $T_2 - T_1$. In presence of acoustics, however, the upstream pressure perturbation may cause a change in upstream temperature, $p_1' \to T_1'$. As a consequence, the mean temperature of heat release $\bar{T}_{ex}$ is also slightly altered.

$$(\bar{s}_2 - \bar{s}_1) + s' = \frac{\bar{q}}{\bar{T}_{ex} + T_{ex}'}. \tag{A.6}$$

These qualitative considerations suggest that when upstream conditions (p_1', T_1') undergo small variations because of acoustic perturbations, a change in downstream entropy occurs, even in absence of unsteady heat release.

In order to determine the dependence of downstream entropy fluctuations on upstream acoustic perturbations, we consider isentropic upstream condition ($s_1' = 0$) and the linearized state equation for perfect gases, and reformulate Eq. (A.1) as:

$$\frac{s_2'}{c_p} = \left(\frac{1}{\lambda}-1\right)\frac{T_1'}{\bar{T}_1} = T_1'\left(\frac{1}{\bar{T}_2} - \frac{1}{\bar{T}_1}\right), \tag{A.7}$$

which shows that the entropy waves downstream are related to the temperature changes occurred upstream because of acoustic fluctuations. For an increase in upstream temperature, the associated entropy change is negative. This is directly explained by the 2nd Law of Thermodynamics, which states that, the higher the temperatures at which the heat addition occurs, the lower the increase in entropy.

The interaction between acoustics and mean heat release is well described in the T–s plane. In Fig. A.2 two isobaric curves are represented in the T–s plane. On the lower curve, points $\bar{1}$ and $\bar{2}$

are the states of the gas before and after the combustion. The process takes place at mean pressure $\bar{p}$.

The heat release per unit of mass is represented by the area under the curve ($\bar{1}$, $\bar{2}$, $\bar{s}_2$, $\bar{s}_1$). Starting from the initial state $\bar{1}$, a perturbation increases the pressure to p. Since the acoustic oscillations are isentropic (see [42]), the end state is at point 1, at temperature T_1. Given the constant heat release per unit of mass:

$$\bar{q} = \int_{\bar{s}_1}^{\bar{s}_2} T(s)ds|_{\bar{p}} = \int_{s_1}^{s_2} T(s)ds|_{p} \tag{A.8}$$

the resultant of the combustion in presence of acoustic perturbations will be at point 2. It is obvious that the entropy at point 2 is lower than the entropy at point $\bar{2}$. In order to suppress any entropy wave downstream, an increase in heat release rate would be required, such that the final state of the combustion is at point 2_{iso}.

It is generally understood that the interaction between acoustics and a heat source produces entropy waves. Our analysis shows that in the case of a *perfectly* premixed flame the generation of entropy waves is only associated with upstream acoustics and *mean* heat release, but not fluctuations of heat release $\dot{Q}'$! Consequently, entropy waves downstream a perfectly premixed flame should not be identified with the fluctuations in the total heat release rate. Moreover, these fluctuations are first order in Mach and are negligible for $M \ll 1$. Of course, this argument assumes complete combustion as well as the absence of heat losses due to convective or radiative heat transfer. These results must be taken into account when discussing the role of entropy waves in thermoacoustic instability or indirect combustion noise.

References

[1] F. Marble, S. Candel, Acoustic disturbance from gas non-uniformities convected through a nozzle, J. Sound Vib. 55 (2) (1977) 225–243.
[2] J. Keller, W. Egli, J. Hellat, Thermally induced low-frequency oscillations, Z. Angew. Math. Phys. 36 (2) (1985) 250–274.
[3] J. Humphrey, F. Culick, Pressure oscillations and acoustic-entropy interactions in ramjet combustion chambers, in: AIAA/SAE/ASME/ASEE 23rd Joint Propulsion Conference, 1987. paper AIAA-1987-1872.
[4] M. Macquisten, A. Dowling, Low-frequency combustion oscillations in a model afterburner, Combust. Flame 94 (3) (1993) 253–264.
[5] W. Polifke, C.O. Paschereit, K. Döbbeling, Constructive and destructive interference of acoustic and entropy waves in a premixed combustor with a choked exit, Int. J. Acoust. Vib. 6 (3) (2001) 1–38.
[6] L. Rayleigh, The theory of sound, Macmillan, London, U.K., 1896.
[7] A. Dowling, G. Bloxsidge, Reheat buzz – an acoustically driven combustion instability, in: AIAA/NASA Aeroacoustics Conference, 1984. paper AIAA-84-2321.
[8] M.A. Heckl, Active control of the noise from a Rijke tube, in: G. Comte-Bellot, J. Ffowcs-Williams (Eds.), Aero- and Hydro-acoustics, Springer, Berlin, Germany, 1985, pp. pp.211–216.
[9] W. Lang, T. Poinsot, S. Candel, Active control of combustion instability, Combust. Flame 70 (3) (1987) 281–289.
[10] A.P. Dowling, The calculation of thermoacoustic oscillations, J. Sound Vib. 180 (4) (1995) 557–581.
[11] U. Krüger, J. Hüren, S. Hoffmann, W. Krebs, P. Flohr, D. Bohn, Prediction of thermoacoustic instabilites with focus on the dynamic flame behaviour for the 3a-series gas turbine of siemens KWU, in: International Gas Turbine & Aeroengine Congress & Exhibition, 1999. paper 99-GT-111.
[12] B.B.H. Schuermans, W. Polifke, C.O. Paschereit, Modeling transfer matrices of premixed flames and comparison with experimental results, in: International Gas Turbine & Aeroengine Congress & Exhibition, 1999. paper 99-GT-132.
[13] S.R. Stow, A.P. Dowling, Thermoacoustic oscillations in an annular combustor, in: International Gas Turbine & Aeroengine Congress & Exhibition, 2001. paper 2001-GT-0037.
[14] M.L. Munjal, Acoustics of ducts and mufflers, John Wiley & Sons, New York, USA, 1987.
[15] J. Kopitz, W. Polifke, CFD-based application of the Nyquist criterion to thermoacoustic instabilities, J. Comput. Phys. 227 (14) (2008) 6754–6778.
[16] C.S. Goh, A.S. Morgans, The influence of entropy waves on the thermoacoustic stability of a model combustor, Combust. Sci. Technol. 185 (2) (2013) 249–268.
[17] M. Bauerheim, F. Nicoud, T. Poinsot, Theoretical analysis of the mass balance equation through a flame at zero and non-zero mach numbers, Combust. Flame 162 (1) (2015) 60–67.
[18] A.P. Dowling, S.R. Stow, Acoustic analysis of gas turbine combustors, J. Propul. Power 19 (5) (2003) 751–764.
[19] P.A. Hield, M.J. Brear, S.H. Jin, Thermoacoustic limit cycles in a premixed laboratory combustor with open and choked exits, Combust. Flame 156 (2009) 1683–1697.
[20] B.T. Chu, On the generation of pressure waves at a plane flame front, Symp. (Int.) Combust. 4 (1) (1953) 603–612.
[21] B.T. Chu, Stability of systems containing a heat source – the Rayleigh criterion, Report No. NACA-RM-56d27, National Advisory Committee for Aeronautics, Washington, USA, 1956.
[22] P.L. Blackshear, Driving standing waves by heat addition, Symp. (Int.) Combust. 4 (1) (1953) 553–566.
[23] H. Merk, An analysis of unstable combustion of premixed gases, Symp. (Int.) Combust. 6 (1) (1956) 500–512.
[24] H. Merk, Analysis of heat-driven oscillations of gas flows, Appl. Sci. Res: Sect. A 7 (2–3) (1958) 175–191.
[25] P. Pelcé, D. Rochwerger, Sound generated by cellular flames, in: M.B. Amar, P. Pelcé, P. Tabeling (Eds.), Growth and Form, Plenum Press, New York, 1991, pp. 245–252.
[26] P. Pelcé, D. Rochwerger, Vibratory instability of cellular flames propagating in tubes, J. Fluid Mech. 239 (1992) 293–307.
[27] B. Schuermans, Modeling and control of thermoacoustic instabilities (Ph.D. thesis), STI, Lausanne, 2003.
[28] T. Lieuwen, Modeling premixed combustion-acoustic wave interactions: a review, J. Propul. Power 19 (5) (2003) 765–781.
[29] B. Schuermans, V. Bellucci, F. Guethe, F. Meili, P. Flohr, O. Paschereit, A detailed analysis of thermoacoustic interaction mechanisms in a turbulent premixed flame, in: International Gas Turbine & Aeroengine Congress & Exhibition, 2004. paper GT2004-53831.
[30] N. Cumpsty, Jet engine combustion noise – pressure, entropy and vorticity perturbations produced by unsteady combustion or heat addition, J. Sound Vib. 66 (4) (1979) 527–544.
[31] A. Dowling, N. Hooper, P. Langhorne, G. Bloxsidge, Active control of reheat buzz, AIAA J. 26 (7) (1988) 783–790.
[32] F. Nicoud, K. Wieczorek, About the zero mach number assumption in the calculation of thermoacoustic instabilities, Int. J. Spray Combust. Dyn. 1 (1) (2009) 67–111.
[33] G.J. Bloxsidge, A.P. Dowling, P.J. Langhorne, Reheat buzz: an acoustically coupled combustion instability. Part 2. Theory, J. Fluid Mech. 193 (1988) 445–473.
[34] J.J. Keller, Thermoacoustic oscillations in combustion chambers of gas turbines, AIAA J. 33 (12) (1995) 2280–2287.
[35] R. LeVeque, Numerical methods for conservation laws, Birkhäuser Verlag, Basel, Switzerland, 1992.
[36] A. Fleifil, A.M. Annaswamy, Z.A. Ghoneim, A.F. Ghoniem, Response of a laminar premixed flame to flow oscillations: a kinematic model and thermoacoustic instability results, Combust. Flame 106 (4) (1996) 487–510.
[37] J.H. Cho, T. Lieuwen, Laminar premixed flame response to equivalence ratio oscillations, Combust. Flame 140 (1) (2005) 116–129.
[38] S. Ducruix, D. Durox, S. Candel, Theoretical and experimental determinations of the flame transfer function of a laminar premixed flame, Proc. Combust. Inst. 28 (1) (2000) 765–773.
[39] S. Candel, Combustion dynamics and control: progress and challenges, Proc. Combust. Inst. 29 (1) (2002) 1–28.
[40] A. Huber, W. Polifke, Dynamics of practical premix flames. Part I. Model structure and identification, Int. J. Spray Combust. Dyn. 1 (2) (2009) 199–229.
[41] W. Polifke, C.J. Lawn, On the low-frequency limit of flame transfer functions, Combust. Flame 151 (3) (2007) 437–451.
[42] S. Rienstra, A. Hirschberg, An introduction to acoustics (Report no. IWDE 92-06), Eindhoven University of Technology, Eindhoven, Netherlands, 2014.

Please cite this article as: L. Strobio Chen et al., Propagation and generation of acoustic and entropy waves across a moving flame front, Combustion and Flame (2016), http://dx.doi.org/10.1016/j.combustflame.2016.01.015

ASME Turbo Expo 2016: *On generation of entropy waves by a premixed flame*

Proceedings of ASME Turbo Expo 2016: Turbomachinery Technical Conference and Exposition
GT2016
June 13-17, 2016, Seoul, South Korea

GT2016-57026

ON GENERATION OF ENTROPY WAVES BY A PREMIXED FLAME

Lin Strobio Chen *, Thomas Steinbacher , Camilo Silva , Wolfgang Polifke
Professur für Thermofluiddynamik
Technische Universität München
Boltzmannstrasse 15, D-85747,
Garching bei München, Germany
Email: strobio@tfd.mw.tum.de

ABSTRACT

It is understood that so-called "entropy waves" can contribute to combustion noise and play a role in thermoacoustic instabilities in combustion chambers. The prevalent description of entropy waves generation regards the flame front as a source of heat at rest. Such a model leads - in its simplest form - to an entropy source term that depends exclusively on the unsteady response of the heat release rate and upstream velocity perturbations. However, in the case of a perfectly premixed flame, which has a constant and homogeneous fuel / air ratio and thus constant temperature of combustion products, generation of entropy waves (i.e. temperature inhomogeneities) across the flame is not expected. The present study analyzes and resolves this inconsistency, and proposes a modified version of the quasi 1-D jump relations, which regards the flame as a moving discontinuity, instead of a source at rest. It is shown that by giving up the hypothesis of a flame at rest, the entropy source term is related upto leading order in Mach number to changes in equivalence ratio only.

To supplement the analytical results, numerical simulations of a Bunsen-type 2D premixed flame are analysed, with a focus on the correlations between surface area, heat release and position of the flame on the one hand, and entropy fluctuations downstream of the flame on the other. Both perfectly premixed as well as flames with fluctuating equivalence ratio are considered.

*Address all correspondence to this author.

NOMENCLATURE

A_D	duct cross-sectional area
A_f	flame surface area
c_p	specific heat capacity at constant pressure
F	frequency response of heat release rate
f	frequency
E	frequency response of entropy
M	Mach number
p	pressure
$\dot{Q}$	total heat release rate
u	velocity
u_s	velocity of flame front in lab frame of reference
s	entropy
S_f	flame speed
T	temperature
$\dot{V}$	volume consumption rate per duct area
Y	mass fraction
ϕ	equivalence ratio
γ	ratio of specific heats
λ	mean temperature ratio $\bar{T}_2/\bar{T}_1$
ρ	density
ω	frequency (in radians)
$\bar{a}$	superscript, temporal mean value of a
a'	superscript, fluctuation of a, $(a' = a - \bar{a})$
1	subscript, refering to conditions upstream of the flame
2	subscript, refering to conditions downstream of the flame

INTRODUCTION

One of the challenges in the study of thermoacoustic systems is the control of instabilities that involve entropy waves. Entropy waves (also called "hot spots") are related to temperature inhomogeneities generated by the unsteady combustion process. As first observed by Marble and Candel [1], the downstream temperature inhomogeneities, when accelerated (e.g. through a nozzle), generate acoustic waves from the acceleration zone. The upstream propagating component of these acoustic waves impinge on the flame and may trigger low-frequency thermoacoustic instabilities. This mechanism of combustion instability has been studied by several authors [2–9]. A number of studies considered the dispersion of entropy waves [5,7], and the generation of acoustic waves from entropy waves in a nozzle [10]. Comparatively, little research has been done on the generation of entropy waves by a premix flame and, to the best knowledge of the authors, a critical validation of the proposed relations between entropy fluctuations s' and unsteady heat release rate $\dot{Q}'$, has not yet been carried out. Understanding such interdependency is crucial for the identification of entropy sources and the control of instabilities generated by the indirect combustion noise. The present study analyzes the mechanism of generation of entropy waves across a premixed flame. The goal is to clarify the relation between perturbations of velocity or equivalence ratio, flame movement, unsteady heat release rate and generation of entropy waves. It will be demonstrated that the proper analytical modeling of entropy generation should adopt the description of the flame front as a *moving* discontinuity, and how the model of the flame at rest gives an incorrect estimation of downstream entropy. To support the analytical models, numerical results from simulations of laminar premixed flames will be analyzed and discussed.

ESTIMATION OF ENTROPY PRODUCTION BY THE MODEL OF A FLAME AT REST

In the formulation of the jump conditions across a compact flame, the flame sheet is often regarded as a discontinuity of negligible thickness, fixed at a mean position. Across the flame front, the conservation equations for linear perturbations in mass, momentum and energy up to first order in Mach number read [3]:

$$\frac{\rho_2'}{\bar{\rho}_2} - \frac{\rho_1'}{\bar{\rho}_1} + \frac{u_2'}{\bar{u}_2} - \frac{u_1'}{\bar{u}_1} = 0, \tag{1}$$

$$\frac{p_2'}{\bar{p}_2} = \frac{p_1'}{\bar{p}_1} + \mathscr{O}(M^2), \tag{2}$$

$$\frac{\dot{Q}'}{\bar{\dot{Q}}} = \frac{c_p(T_2' - T_1')}{c_p(\bar{T}_2 - \bar{T}_1)} + \mathscr{O}(M^2) \tag{3}$$

where $c_p(\bar{T}_2 - \bar{T}_1)$ is the increase in mass-specific sensible enthalpy ($\Delta\bar{h}$). Considering the linear relation between the fluctuation in entropy and the thermodynamic variables p, ρ and T:

$$\frac{s'}{c_p} = \frac{p'}{\bar{p}\gamma} - \frac{\rho'}{\bar{\rho}} = \Big(\frac{1}{\gamma} - 1\Big)\frac{p'}{\bar{p}} + \frac{T'}{\bar{T}} \tag{4}$$

and isentropic upstream flow ($s_1' = 0$), the downstream variation in entropy reads [3, 11]:

$$\frac{s_2'}{c_p} = \Big(1 - \frac{1}{\lambda}\Big)\Big(\frac{\dot{Q}'}{\bar{\dot{Q}}} - \frac{u_1'}{\bar{u}_1} - \underbrace{\frac{p_1'}{\bar{p}_1}}_{\mathscr{O}(M)}\Big). \tag{5}$$

Equation (5) relates the entropy produced by a flame front to the unsteady heat release rate and the acoustic perturbations in velocity and pressure. Since the non-dimensional fluctuations in pressure are first order in Mach number, they are neglected in the following. Equation (5) suggests that entropy is always produced downstream of a heat source, if the change in heat release rate $\dot{Q}'/\bar{\dot{Q}}$ is not equal to the change in upstream velocity $u'/\bar{u}$. Physically, such condition states that the perturbations in entropy are due to the unsteadiness in the mass-specific heat release rate, as noted by Dowling and Stow [11]. Further discussion of this equation and its implications are given by Strobio Chen et al. [24].

The frequency response of the heat release rate of the flame[1] to upstream velocity perturbations is defined as:

$$F(\omega) \equiv \frac{\dot{Q}'(\omega)/\bar{\dot{Q}}}{u_1'(\omega)/\bar{u}_1}. \tag{6}$$

Eq. (5) can now be reformulated as:

$$\frac{s_2'(\omega)}{c_p} = \Big(1 - \frac{1}{\lambda}\Big)\Big(F(\omega) - 1\Big)\frac{u_1'}{\bar{u}_1} + \mathscr{O}(M), \tag{7}$$

which yields for the frequency response of entropy to upstream velocity:

$$E(\omega) \equiv \frac{s_2'(\omega)/c_p}{u_1'/\bar{u}_1} = \Big(1 - \frac{1}{\lambda}\Big)\Big(F(\omega) - 1\Big) + \mathscr{O}(M). \tag{8}$$

Obviously, the model of a flame at rest implies that leading order entropy waves will be generated by flow perturbations unless the flame frequency response $F(\omega)$ is unity.

[1] This quantity if often called the *flame transfer function* (FTF), but strictly speaking it should be called the frequency response.

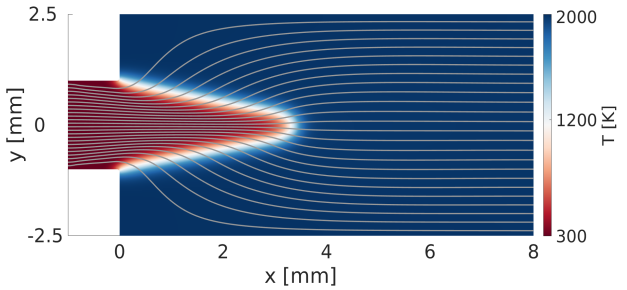

FIGURE 1. VELOCITY STREAMLINES AND TEMPERATURE FIELD OF THE 2D SLIT FLAME

Considerations on perfectly premixed flames

Now perfectly premixed flames are considered, where equivalence ratio is constant and thus $\phi' = 0$. In the limit of zero frequency, the flame frequency response of a perfectly premixed flame approaches unity, $F \to 1$, as discussed by Polifke and Lawn [12]. In this limit, no entropy perturbations up to leading order in Mach number are produced. However, as frequency ω increases, $|F(\omega)|$ deviates from unity in general and Eqs. (7) and (5) imply that leading order entropy waves are generated.

Yet, the generation of leading order temperature inhomogeneities is unphysical. This is due to the fact that perfectly premixed flames feature a constant air/fuel ratio, i.e., a constant mass-specific enthalpy and temperature jump. It would be more physically intuitive to state that downstream temperature inhomogeneities take place, only when fluctuations of equivalence ratio are present in the premixture. Equation (5), however, does not give any information on the dependency of the total heat release rate on the equivalence ratio of the premixture.

At this stage, it is necessary to develop a better understanding of the mechanism involved in the generation of temperature inhomogeneities downstream. The goal of this study is to to shed light on the interplay among upstream acoustic and equivalence ratio perturbations (u_1', ϕ_1'), and the system response, in terms of unsteady heat release, and entropy generation $(\dot{Q}', s_2')$.

To this end, 2D numerical simulations of a premixed, laminar flame are carried out, in presence of fluctuations of velocity and equivalence ratio.

Numerical study of a 2D premixed flame

The system considered for this analysis is a lean premixed "slit flame" stabilized downstream of a sudden expansion. The CFD domain, which is 2D and Cartesian, is depicted in Fig. 1. The inlet duct has a width of 1 mm, while the combustion chamber has a width of 2.5 mm, as in the work of Kornilov et al. [13] and Silva et al. [14]. The methane/air premixture has an equivalence ratio of $\bar{\phi} = 0.8$. Mean velocity and temperature at the inlet are, respectively, $\bar{u}_1 = 1.0$ m/s and $\bar{T}_1 = 293$ K. Adiabatic conditions are imposed at the walls, in order to rule out possible sources of heat dispersion and entropy generation. Under these conditions, the mean temperature of the burnt gases is $\bar{T}_2 = 2003$ K. The ratio between downstream and upstream temperatures is $\lambda \approx 6.3$. A two-step chemistry is used for the combustion model, c.f. [14].

The 2D compressible Navier-Stokes equations are solved by means of the CFD software AVBP, developed at CERFACS and IFP-EN[2]. A second-order Lax-Wendroff scheme is used for spatial and temporal discretization. The maximum CFL number is set to 0.7. To allow both the transmission of acoustic waves across the inlet and outlet boundaries without reflection, and the imposition of an acoustic excitation signal at the inlet, the Navier-Stokes Characteristic Boundary Conditions with wave-masking are adopted (see Poinsot et al [15] and Polifke et al. [16]). A random-binary signal with low levels of autocorrelation has been imposed at the inlet, as in [14]. The frequency of the excitation ranges between 0 and 1000 Hz.

For a more profound analysis of the entropy generation mechanism, the influence of fluctuations of velocity u' and equivalence ratio ϕ' on the unsteady heat release rate $\dot{Q}'(u')$ are investigated separately. Therefore, two test-cases have been taken into consideration:

1. a *perfectly* premixed flame with only velocity perturbations u' imposed at the inlet;
2. a *non-homogeneously* premixed flame, where fluctuations in equivalence ratio ϕ' are imposed at the inlet, while velocity perturbations are absent ($u_1' = 0$). The results of this case are particularly relevant for "technically premixed" flames (also called "practical premixed" flames by some authors), where acoustic perturbations at the fuel injector can modulate the equivalence ratio of the premixture.

The perturbation in equivalence ratio for case 2.) is defined as:

$$\frac{\phi'}{\bar{\phi}} = \frac{Y'_{CH4}}{\bar{Y}_{CH4}} - \underbrace{\frac{Y'_{O2}}{\bar{Y}_{O2}}}_{=0}, \tag{9}$$

where fluctuations in oxygen mass fraction are imposed to be zero. In order to maintain disturbances of the incoming mass flow equal to zero, so that the inlet velocity perturbations are zero, we must assure that $Y'_{CH4} + Y'_{O2} + Y'_{N2} = 0$. Therefore, $Y'_{N2} = -Y'_{CH4}$ is imposed at the inflow boundary.

RESULTS AND DISCUSSION

Frequency responses for heat release rate and entropy are identified by a Box-Jenkins parametric model [17] from time series data generated with unsteady CFD calculations forced by a

[2] www.cerfacs.fr/4-26334-The-AVBP-code.php

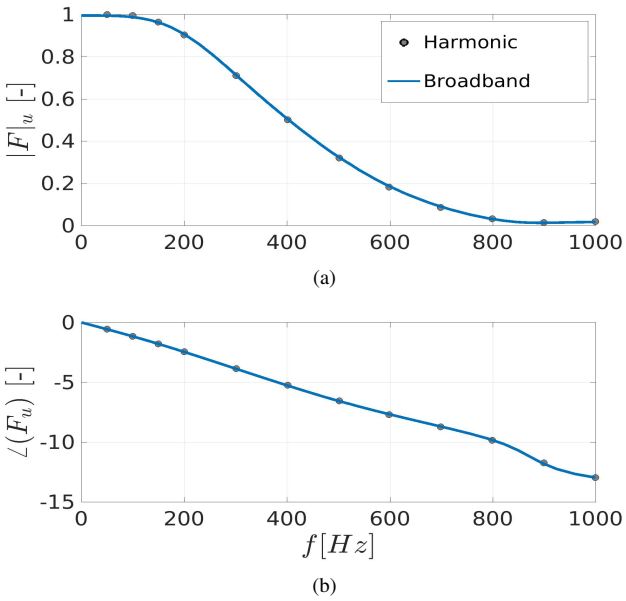

FIGURE 2. GAIN AND PHASE OF THE FREQUENCY RESPONSE OF HEAT RELEASE RATE TO UPSTREAM VELOCITY PERTURBATIONS, $F_u(\omega)$

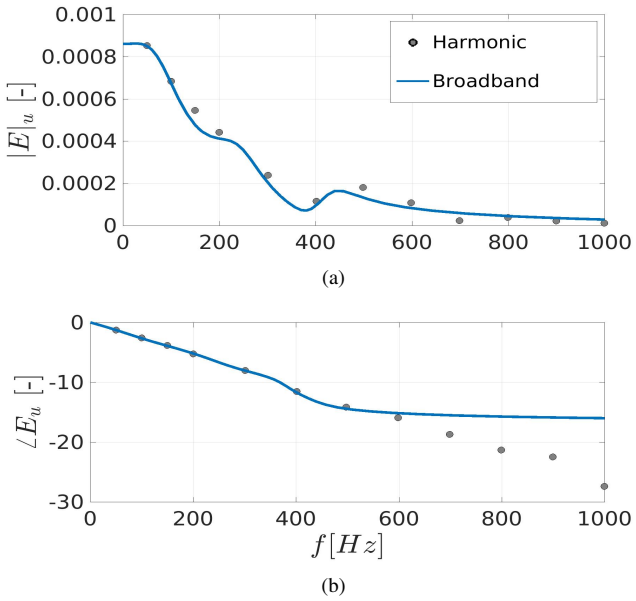

FIGURE 3. GAIN AND PHASE OF THE FREQUENCY RESPONSE OF ENTROPY TO UPSTREAM VELOCITY PERTURBATIONS, $E_u(\omega)$

random binary excitation signal. In the case of a perfectly premixed flame, perturbations of 10% of mean velocity are imposed at the inlet, while for the non-perfectly premixed case, the magnitude of the relative perturbations in mean equivalence ratio is 4.5%. A lower amplitude is chosen for equivalence perturbations in order to keep the flame response in the linear regime [18].

For the perfectly premixed flame, the respective frequency responses for heat release rate and entropy to velocity perturbations are defined as:

$$F_u(\omega) \equiv \frac{\dot{Q}'(\omega)/\bar{\dot{Q}}}{u_1'(\omega)/\bar{u}_1}, \qquad E_u(\omega) \equiv \frac{s_2'(\omega)/c_p}{u_1'(\omega)/\bar{u}_1}. \tag{10}$$

For the non-perfectly premixed case, one describes the response to fluctuations of equivalence ratio perturbations with frequency responses

$$F_\phi(\omega) \equiv \frac{\dot{Q}'(\omega)/\bar{\dot{Q}}}{\phi_1'(\omega)/\bar{\phi}_1}, \qquad E_\phi(\omega) \equiv \frac{s_2'(\omega)/c_p}{\phi_1'(\omega)/\bar{\phi}_1}. \tag{11}$$

The entropy fluctuations s_2' are evaluated at the outlet of the domain, at a single point on the centerline, 4 mm downstream from the tip of the flame, by means of Eq. (4). For quasi-1D analysis, entropy fluctuations could also be determined as averages over the duct cross sectional area, in order to take into account the effects of dispersion along various streamlines [5, 7]. Note that in the present case, averages over the outlet area yield frequency response functions that are virtually identical to the results presented below (not shown).

Entropy produced by a 2D perfectly premixed flame

Fig. 2(a) and 2(b) show gain and phase of the flame frequency response $F_u(\omega)$ identified for the system in Fig. 1. Simulations with harmonic excitations are performed to validate the results obtained from random binary excitation signal. Good agreement is found between the two datasets. The flame frequency response in Fig. 2(a) shows a typical low-pass filter behavior. The low-frequency limit equals unity, and is therefore correctly captured (see Polifke and Lawn [12]).

Equation (8) suggests that in the frequency domain the entropy frequency response should be specular to the flame frequency response, i.e. exhibit high-pass filter behavior: At higher frequencies, as $|F_u(\omega)|$ approaches zero, the entropy fluctuations should reach a maximum amplitude of $(1/\lambda - 1)u_1'/\bar{u}_1$. However, such behavior is not exhibited by the CFD results: Fig. 4(b) shows that in the time domain the fluctuations in entropy (and temperature) are highest at low frequency, and decrease to zero for higher frequencies. The entropy frequency response, therefore, has also a low-pass filter behavior. The small differences in the magnitude of $|E_u(\omega)|$ between broadband and harmonic excitation is due to the low amplitude of the response, which influences the signal-to-noise ratio, and therefore the quality of the

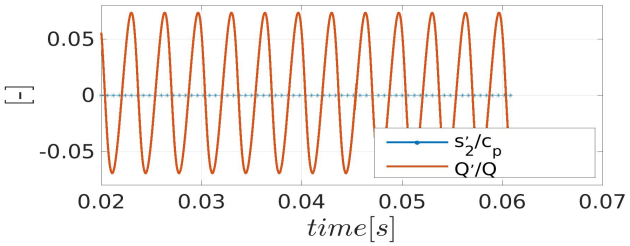

(a) FLUCTUATION IN HEAT RELEASE RATE $\dot{Q}'/\bar{\dot{Q}}$ AND IN DOWNSTREAM ENTROPY s_2'/c_p FOR 300 HZ

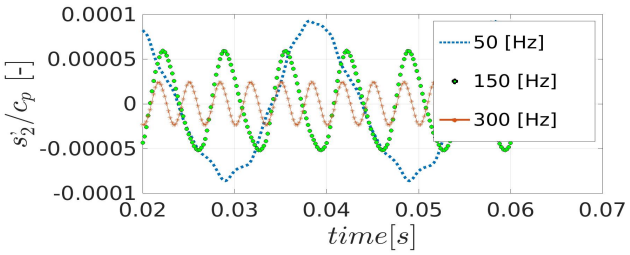

(b) FLUCTUATION IN DOWNSTREAM ENTROPY s_2'/c_p FOR 50, 150 and 300 HZ

FIGURE 4. TIME SERIES OF ENTROPY WAVES AND UNSTEADY HEAT RELEASE RATE

identification.

Figs. 3(a) (frequency domain) 4(a) (time domain) show that the amplitude $|E_u(\omega)|$ obtained from numerical simulation is several orders of magnitude smaller than $|F_u(\omega)|$. Indeed, the fluctuations are first order in Mach number: The maximum amplitude of the entropy frequency response is approximately 0.9×10^{-3}, which translates to fluctuations of downstream temperature T_2' of less than 2 K. Strobio Chen et al. [24] elucidate this mechanism of entropy wave generation and argue that it result from an interaction of acoustics with *mean* heat release rate. Details are given in the Appendix of [24].

Kinematic balance at the flame front It becomes evident, from the results in the previous section, that Eq. (7) does not give a correct prediction of the entropy production across a perfectly premixed flame. In order to provide a valid model for such prediction, it is necessary to take the kinematic matching conditions at the flame front into consideration. The kinematic balance was first used by Chu [19] for the case of a plane flame, by Blackshear [20] in 2-D premixed flames and later by Schuermans [21,22] in the modeling of swirl-stabilized turbulent flames. The mean heat release for a premixed flame is expressed as [23]:

$$\bar{\dot{Q}} = \bar{A}_f \bar{S}_f \bar{\rho}_1 \Delta\bar{h} = \bar{\dot{V}} A_D \bar{\rho}_1 \Delta\bar{h}, \tag{12}$$

where $\bar{A}_f$ is the mean flame surface, $\bar{S}_f$ is the mean local flame speed, $\bar{\rho}_1$ the mean flow density and $\Delta\bar{h}$ is the increase in sensible enthalpy per unit of mass. The flame surface and flame local speed contribute to the volume of premixture being burnt across the flame front at a given instant of time. $\bar{\dot{V}}$ represents the volume consumption rate of the flame per unit of duct area A_D.

The linear perturbations in heat release rate in a perfectly premixed flame are expressed as:

$$\frac{\dot{Q}'}{\bar{\dot{Q}}} = \frac{A_f'}{\bar{A}_f} + \frac{S_f'}{\bar{S}_f} + \frac{\rho_1'}{\bar{\rho}_1} + \frac{\Delta h'}{\overline{\Delta h}} = \frac{\dot{V}'}{\bar{\dot{V}}} + \frac{\rho_1'}{\bar{\rho}_1} + \frac{\Delta h'}{\overline{\Delta h}}. \tag{13}$$

The unsteadiness in the total heat release rate is mainly due to the contribution of unsteady mass flow $\rho_1'/\bar{\rho}_1 + A_f'/\bar{A}_f + S_f'/\bar{S}_f$ and to the change in sensible enthalpy per unit of mass $\Delta h'/\overline{\Delta h}$. For a perfectly premixed flame, $\Delta h' = 0$ and $S_f' = 0$ (neglecting effects of flame front curvature on the laminar flame speed). Moreover, in absence of upstream entropy waves $s_1' = 0$, the fluctuations in upstream density are first order in Mach number $\rho_1'/\bar{\rho}_1 \sim \mathcal{O}(M)$, and therefore could be neglected. The response in flame surface represents the main contribution to the unsteady heat release rate. In the steady state, the mean volume flux $\bar{u}_1 A_D$ is in equilibrium with the mean volume consumption rate of the flame:

$$A_D \bar{u}_1 = \bar{A}_f \bar{S}_f = \bar{\dot{V}} A_D. \tag{14}$$

In presence of velocity perturbations, the equilibrium condition expressed by Eq. (14) is not valid anymore, since the flame responds to upstream perturbations by changing the flame surface A_f. However, such response does not match the upstream perturbations instantaneously, but is subject to convective time lags. The difference between u_1' and $\dot{V}'$ causes the flame to move from its mean position:

$$\frac{u_1'}{\bar{u}_1} = \frac{\dot{V}'}{\bar{u}_1} + \frac{u_s'}{\bar{u}_1}, \tag{15}$$

where u_s' is the movement of the flame front with respect to the lab frame of reference, in the quasi-1D framework. In the steady state, the flame front does not move, since $\bar{u}_1 = \bar{\dot{V}}$ (see Eq. (14)). Consequently, the mean value of the flame front velocity $\bar{u}_s$ is zero and in the unsteady case $u_s(t) = u_s'(t)$. Considering Eq. (15), the unsteady heat release rate for a perfectly premixed flame can be rewritten as:

$$\frac{\dot{Q}'}{\bar{\dot{Q}}} = \frac{u_1'}{\bar{u}_1} - \frac{u_s'}{\bar{u}_1}. \tag{16}$$

The movement of the flame front must be taken into account in the conservation of mass flow. In fact, while the mass flowing through a fixed heat source (i.e. a heat exchanger) depends

only on the upstream flow velocity, in the case of a moving heat source, such as the premixed flame, the mass crossing the discontinuity depends not only on the upstream flow speed u_1, but also on the speed of the discontinuity itself u_s:

$$\dot{m}(t) = \rho_1(u_1 - u_s) = \rho_2(u_2 - u_s). \tag{17}$$

Equation (1) across a flame front is rewritten as:

$$\frac{\rho_2'}{\bar{\rho}_2} - \frac{\rho_1'}{\bar{\rho}_1} + \frac{u_2'}{\bar{u}_2} - \frac{u_1'}{\bar{u}_1} = \left(\frac{1}{\lambda} - 1\right)\frac{u_s'}{\bar{u}_1}. \tag{18}$$

Across a moving flame front, the solution of the linearized conservation equations in terms of $u_2'/\bar{u}_2$, $p_2'/\bar{p}_2$ and s_2'/c_p is:

$$\begin{pmatrix} \frac{u_2'}{\bar{u}_2} \\ \frac{p_2'}{\bar{p}_2} \\ \frac{s_2'}{c_p} \end{pmatrix} = \begin{bmatrix} \frac{1}{\lambda} & \left(\frac{1}{\lambda} - 1\right) & 0 \\ 0 & 1 & 0 \\ \left(\frac{1}{\lambda} - 1\right) & \left(\frac{1}{\lambda} - 1\right) & 1 \end{bmatrix} \begin{pmatrix} \frac{u_1'}{\bar{u}_1} \\ \frac{p_1'}{\bar{p}_1} \\ \frac{s_1'}{c_p} \end{pmatrix} + \begin{bmatrix} \left(1 - \frac{1}{\lambda}\right) \\ 0 \\ \left(1 - \frac{1}{\lambda}\right) \end{bmatrix} \frac{\dot{Q}'}{\bar{\dot{Q}}} + \begin{bmatrix} 0 \\ 0 \\ \left(1 - \frac{1}{\lambda}\right) \end{bmatrix} \frac{u_s'}{\bar{u}_1} \tag{19}$$

A detailed derivation of the linearized conservation equations across a moving flame front is given in [24]. Substituting Eq. (16) in the solution matrix Eq. (19) yields for the entropy production:

$$\frac{s_2'}{c_p} = \underbrace{\left(1 - \frac{1}{\gamma}\right)\left(\frac{1}{\lambda} - 1\right)\frac{p_1'}{\bar{p}_1}}_{\mathcal{O}(M)} + \underbrace{\frac{s_1'}{c_p}}_{=0}. \tag{20}$$

Equation (20) gives a reasonable estimation of the entropy fluctuations downstream a perfectly premixed flame. Fig. 5 shows that the order of magnitude for low-frequency limit is correctly captured. The phase delay between the entropy estimation and the actual entropy generation is due to the convective time between the upstream plane at which upstream fluctuations are evaluated and the outlet plane, at which entropy is evaluated.

ENTROPY PRODUCTION BY A NON-PERFECTLY PREMIXED FLAME

The flame and entropy frequency responses in presence of equivalence ratio perturbations are given in Fig. 6(a), 6(b) and Fig. 7(a), 7(b). The fluctuations of equivalence ratio are measured at the inlet, at 1 [mm] from the flame holder. In presence of

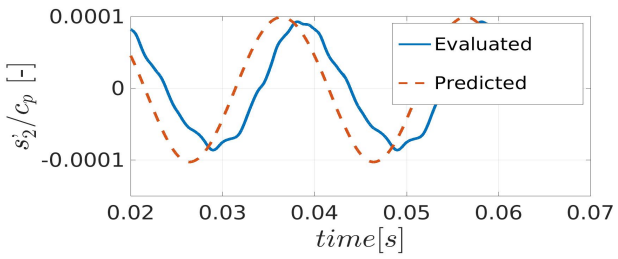

FIGURE 5. THE RELATIVE AMPLITUDE OF THE ENTROPY WAVES AS PREDICTED IN EQ. (20) AND THE ENTROPY EXTRACTED AT THE OUTLET FOR THE CASE OF 50HZ

equivalence ratio perturbations, the unsteady heat release rate has a more complex formulation than in Eq. (16), since the perturbations in local flame speed and in mass-specific sensible enthalpy cannot be neglected anymore. In fact, the local flame speed is sensitive to the upstream equivalence ratio fluctuations. Abu-Orf and Cant [25] have suggested the relation

$$S_f(\phi) = A\phi^B e^{-c(\phi - D)^2}, \tag{21}$$

where A, B, C and D are empirical coefficients. The change in mass-specific sensible enthalpy is also a function of ϕ'. For small perturbation in ϕ', we can write [23]:

$$\frac{\Delta h'}{\Delta \bar{h}} = \frac{\phi'}{\bar{\phi}}. \tag{22}$$

According to Lieuwen [26], the flame frequency response in presence of equivalence ratio $\dot{Q}'/\bar{\dot{Q}}|_\phi$ consists of several contributions:

$$F_\phi(\omega) = \frac{\dot{Q}'(\omega)/\bar{\dot{Q}}}{\phi'(\omega)/\bar{\phi}} = F_H(\omega) + F_S(\omega) \tag{23}$$

in which F_H represents the change in the increase of mass-specific sensible enthalpy $\Delta h'$ of the premixture in presence of ϕ' and F_S represents the effects on the volume consumption at the flame front. The change in volume consumption, in this case, is due to the fluctuations in local flame speed, which is sensitive to the equivalence ratio of the premixture (see Eq. (21)), and due to the subsequent change in flame surface. The relation between ϕ' and $\dot{V}'$ is non-trivial, since several effects act on the flame shape and flame surface. However, such complexity does not affect the modeling of the entropy frequency response. In fact, the change in flame surface governs the total mass consumption of the premixture across the flame. On the other hand, entropy, as

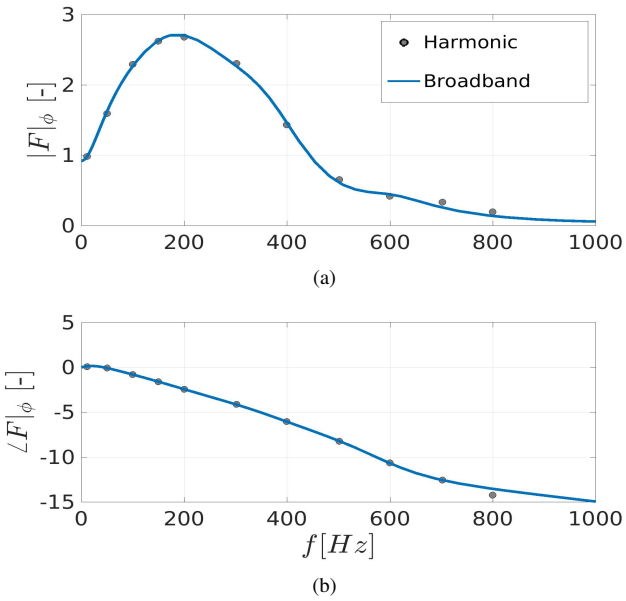

FIGURE 6. FREQUENCY RESPONSE OF HEAT RELEASE RATE TO PERTURBATIONS OF EQUIVALENCE RATIO, $F_\phi(\omega)$

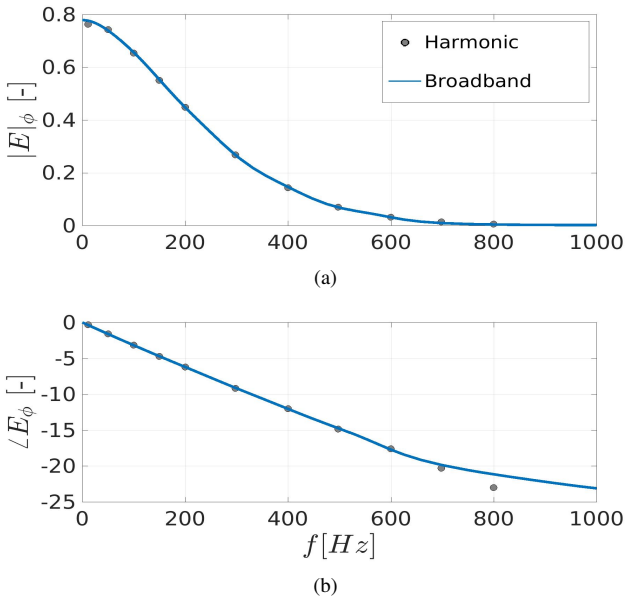

FIGURE 7. FREQUENCY RESPONSE OF HEAT RELEASE RATE TO PERTURBATIONS OF EQUIVALENCE RATIO, $E_\phi(\omega)$

well as temperature, is a mass specific quantity and does not depend on the total mass consumption, but on the inhomogeneities in the premixture ϕ' (see [24]). In fact, considering Eq. (22), we can express the unsteady heat release rate as:

$$\frac{\dot{Q}'}{\bar{\dot{Q}}} = \frac{u_1'}{\bar{u}_1} - \frac{u_s'}{\bar{u}_1} + \frac{\phi'}{\bar{\phi}} \tag{24}$$

and substituting in Eq. (19), the solution for the downstream entropy is:

$$\frac{s_2'}{c_p} = \underbrace{\left(1-\frac{1}{\lambda}\right)\frac{\phi'}{\bar{\phi}}}_{\mathscr{O}(1)} + \underbrace{\left(1-\frac{1}{\gamma}\right)\left(\frac{1}{\lambda}-1\right)\frac{p_1'}{\bar{p}_1}}_{\mathscr{O}(M)} + \underbrace{\frac{s_1'}{c_p}}_{0} . \tag{25}$$

Equation (25) expresses the fact that across a moving premixed flame front, leading order entropy generation depends solely on the presence of upstream fluctuations in equivalence ratio. Fig. 7(a) and 7(b) show that the entropy generation has a low-pass filter behavior. This result agrees qualitatively with the analytical derivations of F_H in the G-equation framework made by Lieuwen [26], Cho et al. [27] and Humphrey et al. [28].

The low-frequency limit of the entropy frequency response

In the quasi-steady framework, the amplitude of E_ϕ should equal the factor $(1-1/\lambda)$, which is 0.85 in our case. However, as shown in Fig. 7(a), the low frequency limit of the entropy frequency response is lower than $(1-1/\lambda)$, reaching a value close to 0.8 at low-frequency limit. This discrepancy, also shown in Fig. 8 for the case of 10 Hz, is due to several reasons. First, the ratio between $\Delta h'/\overline{\Delta h}$ and $\phi'/\bar{\phi}$ is not exactly unity, because the conversion to products species is not complete. For lean premixtures, Abu-Orf and Cant [25] proposed the following empirical relation:

$$\Delta h = \frac{2.9\times10^6\phi}{1+0.05825\phi}. \tag{26}$$

For $\bar{\phi}=0.8$ this yield for the proportionality factor $(\Delta h'/\overline{\Delta h})/(\phi'/\bar{\phi}) \approx 0.95$. This impacts on the entropy, since $\Delta h' \approx c_p T_2'$. The second reason is found in the fact that in real gases, c_p is not constant, but a function increasing with temperature (see further considerations in Appendix A). Therefore, at higher temperatures, a higher variation in enthalpy is needed for a given ΔT. These two considerations suggest that the proportionality factor $(1-1/\lambda)$ represents an "upper limit" to entropy generation.

CONCLUSIONS AND OUTLOOK

The correct estimation of entropy wave generation by unsteady combustion is crucial for prediction and control of thermoacoustic instabilities and indirect combustion noise. In this

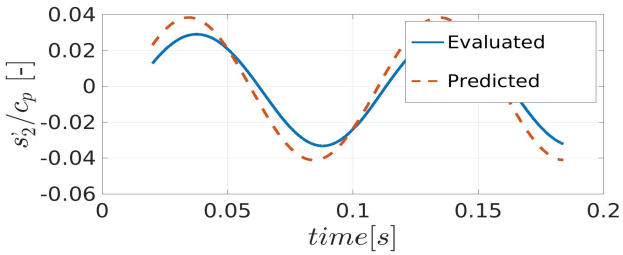

FIGURE 8. THE RELATIVE AMPLITUDE OF THE ENTROPY WAVES AS PREDICTED BY EQ. (25) AND THE ENTROPY EVALUATED AT THE OUTLET AS IN EQ. (4) FOR THE CASE OF 10HZ

paper, the mechanism of entropy waves generation in premixed flames has been investigated.

Numerical simulations, supported by analytical modeling, show that in the case of a perfectly premixed flame, the generation of entropy waves is negligible. In presence of equivalence ratio perturbations, on the other hand, leading order entropy waves are produced. In frequency domain, these waves have a low-pass filter behavior. The low-frequency limit of the entropy frequency response exhibits the highest gain, which is function of the temperature jump λ.

It has been argued, by means of numerical results and physical arguments, that the model of a heat source at rest cannot properly predict the amplitudes of temperature inhomogeneities downstream of a premixed flame. Instead, it is necessary to reformulate the conservation equations, by considering the flame front as a moving discontinuity. This model relates the leading order downstream entropy to the equivalence ratio perturbations only.

However, it should be noted that equivalence ratio perturbations are in general not the only source of entropy waves in complex combustion systems. The presence of non-adiabatic walls, cold gas injection and incomplete combustion might as well contribute to temperature inhomogeneities and thus to indirect combustion noise. Indeed, heat loss at combustor walls as well as injection of cold flow (see [9], [8]) are frequently found in real combustor configurations. It would be beneficial to extend the analytical model in the present work, such that "secondary" entropy sources, due to heat loss, are also taken into account. This would require to resolve the variability of entropy wave generation across various streamlines. A first step in this direction is the formulation of a quasi-1D model for the entropy frequency response that includes both molecular dissipation and streamline dispersion. This is the subject of ongoing work.

Note that the model of a compact premixed flame as a moving discontinuity also resolve paradoxical results concerning the conservation of mass and volume flow rates in the limit of vanishing Mach number (see Bauerheim et al. [29]). For details, the interested reader is referred to Strobio Chen et al. [24].

ACKNOWLEDGMENT

The presented work is part of the Marie Curie Initial Training Network Thermo-acoustic and aero-acoustic nonlinearities in green combustors with orifice structures (TANGO). We gratefully acknowledge the financial support from the European Commission under call FP7-PEOPLE-ITN-2012.

Appendix A: Thermodynamic properties of real gases

In real gases, the thermodynamic properties c_p and γ are not constant, but vary in function of temperature. Since the combustion process can be approximated to an isobaric heating process, the variation in sensible enthalpy per unit of mass is:

$$\Delta h = \int_{T_1}^{T_2} c_p(T)dT \tag{27}$$

In the present work, to evaluate enthalpy, a mean value of c_p is chosen:

$$\bar{c}_p = \frac{\int_{\bar{T}_1}^{\bar{T}_2} c_p(T)dT}{(\bar{T}_2 - \bar{T}_1)} \tag{28}$$

such that: $\overline{\Delta h} = \bar{c}_p(\bar{T}_2 - \bar{T}_1)$. However, the choice of c_p and γ do not change the conclusions reached in this paper on entropy generation, since they only affect the pressure term (see Eq. (4)), which is negligible.

REFERENCES

[1] Marble, F., and Candel, S., 1977. "Acoustic disturbance from gas non-uniformities convected through a nozzle". *Journal of Sound and Vibration,* ***55***(2), pp. 225–243.

[2] Keller, J., Egli, W., and Hellat, J., 1985. "Thermally induced flow frequency oscillations". *J. of Appl. Math. Physics*.

[3] Dowling, A. P., 1995. "The calculation of thermoacoustic oscillations". *J. of Sound and Vibration,* ***180***(4), pp. 557–581.

[4] Polifke, W., Paschereit, C. O., and Döbbeling, K., 2001. "Constructive and destructive interference of acoustic and entropy waves in a premixed combustor with a choked exit". *Int. J. of Acoustics and Vibration,* ***6***(3), pp. 1–38.

[5] Sattelmayer, T., 2003. "Influence of the combustor aerodynamics on combustion instabilities from equivalence ratio fluctuations". *Journal of Engineering for Gas Turbines and Power(Transactions of the ASME),* ***125***(1), pp. 11–19.

[6] Eckstein, J., and Sattelmayer, T., 2006. "Low-order modeling of low-frequency combustion instabilities in aeroengines". *Journal of propulsion and power,* ***22***(2), pp. 425–432.

[7] Goh, C. S., and Morgans, A. S., 2012. "The influence of entropy waves on the thermoacoustic stability of a model combustor". *Combustion Science and Technology,* ***185***, pp. 249–268.

[8] Motheau, E., Nicoud, F., Mery, Y., and Poinsot, T., 2013. "Analysis and modelling of entropy modes in a realistic aeronautical gas turbine". In Proceedings of ASME Turbo Expo 2013.

[9] Motheau, E., Nicoud, F., and Poinsot, T., 2014. "Mixed acoustic–entropy combustion instabilities in gas turbines". *Journal of Fluid Mechanics,* ***749***, pp. 542–576.

[10] Bake, F., Kings, N., and Roehle, I., 2008. "Fundamental mechanism of entropy noise in aero-engines: Experimental investigation". *Journal of Engineering for Gas Turbines and Power,* ***130***(1), pp. 11–20.

[11] Dowling, A. P., and Stow, S. R., 2003. "Acoustic analysis of gas turbine combustors". *Journal of Propulsion and Power,* ***19***(5), pp. 751–764.

[12] Polifke, W., and Lawn, C. J., 2007. "On the low-frequency limit of flame transfer functions". *Combust. Flame,* ***151***(3), pp. 437–451.

[13] Kornilov, V., Rook, R., ten Thije Boonkkamp, J., and de Goey, L., 2009. "Experimental and numerical investigation of the acoustic response of multi-slit bunsen burners". *Combustion and Flame,* ***156***(10), pp. 1957 – 1970.

[14] Silva, C. F., Emmert, T., Jaensch, S., and Polifke, W., 2015. "Numerical study on intrinsic thermoacoustic instability of a laminar premixed flame". *Combustion and Flame,* ***162***(9), pp. 3370 – 3378.

[15] Poinsot, T., and Lele, S., 1992. "Boundary conditions for direct simulation of compressible viscous flows". *Journal of Compuational Physics,* ***101***, pp. 104–129.

[16] Polifke, W., Wall, C., and Moin, P., 2006. "Partially reflecting and non-reflecting boundary conditions for simulation of compressible viscous flow". *J. of Comp. Physics,* ***213***, pp. 437–449.

[17] Ljung, L., 1998. *System identification*. Springer.

[18] Hemchandra, S., 2011. "Direct numerical simulation study of premixed flame response to fuel-air ratio oscillations". In Proceedings of ASME Turbo Expo 2011.

[19] Chu, B. T., 1953. "On the generation of pressure waves at a plane flame front". *4th Symposium on Combustion*.

[20] Blackshear, P. L., 1953. "Driving standing waves by heat addition". In Symposium (International) on Combustion, Vol. 4, Elsevier, pp. 553–566.

[21] Schuermans, B., 2003. "Modeling and control of thermoacoustic instabilities". PhD thesis, STI, Lausanne.

[22] Schuermans, B., Bellucci, V., Guethe, F., Meili, F., Flohr, P., and Paschereit, O., 2004. "A detailed analysis of thermoacoustic interaction mechanisms in a turbulent premixed flame". In ASME Turbo Expo 2004, Vienna, Austria, June 14-17.

[23] Schuermans, B. B. H., Polifke, W., and Paschereit, C. O., 1999. "Modeling transfer matrices of premixed flames and comparison with experimental results". No. 99-GT-132 in Int. Gas Turbine & Aeroengine Congress & Exhibition, Indianapolis, Indiana, USA, June 7 -10.

[24] Strobio Chen, L., Bomberg, S., and Polifke, W., 2016. "Propagation and Generation of Acoustic and Entropy Waves Across a Moving Flame Front". *Comb. and Flame*, DOI 10.1016/j.combustflame.2016.01.015.

[25] Abu-Orf, G., and Cant, R., 1996. "Reaction rate modelling for premixed turbulent methane-air flames". No. 1996-4-1 to 1996-4-4, Joint Meeting of the Portuguese, British, Spanish and Swedish Sections of the Combustion Institute.

[26] Lieuwen, T., 2003. "Modeling premixed combustion-acoustic wave interactions: A review". *Journal of Propulsion and Power,* ***19***(5), pp. 765–781.

[27] Cho, J. H., and Lieuwen, T., 2005. "Laminar premixed flame response to equivalence ratio oscillations". *Combustion and Flame,* ***140***(1), pp. 116–129.

[28] Humphrey, L., Acharya, V., Shin, D.-H., and Lieuwen, T., 2014. "Technical note coordinate systems and integration limits for global flame transfer function calculations". *International Journal of Spray and Combustion Dynamics,* ***6***(4), pp. 411–416.

[29] Bauerheim, M., Nicoud, F., and Poinsot, T., 2014. "Theoretical analysis of the mass balance equation through a flame at zero and non-zero Mach numbers". *Combustion and Flame,* ***162***, pp. 60–67.

ICSV22: *Thermo-acoustic characterization of a heat exchanger in cross flow using compressible and weakly compressible numerical simulation*

Florence, Italy 12-16 July 2015
ICSV22
The 22nd International Congress on Sound and Vibration

THERMO-ACOUSTIC CHARACTERIZATION OF A HEAT EXCHANGER IN CROSS FLOW USING COMPRESSIBLE AND WEAKLY COMPRESSIBLE NUMERICAL SIMULATION

Strobio Chen Lin, Witte Armin, Polifke Wolfgang
Professur für Thermofluiddynamik, TU München, D-85747, Garching, Germany
email: strobio@tfd.mw.tum.de

In the present work, a heat exchanger as used for hot water supply in domestic boilers is investigated numerically. The objective of the study is to identify the frequency response of the heat transfer rate with respect to perturbations of flow velocity, and the acoustic scattering matrix of the heat exchanger. These response functions are determined by CFD simulation of flow with heat transfer combined with system identification. Unsteadiness is imposed on the simulations by broad-band excitation of the variables at the boundaries. The resulting time series are post-processed to obtain the frequency responses. Particular emphasis is placed on the comparability between compressible and weakly compressible simulations in terms of heat release response. The response functions may be used subsequently in thermo-acoustic stability analysis of combustion systems.

1. Introduction

The presence of heat exchangers in industrial applications is ubiquitous. Tthey can be found in most energy conversion systems, and are used in both cooling (industrial turbines, internal combustion engines) and hot water production systems (domestic heating, industrial boilers). Despite the wide range of applications, little is known about the thermo-acoustic scattering properties of heat exchangers, and about their role in system stability. This is due to the fact that heat exchangers are classified as heat sinks, which are often erroneously regarded as damping elements. Indeed, according to the Rayleigh criterion, instability may occur whenever the global Rayleigh index (evaluated in the volume of heat release V) is positive over an oscillation cycle of period T [10]:

$$G = \int_V \frac{1}{T} \int_T \dot{q}'(x,t) p'(x,t) \mathrm{d}t \, \mathrm{d}v > 0, \tag{1}$$

where $\dot{q}'(x,t)$ is the heat release rate fluctuation per unit volume and $p'(x,t)$ is the fluctuation in pressure. This means that, in presence of acoustics, a heat sink might either damp or drive system instability, depending on the phase between the heat release fluctuations and the pressure field. In the present work, a typical configuration of heat exchanger employed in domestic boilers (Fig. 2) is investigated numerically. The aim is to characterize the behavior of the heat exchanger in terms of its acoustic scattering matrix and its heat release response to upstream acoustic perturbations. The

results of the identification can subsequently be used as input for an acoustic network model, in order to perform stability analysis.
The choice of a numerical approach is justified by the fact that in experimental test rigs, it is very difficult to measure the local instantaneous heat release rate. However, fully resolving the acoustics leads to very high computational costs. Therefore, in presence of low Mach and Helmholtz numbers, it is more convenient to treat the flow as incompressible [3],[6]. For compact heat sources ($He \ll 1$), in which the geometrical length is much smaller than the acoustic wavelength, the incompressible-flow approximation has some advantages: it is, in fact, computationally less expensive, and no acoustic reflections occur at the boundaries. Yet, in this specific case, the compactness is not always satisfied, since the Helmholtz number is in the range of $He \in [0, 0.5]$ (see Section 2.2.1). For this reason, is necessary to compare the incompressible simulation to a fully compressible case, in order to validate or discuss possible discrepancies. In the present study, since heat transfer takes place, a "weakly compressible" solver is proposed (see Section 2), which allows for changes in density depending solely on temperature.
In section 2, the details of the simulation and system identification procedure are given for both compressible and incompressible cases. In section 3, the results in terms of heat release fluctuations will be discussed. In section 4, an analytical modeling of the heat exchanger element has been carried out, in order to shed light on the physical phenomena governing the acoustic scattering of the heat exchanger. The results are discussed in terms of acoustic scattering matrix coefficients, and compared against the results from the fully compressible simulation, where direct identification of the scattering behavior is possible.

2. Numerical Approach

2.1 Compressible and weakly-compressible simulation

To create the time series necessary for system identification, CFD simulations were used. For the fully compressible simulations (FCS), the standard solver buoyantPimpleFoam, developed in OpenFOAM®, is used. buoyantPimpleFoam is apt for solving unsteady problems involving heat transfer and buoyancy effects. Neglecting the buoyancy effects, the local total pressure in buoyantPimpleFoam is expressed as:

$$p(t, x) = p_d(t, x) + p_\infty, \tag{2}$$

in which the instantaneous total pressure is a sum of the dynamic pressure (p_d) and of the constant reference pressure (p_∞).
The weakly compressible simulation (WCS), on the other hand, adopts a modified version of the original solver. The main modification concerns the relation density-pressure. In the WCS, the instantaneous pressure $p(t)$ is used for the transport equations, while the thermodynamic model follows an isobaric approach. The equation of state for a perfect gas is in fact changed to:

$$\rho(t, x) = \frac{p_\infty}{R\,T(t, x)}, \tag{3}$$

where R is the gas constant, T is the instantaneous temperature. p_∞ is not the instantaneous pressure, but constant over time. Hence, density variations depend solely on temperature variations.

2.2 Simulation domain and boundary conditions

2.2.1 General numerical details

In most hot water production systems, the heat exchanger (HX) and the hot gases are in a cross-flow configuration. The hot gases flow through a row of cylinders and heat is transferred to the water

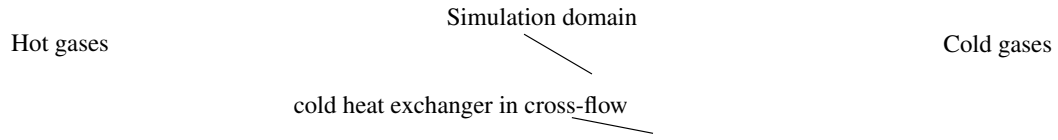

Figure 1. The geometry of a combustion system with row of HX cylinders in cross-flow

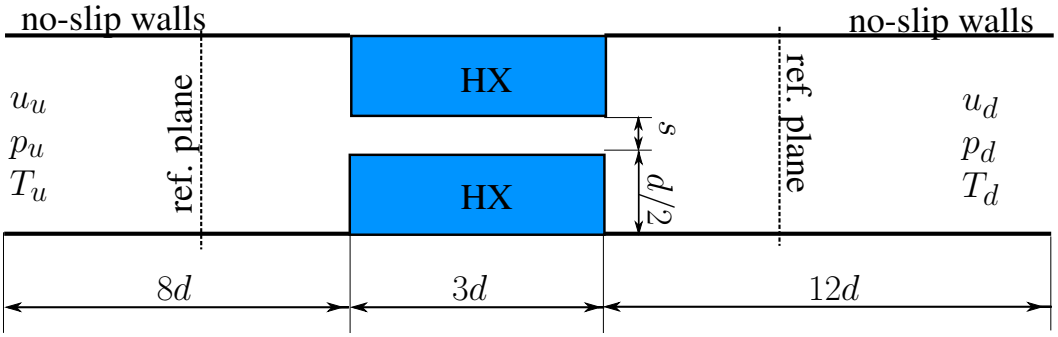

Figure 2. The geometry of the domain. The blue region represents the HX filled with water at constant temperature $T_{HX} = 300K$. The figure is not drawn to scale.

(see Fig. 1). In most applications, in order to optimize the heat exchange process, the surface of the cylinders is maximized with respect to the volume, therefore the cross section of the tubes are not circular, but elongated. In this study, we consider a simple 2D model (see Fig. 2), with two rectangular half tubes inside a channel. The height of the narrow channel between the tubes is $s = 0.8\,[mm]$, while the diameter of the HX tube is $d = 12.8\,[mm]$. This domain represents a single portion of the periodic configuration in Fig. 1. For the upper and lower boundaries, an adiabatic, no-slip wall condition is adopted instead of the cyclic boundary condition, in order to stabilize the downstream flow, which shows relevant transversal velocity components after the sudden area expansion. The velocity of the hot gases at the inlet is $\bar{u}_u = 0.89\,[m/s]$, which corresponds to a Mach number of $M_u = 1.28 \cdot 10^{-3}$. The maximum velocity is reached at the beginning of the narrow channel, $\bar{u}_{max} \approx 12\,[m/s]$. At the outlet, a constant pressure boundary condition has been set to $\bar{p}_d = 100\,[kPa]$. The temperature at the inlet is imposed at $\bar{T}_u = 1200\,[K]$, while the temperature at the heat exchanger is assumed to be constant $\bar{T}_{HX} = 300\,[K]$. The constant temperature assumption simplifies the analysis. However, the 'oversized' cooling in the HX implies that the temperature at the exit, $\bar{T}_d = 320\,[K]$, is lower than in the real case. The flow regime is laminar, since the highest Reynolds number in the domain is $Re_{max} = 180$.
Taking the upstream speed of sound as reference value, the Helmholtz number ($He = \omega L_{HX}/\bar{c}_u$) ranges from 0 to 0.45 for frequency range between 0 and 1500 Hz. A grid independence study has been carried out, in order to determine the level of refinement in the HX channel which properly resolves the boundary layer, where most of the heat exchange takes place. As a result, the channel height (s) has been divided into 16 squared cells.

2.2.2 Fully compressible simulation

In the fully compressible simulation the propagation of sound waves has to be resolved. The largest time step which allows to resolve the acoustic propagation properly is $\Delta t_{max} = \frac{Co_{max} \cdot \Delta x_{min}}{\bar{u}_u + \bar{c}_u} \approx 7 \cdot 10^{-8}\,[s]$, in which Co_{max} equals unity, according to the Courant-Friedrichs-Lewy condition.
The time step used in the simulation is $\Delta t_{fcs} = 5 \cdot 10^{-8}\,[s]$, which corresponds to a maximum Courant number of $Co_{max} = 0.7$.

Because of the presence of acoustically reflecting boundary conditions, the steady state solution was obtained by applying the Navier-Stokes Characteristic Boundary Conditions (NSCBCs) [8] at inlet and outlet. These boundary conditions ensure an exponential decay (w.r.t. frequency) of the reflection coefficient at the boundaries. However, partial reflection is still present at lower frequencies.

2.2.3 Weakly compressible simulation

Concerning the weakly compressible simulation, the considerations on the mesh refinement and initial conditions ($\bar{u}$, $\bar{p}$, $\bar{T}$) are unchanged. However, since there is no propagation of acoustic waves in the domain, no manipulations are needed for the inlet and outlet boundary conditions. Moreover, the time step adopted ($\Delta t_{wcs} = 2 \cdot 10^{-6}\,[s]$) has only to satisfy the fluid-dynamic CFL number and is roughly two orders of magnitude larger than the Δt_{fcs}. This makes the WCS suitable for generation of long time series (in the order of seconds), which is useful in the identification of the acoustic response at low frequencies.

2.3 System excitation and identification

The behavior of a system in presence of acoustic disturbances is characterized by its heat release response to upstream velocity perturbations $\mathcal{F}(\omega)$:

$$\mathcal{F}(\omega) = \frac{\dot{Q}'(\omega)/\bar{\dot{Q}}}{u'_u(\omega)/\bar{u}_u}, \tag{4}$$

where $\dot{Q}'$ is the fluctuation in heat release rate of the heat exchanger and u'_u is the velocity probe at the reference plane (see Fig. 2); and by its acoustic scattering matrix:

$$\begin{pmatrix} f_d \\ g_u \end{pmatrix} = \begin{bmatrix} T_{u\to d} & R_d \\ R_u & T_{d\to u} \end{bmatrix} \begin{pmatrix} f_u \\ g_d \end{pmatrix}, \tag{5}$$

where f and g are, respectively, the waves propagating in downstream and upstream direction. They are related to the acoustic perturbations (p',u') as follows:

$$f = \frac{1}{2}\left(\frac{p'}{\bar{\rho}\bar{c}} + u'\right) \qquad g = \frac{1}{2}\left(\frac{p'}{\bar{\rho}\bar{c}} - u'\right). \tag{6}$$

For the identification of the heat release response $\mathcal{F}(\omega)$ in the FCS, a Single-Input Single-Output (SISO) approach is adopted. After imposing an excitation signal (f) at the inlet, the model is identified by considering the upstream velocity fluctuations as the input and the fluctuations in the instantaneous total heat release as the output. As for the scattering matrix, a Multi-Input Multi-Output (MIMO) approach is used, in which excitation signals (f_u, g_d) are applied respectively at the inlet and outlet, and the outputs (f_d, g_u) are measured at the reference planes (see Fig. 2). The wavelet-based excitation signals present a constant power spectral density in the frequency range under investigation ($f \in [0; 1500]$ Hz) and are statistically uncorrelated [1]. The identification of the models from the time series is performed with the Box-Jenkins parametric model structure [7], in order to handle the noise deriving from the NSCBC partially reflecting boundaries. In the WCS a similar identification process is pursued. However, the excitation signals imposed correspond to u' at the inlet in the SISO approach and to u' and p' respectively at inlet and outlet in the MIMO approach. This is because, in an incompressible simulation, all disturbances travel at infinite speed and no acoustic wave (as f and g) can propagate across the domain.

3. Results from Compressible and Weakly Compressible Simulations

In this section, the frequency response from the FCS and WCS are compared. Before analyzing the results, it is necessary to point out that the time series of the two simulations are not immediately

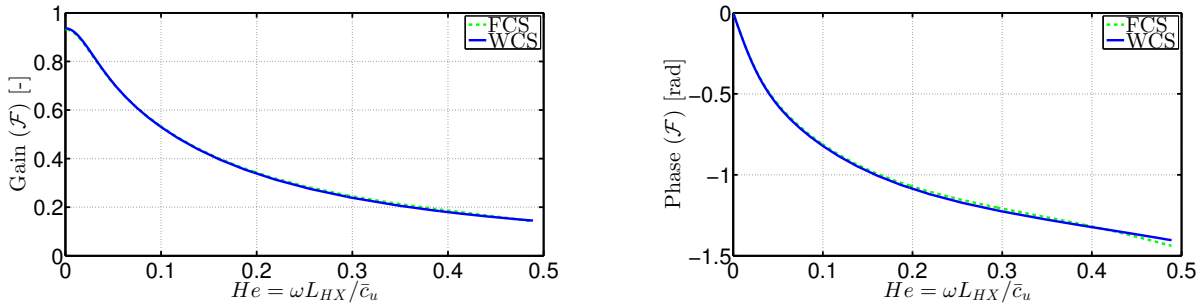

Figure 3. Gain and phase of the HX transfer function for compressible (green-dashed line) and weakly-compressible (blue line) simulations

comparable. In fact, in the compressible simulation, the signals of $u'/\bar{u}$ vary according to the position of the reference plane, since they are non-causal and derive from the superposition of the Riemann invariants f and g at the reference plane. In order to make the velocity signal space-invariant, it is necessary to first manipulate the Riemann invariants of the reference plane, by shifting them to the position of the heat exchanger. Since f and g travel in opposite directions, the time series of f is shifted forward, while g is shifted backwards for the upstream velocity. The time associated to the shift for f is: $\tau(f) = \Delta x/(\bar{c} + \bar{u})$, while for g is: $\tau(g) = \Delta x/(\bar{c} - \bar{u})$, where Δx is the distance between the reference plane and the HX and $\bar{c}$ and $\bar{u}$ are the mean speed of sound and flow velocity, respectively. Being the shifted time series f^* and g^*, it is possible to reconstruct the space-invariant velocity signal as $u'^* = f^* - g^*$. The heat exchanger transfer function for the compressible simulation is therefore expressed as in Eq. (4), with u'^* as fluctuating velocity.

3.1 Frequency response of heat transfer

Given the quasi-steady approximation used in the WCS, differences in gain and phase are expected for higher frequencies. However, the results in Fig 3 do not show any substantial difference between the transfer functions. Slight departures show at $He = 0.2$, but the difference in both gain and phase are negligible. This means that the weakly compressible simulation can capture with a good approximation all the fluid-dynamic features of the system, such as heat release and the changes in the velocity field, up to the frequency range considered ($f \in [0, 1500]Hz$). Significant difference only shows in the phase startin from $He \approx 0.48$.

3.2 Low frequency limit of the heat release response

The transfer function of the HX shows a low-pass filter behavior. Such behavior is common in the transfer functions of most heat sources, particularly in flames. However, as argued in [9] and experimentally demonstrated in [5], the zero-frequency limit of the transfer function in perfectly premixed flames should equal unity. Here, the low frequency limit of the heat exchanger transfer function is lower than 1. In order to explain such difference, it is necessary to analyze the physics involved in the heat exchanger. In [9] it is shown how the response of heat sources in the low-frequency limit can be derived from global conservation equations in quasi steady state.
The enthalpy balance for the HX is:

$$\dot{Q} = \dot{m}\Delta h = A_{\text{flow}} u_u \rho_u c_p (T_u - T_d), \tag{7}$$

where A_{flow} is the cross section of the channel, $u_u\rho_u$ is the mass flow rate and $c_p(T_u - T_d)$ is the specific enthalpy transferred from the hot gases to the HX. Considering that, in presence of low Mach numbers and acoustic disturbances only, the normalized density fluctuation is negligible w.r.t. the

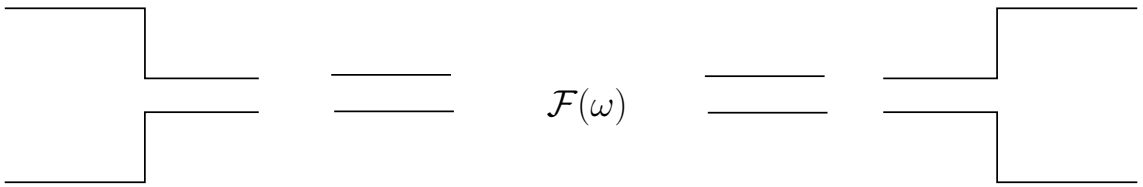

Figure 4. Acoustic model of the heat exchanger as: area change - duct - heat sink - duct - area change

velocity fluctuations, we have for the transfer function

$$\lim_{\omega\to 0}\mathcal{F} = \frac{\dot{Q}'/\overline{\dot{Q}}}{u'_u/\overline{u}_u} = 1 - \left(\frac{T'_d}{\overline{T}_u - \overline{T}_d}\Big/\frac{u'_u}{\bar{u}_u}\right). \tag{8}$$

Eq. (8) shows that the transfer function of the HX is lower than unity, whenever the fluctuation in downstream temperature is positive. In order to correlate the downstream temperature fluctuation T'_d to the velocity fluctuation u'_u, we consider the local temperature function in a simple 2D channel geometry:

$$T_d = T_{\mathrm{HX}} + (T_u - T_{\mathrm{HX}})\exp\left(\frac{-\mathrm{Nu}_\infty \lambda L}{2\rho_u u_u s^2 c_p}\right). \tag{9}$$

Assuming that fluctuations in temperature are only caused by velocity fluctuations, it may be argued that T'_d can be approximated as $T'_d(u'_u) \approx \frac{d\bar{T}_d}{d\bar{u}_u}u'_u$, which gives for the low frequency limit of $\mathcal{F}$:

$$\lim_{\omega\to 0}\mathcal{F} = 1 - \frac{\bar{T}_u - T_{\mathrm{HX}}}{\bar{T}_u - \bar{T}_d}\frac{\mathrm{Nu}_\infty \lambda L}{2\bar{\rho}_u\overline{u}_u s^2 c_p}\exp\left(\frac{-\mathrm{Nu}_\infty \lambda L}{2\bar{\rho}_u\overline{u}_u s^2 c_p}\right). \tag{10}$$

Eq. (10) shows that the lower frequency limit of the transfer function differs from unity, except from some limit cases, in which the product on the r.h.s is zero. This condition is verified for two cases: $L \to \infty$ and $s \to 0$. The first limit case shows that only when a heat exchanger has infinite surface, the downstream temperature fluctuation is zero. In the second case, the height of the channel is infinitesimally small, so the heat exchange takes place instantaneously via heat conduction. In real applications, neither of the cases cited above is verified. Therefore, the zero frequency limit of the heat exchanger transfer function is generally below unity.
There are no exact analytical relations for the geometry of the HX under analysis, so no quantitative values of $\lim_{\omega\to 0}\mathcal{F}$ can be given for comparison. However, regardless of the geometry, the qualitative considerations given above are valid for any heat source (or sink) in which heat exchange is involved.

4. System Modeling

As previous works have shown [1], the fully compressible simulation, combined with system identification can give very reliable results in terms of acoustic scattering matrix and heat release response. The results obtained for scattering matrix from the identification are shown in Fig. 5 (green line). Fully resolving the acoustic propagation is, however, more expensive in terms of computation efforts compared to the WCS. In this section, we will try to reproduce the scattering behavior identified with the FCS, using the results for the heat exchange rate obtained from the WCS. This modeling process not only gives insight into the scattering process at the HX, but would also enable the use of the incompressible simulation for describing acoustics of non-compact elements. In this attempt, we have modeled the system in Fig. 2 as a network of basic elements, as depicted in Fig. 4: As shown in Fig. 4, the heat exchanger is represented with all its geometric features, while the heat release is concentrated at the center of the network. This choice is justified by the fact that, for a reasonably high range of frequencies ($f \in [0, 1500]\,Hz$), the weakly compressible transfer function still gives a

good approximation of the heat transfer dynamics. Therefore, the heat source can still be considered as compact, at low Helmholtz numbers. The transfer functions in terms of $\frac{p'}{\bar{\rho}\bar{c}}$ and u' for the area change (ac) and the duct are:

(11)

$$TM_{ac} = \begin{bmatrix} 1 & -i\omega L_{eff}/\bar{c} \\ i\omega L_{red}/\bar{c} & \alpha \end{bmatrix}, \qquad TM_{duct} = \frac{1}{2}\begin{bmatrix} \left(e^{ik^- L} + e^{-ik^+ L}\right) & \left(-e^{ik^- L} + e^{-ik^+ L}\right) \\ \left(-e^{ik^- L} + e^{-ik^+ L}\right) & \left(e^{ik^- L} + e^{-ik^+ L}\right) \end{bmatrix},$$

where $L_{eff} = 0.0064\,[m]$ and L_{red} are end correction coefficients, which depend on the ratio between the cross-sections (α); as shown in [2], the value of L_{red} is negligible. In the transfer matrix of the duct L is the length of the channel and $k^{\pm} = \frac{\omega}{\bar{c}\pm\bar{u}}$. Considering the Rankine-Hugoniot relations for thermoacoustics [4], the transfer matrix across a concentrated heat source is:

(12)
$$TM_{pu,RH} = \begin{bmatrix} \frac{\bar{\rho}_u \bar{c}_u}{\bar{\rho}_d \bar{c}_d} & -\frac{\bar{\rho}_u \bar{c}_u}{\bar{\rho}_d \bar{c}_d}\left(\frac{T_d}{T_u} - 1\right) M_u(1 + \mathcal{F}(\omega)) \\ -\left(\frac{T_d}{T_u}\right)\gamma M_u & 1 + \left(\frac{T_d}{T_u} - 1\right)\mathcal{F}(\omega) \end{bmatrix}.$$

It consists of a 'semi-analytical' approach, since well-known analytical models are employed together with the transfer function $\mathcal{F}(\omega)$ given by the numerical simulation. The total transfer matrix in terms of $p'/\bar{\rho}\bar{c}$ and u' will be given by the product of the transfer matrices of the single elements. The results are shown in Fig. 5 in terms of the scattering matrix (see Eq. (5)), which is obtained from an algebraic manipulation of the transfer matrix. In Fig. 5, the model (blue line) is compared against the scattering matrix identified numerically (green-dashed line). Significant discrepancies are found in the transmission coefficients up and down stream and minor discrepancies in the low frequency region for the other terms. This means that the approximation of a concentrated heat release does not represent the heat exchanger very well. In fact, the model is qualitatively wrong, even if all the main qualitative features are present. Several hypothesis can be made to explain the discrepancies. First, the heat release is not equally distributed along the HX, but occurs for the most part at the front stagnation point and at the beginning of the duct, where the temperature gradient is higher. In addition, the presence of heat release at the front stagnation point might influence the scattering properties of the area change. Moreover, the sudden expansion downstream could also cause acoustic dissipation, due to the presence of sharp edges.

5. Conclusion

In this work, the identification of the transfer function and scattering matrix of a cold heat exchanger in hot cross flow is presented. The objective is not only to obtain a validated model for stability studies, but also to validate the effectiveness of the weakly compressible solver in handling acoustic simulation. The results show that the weakly compressible solver is apt for identifying the leading order effects, such as heat release and velocity fluctuaitons for a wide range of frequencies. At higher frequencies some discrepancies arise. However, such discrepancies do not have much influence, since the gain is close to zero. An attempt to model the HX analytically has been made. Comparison to results from direct identification shows that the approach used in the modeling is not satisfactory. To fully understand the mechanisms of acoustic scattering in a heat exchanger, further studies are needed on the behavior of the single acoustic elements (channel, area change) in presence of heat release.

6. Acknowledgements

The presented work is part of the Marie Curie Initial Training Network Thermo-acoustic and aero-acoustic nonlinearities in green combustors with orifice structures (TANGO). We gratefully acknowledge the financial support from the European Commission under call FP7-PEOPLE-ITN-2012.

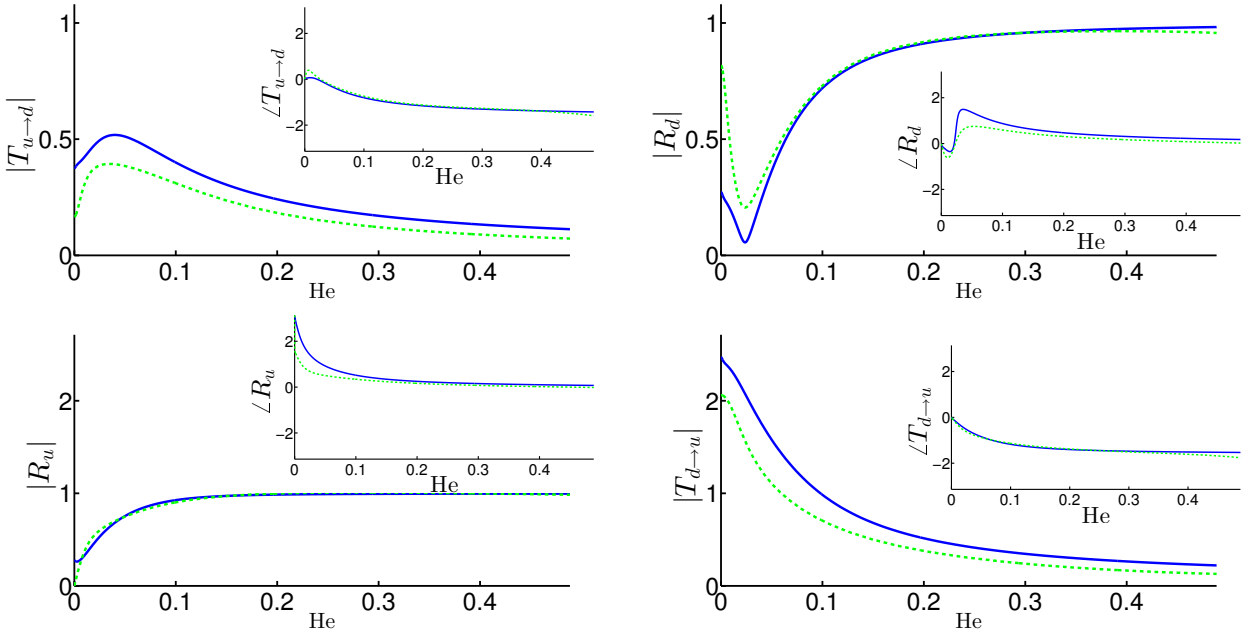

Figure 5. Scattering matrix amplitude (main frames) and phase (insets) for FCS (green-dashed line) and network model (blue line)

Financial support for Armin Witte by the German Research Foundation DFG, project PO 710/15-1 and the Technische Universität München are gratefully acknowledged.

REFERENCES

1. Polifke W Foeller S. Identification of aero-acoustic scattering matrices from large eddy simulation. Application to a sudden area expansion of a duct. *Journal of sound and vibration*, 331(13):3096–3113, 2012.
2. A. Gentemann, A. Fischer, S. Evesque, and W. Polifke. Acoustic transfer matrix reconstruction and analysis for ducts with sudden change of area. In *9th AIAA/CEAS Aeroacoustics Conference and Exhibit*, number AIAA-2003-3142, page 11, Hilton Head, SC, USA, May 2003. AIAA.
3. M. Karlsson and M. Abom. Quasi-steady model of the acoustic scattering properties of a T-junction. *Journal of Sound and Vibration*, 330(21):5131–5137, 2011.
4. J. J Keller. Thermoacoustic oscillations in combustion chambers of gas turbines. *AIAA Journal*, volume 33, number 12:2280–2287, 1995.
5. Kornilov V.N., Rook R., ten Thije Boonkkamp JHM, and de Goey LPH. Experimental and numerical investigation of the acoustic response of multi-slit bunsen burners. *Combustion and Flame*, 156(10):1957–1970, 2009.
6. Lacombe R., Moussou P., and Auregan Y. Identification of whistling ability of a single hole orifice from an incompressible flow simulation. In *ASME 2011 Pressure Vessels and Piping Conference*, pages 261–267. American Society of Mechanical Engineers, 2011.
7. L. Ljung. *System Identification - theory for user*. Prentice Hall, 1999.
8. W. Polifke, C. Wall, and P. Moin. Partially reflecting and non-reflecting boundary conditions for simulation of compressible viscous flow. *J. of Comp. Physics*, 213:437–449, 2006.
9. Polifke Wolfgang and Lawn Chris. On the low-frequency limit of flame transfer functions. *Combustion and flame*, 151(3):437–451, 2007.
10. Lord Rayleigh. *The theory of sound*. Number Rayleigh. Macmillan, 1896.

ICSV23: *Acoustic scattering behavior of a 2D flame with heat exchanger in cross-flow*

23rd International Congress on Sound & Vibration
Athens, Greece 10-14 July 2016
ICSV23

ACOUSTIC SCATTERING BEHAVIOR OF A 2D FLAME WITH HEAT EXCHANGER IN CROSS-FLOW

Lin Strobio Chen and Wolfgang Polifke
Professur für Thermofluiddynamik, Technische Universität München, Garching, München, Germany
email: strobio.chen@tum.de

Naseh Hosseini
Bekaert Combustion Technology BV, Assen, the Netherlands
Mechanical Engineering Department, Eindhoven University of Technology, Eindhoven, the Netherlands

Omke Jan Teerling
Bekaert Combustion Technology BV, Assen, the Netherlands

Ines Lopez Arteaga
Mechanical Engineering Department, Eindhoven University of Technology, Eindhoven, the Netherlands
Department of Aeronautical and Vehicle Engineering, KTH Royal Institute of Technology, Stockholm, Sweden

Viktor Kornilov and Philip de Goey
Mechanical Engineering Department, Eindhoven University of Technology, Eindhoven, the Netherlands

In practical heat production systems, premixed flames with cold heat exchanger in cross-flow is a widely used configuration. Self-excited thermoacoustic instabilities often occur in such systems. A practical way to predict the presence of the instabilities is the network model approach. In the present study, the configuration flame – heat exchanger is analyzed numerically. We first analyze the system as a network of segregated elements. Based on the resulting acoustic scattering matrix, the role of the heat exchanger as an amplifier of the flame resonant frequencies will be discussed. Then, results from the 1D network modeling are compared to results of compressible numerical simulations, performed for several distances between flame and heat exchanger. Finally, the limits to the validity of the segregated network model approach are discussed.

1. Introduction

Premixed flames with cold heat exchanger in cross-flow can be found in practical heat production systems, ranging from residential to industrial scale. A widely used configuration consists of pin or tube heat exchangers downstream a perforated premixed burner plate. In thermoacoustic systems, *heat sources* are known as the main source of acoustic disturbance energy. However, little research has focused on the role of *heat sinks* on the system acoustics. Indeed, the presence of cold heat exchangers introduces additional complexity to the study of such systems, since the heat transfer rate of heat exchangers is also sensitive to velocity perturbations, and the presence of the heat exchanger could either damp or enhance the system instability.

In the stability analysis of complex thermoacoustic systems, a widely adopted approach is the network modelling. In this framework, a combustion system is conceived as a network of segregated elements, each characterized by a set of analytical equations, which relate the downstream acoustics to upstream perturbations [1].

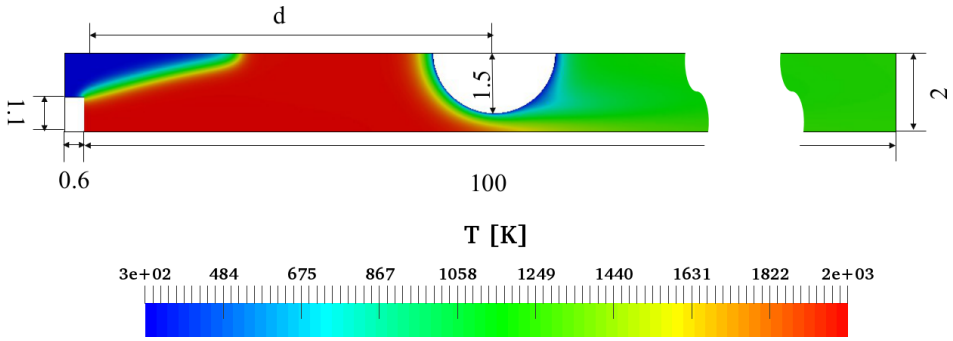

Figure 1: Temperature field of the system featuring flame and cold heat exchanger downstream. All dimensions are expressed in mm. Cases with varying distance d between burner deck and heat exchanger are analyzed. Here, $d = 10\,\mathrm{mm}$.

The network approach can be as well adopted for the case investigated in the present paper, which features a heat source (flame) and a heat sink (heat exchanger). However, depending on the distance between flame and heat exchanger, non-acoustic interactions due to changes in mean flow might occur, which could alter the acoustic scattering properties of the single elements. In particular, when the flame and the heat exchanger are very close to each other, the flame front might impinge on the heat exchanger tubes, altering both the combustion and the heat transfer processes. In this case, the system flame - heat exchanger cannot be modeled as a network of segregated elements anymore, but should be considered as a joint system, because of the mean flow interactions existing between the elements.

The goal of this study is to characterise the system with flame and heat exchanger from an acoustical point of view, and understand the conditions at which the network model approach can be considered valid, i.e. when the mutual influence between sink and source can be neglected. To do so, we first identify the scattering matrices of flame and heat exchanger separately by means of unsteady compressible simulations combined with system identification (Section 2). The scattering behaviour of the total system obtained from semi-analytical network models is discussed (Section 3). In order to prove the validity of the results given by network models, we compare them to scattering matrices obtained from direct identification of the joint system, for several distances between flame and heat exchanger (Section 4).

2. Numerical details

The system considered in the present study consists of a lean premixed 2D slit flame and a cold cylindrical heat exchanger downstream of the flame (see Fig. 1). A similar configuration is found in the previous work of Hosseini et al. [2, 3]. The burner deck consists of a row of slits of $0.6\,\mathrm{mm}$ width and $1.1\,\mathrm{mm}$ height. The heat exchanger consists of a row of cylindrical tubes, with a diameter of $3\,\mathrm{mm}$. The extension of the numerical domain in the direction normal to the flow is $2\,\mathrm{mm}$.

The code used for the compressible simulations is AVBP, developed by CERFACS and IFP-EN [1]. The temporal and spatial discretization is a second order Lax-Wendroff scheme. The unstructured mesh adopted for the direct numerical simulation has a maximum refinement of $2.0 \times 10^{-5}\,\mathrm{m}$ in the combustion zone and $4.0 \times 10^{-5}\,\mathrm{m}$ in the vicinity of the heat exchanger. Imposing an acoustic Courant number of 0.7, the time step used for the computation corresponds to $\sim 1.2 \times 10^{-8}\,\mathrm{s}$. At the inlet and outlet boundaries, acoustically non-reflecting boundary conditions are imposed, by means of the Characteristics Based State-space Boundary Conditions (CBSBC) [4].

A constant velocity and temperature boundary condition ($u_{in} = 1\,\mathrm{m\,s^{-1}}$, $T_{in} = 293\,\mathrm{K}$) is imposed

[1] www.cerfacs.fr/4-26334-The-AVBP-code.php

at the inlet and constant atmospheric pressure ($p_{out} = 101\,325\,\mathrm{Pa}$) at the outlet. The flow regime in the domain is laminar. No-slip wall boundary conditions are assumed for the burner deck and the heat exchanger surfaces. The upper and lower sides of the domain are symmetric in order to account for the presence of neighbouring flames. The premixture of air and methane is assumed as homogeneous at the inlet and has an equivalence ratio of 0.8. The combustion is modelled with a two-step reaction mechanism (see [5]). After combustion, the flow velocity and temperature reach $u_{hot} = 3.71\,\mathrm{m\,s^{-1}}$and $T_{hot} = 2005.5K$, respectively.

An adiabatic boundary condition is imposed on the burner deck, in order to rule out any preheating of the premixture at the inlet. This assumption does not correspond to the actual experimental conditions, in which the burner deck contributes to the heat loss of the flame.

The heat exchanger surface is set to a constant temperature of $323\,\mathrm{K}$. The choice of constant temperature simplifies the analysis, since it rules out the mechanism of conjugate heat transfer. However, the assumption of constant temperature at the heat exchanger surface leads to lower downstream temperature than in experiment. For this reason, in the present simulations the heat exchange between the flow and the cylinder is handled with a modified boundary condition, featuring a thermal resistance term (R_w) in the heat flux equation [2]:

$$\dot{q} = -(T_{wall} - T_{ref})/R_w, \tag{1}$$

where T_{ref} is the temperature at the heat exchanger surface and T_{wall} is the temperature of the hot fluid at the wall. For high values of thermal resistance R_w, the boundary behaves adiabatically, while for values of R_w approaching zero, the boundary behaves as a quasi-isothermal wall (for $R_w = 0$ the boundary condition diverges). In the present analysis, the value chosen for R_w is 0.001, which gives a good compromise between the desired physical effect and the numerical stability. Due to the heat transferred to the heat exchanger tubes, the flow temperature decreases to $T_{out} = 1318\,\mathrm{K}$. It should be noted that the outlet temperature in this study is much higher than the temperature of exhaust gases in real boilers, since in this analysis only a single row of cylindrical tubes has been taken into account.

2.1 External excitation and system identification

The scattering behaviour of an element in the acoustic network is charaterized by its transmission and reflection coefficients upstream and downstream. Equation (2) relates the output signals, f_d and g_u, to the incoming excitation signals f_u and g_d via the acoustic scattering matrix SM:

$$\begin{pmatrix} f_d \\ g_u \end{pmatrix} = \underbrace{\begin{bmatrix} T_{u\to d} & R_d \\ R_u & T_{d\to u} \end{bmatrix}}_{SM} \begin{pmatrix} f_u \\ g_d \end{pmatrix}, \tag{2}$$

in which $T_{u\to d}$, $T_{d\to u}$, R_d and R_u are the complex-valued upstream and downstream transmission and reflection coefficients of the system. f and g are the acoustic waves, related to the perturbations in velocity and pressure as:

$$f = \frac{1}{2}\left(\frac{p'}{\bar{\rho}\bar{c}} + u'\right) \qquad g = \frac{1}{2}\left(\frac{p'}{\bar{\rho}\bar{c}} - u'\right), \tag{3}$$

where $\bar{\rho}$ and $\bar{c}$ are the mean density and mean speed of sound. In this paper, we adopt a wavelet-based broadband signal as external excitation. This type of signals ensures a constant power spectrum in the frequency range of interest ($f = [0, 800]Hz$ for the present case), with low auto-correlation and zero cross-correlation. The amplitude of the excitation signals f_u and g_d is set to 5% with respect to the mean velocity at the inlet and outlet. Output signals f_d and g_u are registered at the same planes. In

[2] a detailed description of the boundary condition can be found at:
www.cerfacs.fr/avbp/AVBP_V6.X/AVBPHELP/avbphelp.php

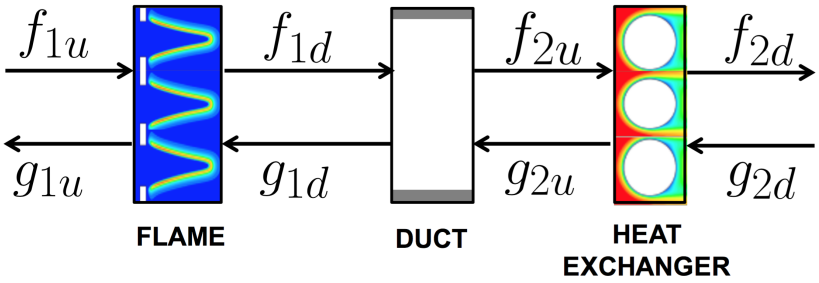

Figure 2: Network model of segregated elements

the post-processing, the unsteady time series are shifted, in order to compensate for the acoustic time delay between the reference planes and the position of the activ elements. The output error parametric model structure has been used for the identification of the Multi-Input Multi-Output system from the unsteady simulations [6, 7].

3. Network model of segregated elements

In this section, we first simulate the flame and heat exchanger separately, and then the joint system with varying distance d. In the acoustic network model approach, complex thermoacoustic systems are conceived as a network of segregated elements. This implies that the acoustic scattering behaviour of a single element does not depend on the presence of other elements in the acoustic network. In this study, the system under investigation is divided into 3 subsystems: a heat source (flame), a duct of length d and a heat sink (heat exchanger), as in Fig 2. The scattering matrices of flame and heat exchanger are identified separately, by means of compressible simulations. We use the single element sub-models as building-blocks for the complete acoustic network. The propagation of acoustic waves between the two elements is modelled by means of a lossless duct of length d. The varying acoustic propagation speed in the domain is accounted for in the present network model. In this section, we make use of the network model to understand how the presence of the heat exchanger - and its distance from the flame - impacts on the behaviour of the whole system. For our analysis, the in-house developed state-space based toolbox *taX* is used [8]. The results of this analysis are shown in Fig. 3. The gain of the scattering matrix is represented in the logarithmic scale, in order to visualize properly the heat exchanger behaviour. The scattering matrix of the flame in Fig. 3 shows a maximum at $f = 255Hz$. According to Bomberg et al. [9], the pronounced peaks in the acoustic response of the flame are due to intrinsic thermo-acoustic feedback (ITA). Such feedback mechanism is due to the unsteady thermal response of the flame to velocity perturbations, which generates acoustic waves travelling upstream and downstream. The upstream propagating component of these acoustic waves modulates the upstream velocity perturbations. As suggested in [9], the frequency at which such feedback loop exhibit resonance corresponds to the frequency at which the phase of the flame transfer function $\angle F(\omega)$ reaches $-\pi$. This can be easily verified in Fig. 4.

In the numerical simulation of the heat exchanger, the velocity profile at the inlet is assumed as uniform, in order to exclude any mean field effect deriving from the flame. This assumption should be accounted for, in the comparison between network model and the results of the joint system, since the flow field downstream the flame has a 2D distribution, which recovers to 1D at longer distances. Other inlet conditions such as temperature, density and mass fractions are taken from the downstream conditions of the flame.

Fig. 3 shows that the heat exchanger is almost acoustically transparent: the magnitude of the reflection coefficients upstream R_u and downstream R_d are close to zero, with a maximum of 0.2 at 800 Hz. The transmission coefficient upstream T_d is almost constant in the frequency range con-

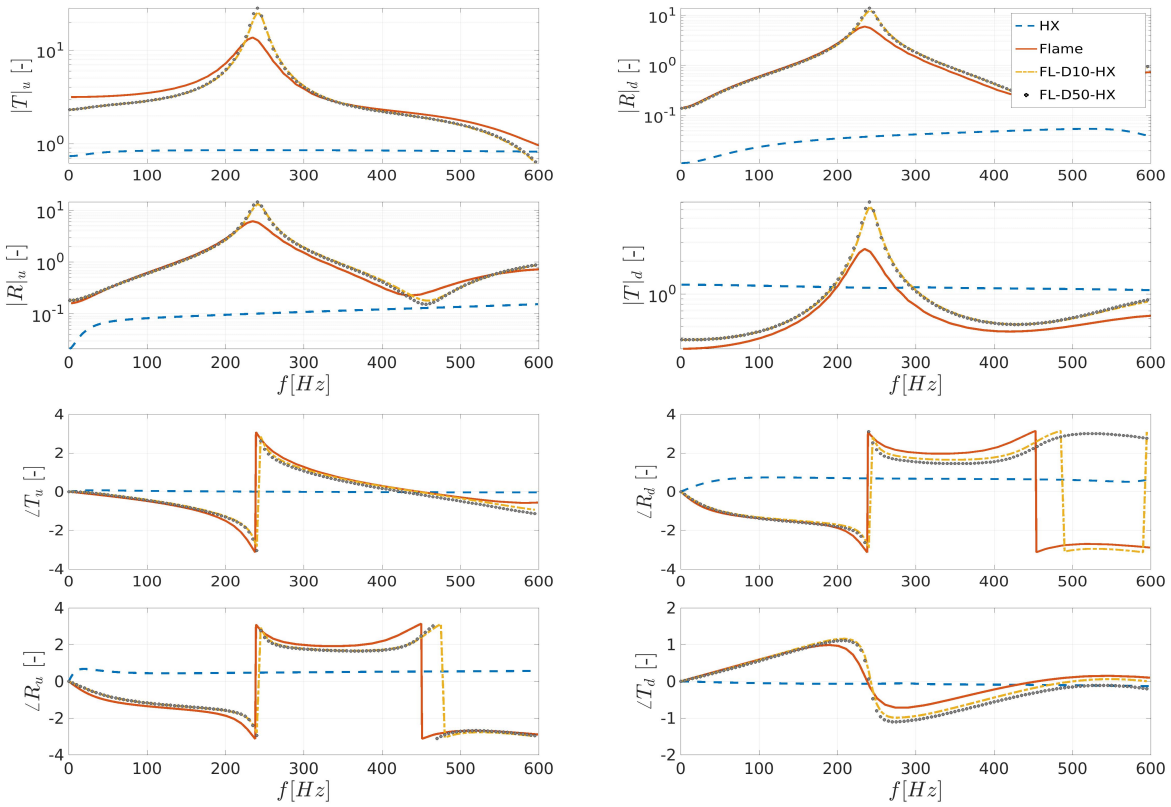

Figure 3: *Gain* and *Phase* of the scattering matrix for the heat exchanger (**HX**), flame (**FL**), the network model with flame–10 mm duct–heat exchanger (**FL-D10-HX**) and the network model consisting of flame–50 mm duct–heat exchanger (**FL-D50-HX**)

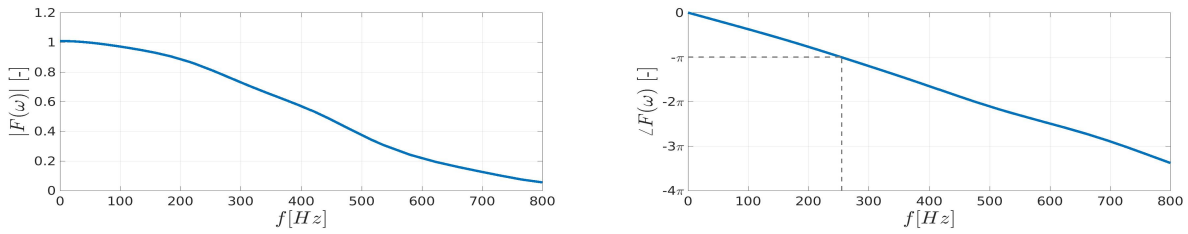

Figure 4: Gain and phase of the flame transfer function $F(\omega) = (\dot{Q}'/\bar{\dot{Q}})/(u'_{in}/\bar{u}_{in})$ without heat exchanger

sidered, and has a magnitude slightly below unity (~ 0.9). Similarly, the magnitude of downstream transmission coefficient T_d is also frequency invariant and is slightly above unity (~ 1.2).

As Fig. 3 shows, the scattering matrix of the total system shows higher peaks than the flame itself. These peaks are found at about 257 Hz, close to the resonant frequency of the flame. In the total system the heat exchanger acts as an amplifier of the intrinsic thermo-acoustic resonance. Analytically, such amplification can be explained as follows: referring to the scattering matrix in Eq. (2), the relation between the global acoustic scattering matrix and the single subsystems is described in Eqs. (4) . Terms with subscripts 1 refer to the flame, and terms with subscript 2 refer to the heat exchanger. The peaks in the scattering matrix depend mainly on $1 - (R_{1d}R_{2u}e^{-2ikL})$, which is the denominator of all four terms. Resonance sets in when the product between the flame downstream reflection coefficient, R_{1d} and the heat exchanger upstream reflection coefficient approach unity. In presence of a duct of length L, resonance also depends on the time lag e^{-ikL}, where $k = \omega/c$ and c is

the speed of sound downstream the flame front.

$$T_{u\to d} = \frac{T_{1u}T_{2u}e^{-ikL}}{1 - R_{1d}R_{2u}e^{-2ikL}}, \qquad R_d = \frac{R_{1d}T_{2u}T_{2d}e^{-2ikL}}{1 - R_{1d}R_{2u}e^{-2ikL}} + R_{2d} \tag{4}$$

$$R_u = \frac{T_{1u}T_{1d}R_{2u}e^{-2ikL}}{1 - R_{1d}R_{2u}e^{-2ikL}} + R_{1u}, \qquad T_{d\to u} = \frac{T_{1d}T_{2d}e^{-ikL}}{1 - R_{1d}R_{2u}e^{-2ikL}}.$$

Away from the resonant frequency, the behaviour of the system mainly follows the flame scattering properties. Moreover, the results in Fig. 3 show that the variation of the distance between flame and heat exchanger does not impact significantly on the system acoustic response. In fact, the cases $d = 50\,\mathrm{mm}$ and $d = 10\,\mathrm{mm}$ do not differ noticeably in the scattering matrix magnitude. The difference in phase becomes non-negligible only at higher frequencies, when the compactness is not satified anymore.

In the present study, the minimum length considered for d is $8\,\mathrm{mm}$. For distances lower than $8\,\mathrm{mm}$, it is reasonable to question the validity of the results from the network model. As noted above, the distance is intended as between the burner deck and the center of the heat exchanger tube. In the actual system, the flame is about $4\,\mathrm{mm}$ high and the heat exchanger has a radius of $1.5\,\mathrm{mm}$. It follows that for a distance of $8\,\mathrm{mm}$, the flame tip is in fact only $2.5\,\mathrm{mm}$ away from the tube row. At shorter distances, as already shown by Hosseini et al. [2] [3], the presence of the heat exchanger in the nearfield of the flame can deeply impact on the nature of the system, which might show non-linear behaviour.

4. Identification of the joint thermoacoustic system

In order to explore the validity of the network model approach, direct numerical simulation of the joint system featuring flame and heat exchanger are carried out for the case of d=$50\,\mathrm{mm}$, $20\,\mathrm{mm}$, $10\,\mathrm{mm}$ and for the "limit case" of $d = 8\,\mathrm{mm}$. The results have been compared to the scattering matrix in Fig. 3. Discrepancies arising between CFD and network model are then discussed and explained.

4.1 Case d>20 mm

At a distance of 20 mm between the two elements, it is reasonable to presume that no mean field effects exist between flame and heat exchanger. The flow profile approaching the heat exchanger can in fact be approximated as block profile, since only 0.1% deviation in the incoming velocity profile is found and non-uniformities in temperature profile are negligible. As shown in Fig. 5, the scattering matrix resulting from CFD gives very good agreement with respect to the network model. The gain is well resolved for all the frequencies and, in particular, the resonant peak is correctly captured for all the terms in the scattering matrix. Minor discrepancies can be found in the phase at higher frequencies, see Fig. 5. Such discrepancies mainly occur in the terms involving downstream signals and are caused by the error made in the time delay estimation of the acoustic waves propagating from the heat exchanger to the outlet reference plane, at which the signals are registered. In fact, the temperature field downstream the heat exchanger is mainly 2D, due to the wake after the cylindrical tubes. Indeed, the non-uniform temperature field represents a source of error for the estimation of the speed of sound, and thus, for the phase of the total scattering matrix.

4.2 Case d<10 mm

As the distance between flame and heat exchanger descreases, CFD simulations show that the value of the resonant peak also decreases. In fact, results in Fig. 5 show that the scattering matrix for the cases of $10\,\mathrm{mm}$ duct has a resonance peak which is significantly lower than the case of $50\,\mathrm{mm}$ duct. This means that the network model obtained from segregated elements is not valid anymore when

the distance between burner deck and heat exchanger is approximately 10 mm. The reason behind such discrepancy is the different response of the heat exchanger in presence of a 2D distribution in the incoming velocity profile. For d=10 mm, the velocity downstream the flame front presents a maximum deviation of 5% along the Y direction. Such deviation slightly changes the acoustic scattering behaviour of the heat exchanger, as shown in Fig. 6. The scattering matrices in Fig. 6 are identified directly from the compressible simulations of the joint system, and the input and output

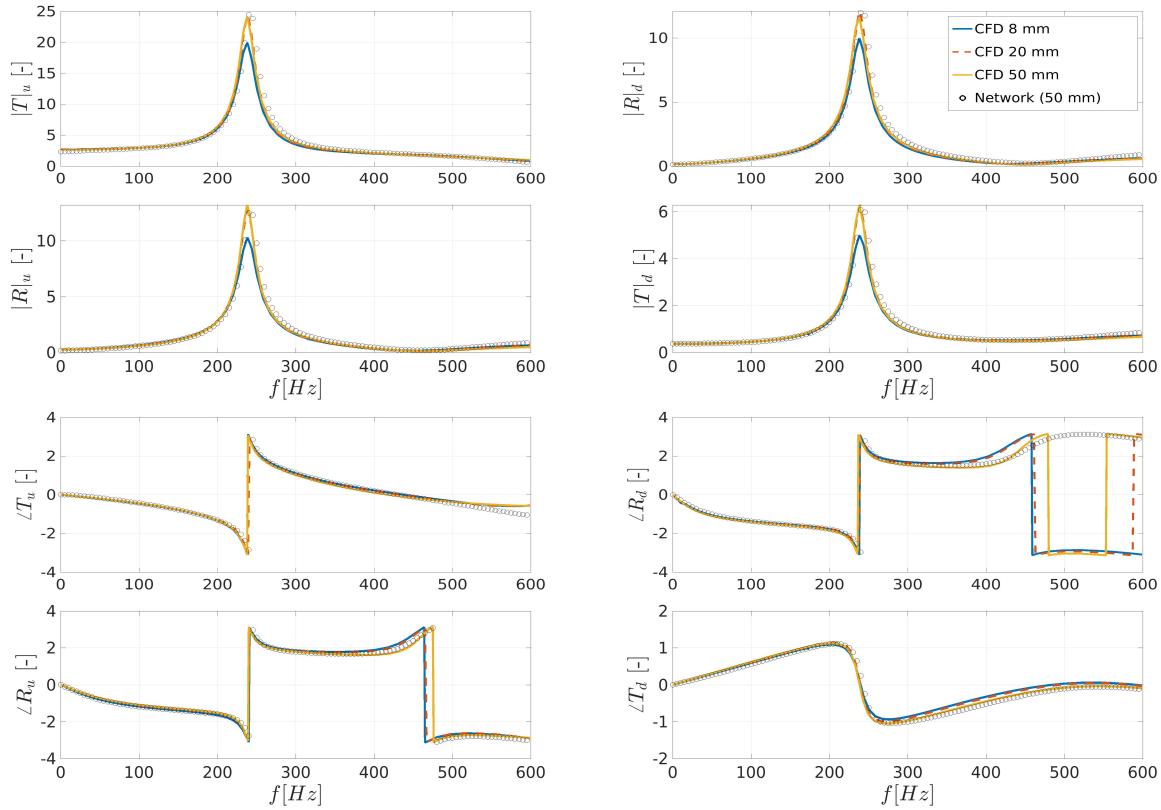

Figure 5: Gain and phase of the scattering matrix resulting from CFD of the joint system with ducts of 8 mm (**CFD08**), 20 mm (**CFD20**) and 50 mm (**CFD50**) between flame and HX , compared to the network model consisting of flame – 50 mm duct – heat exchanger (**FL-D50-HX**). The case with duct length of 10 mm (**CFD10**) is omitted, but shows similar values as the case (**CFD08**) . The frequency range is restricted to [0,600] Hz to better visualize the resonance peak.

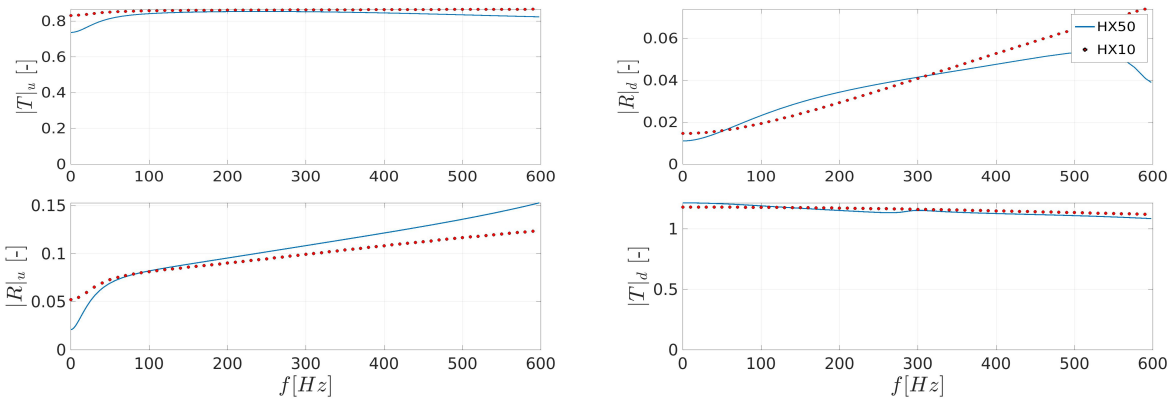

Figure 6: HX scattering matrix gain identified from the simulations of joint systems featuring 10 mm duct (HX10) and 50 mm duct (HX50)

signals f and g are registered at reference planes placed just up and downstream of the heat exchanger, for both cases considered in the paper. Due to the high sensitivity of the system at resonant frequencies (see Eqs. (4)), the small change in heat exchanger scattering properties results in a conspicuous decrease of the peak response.

5. Conclusions

In the present study, we analyzed and discussed the acoustic scattering behaviour of a thermoacoustic system consisting of a 2D slit premixed flame and a cylindrical heat exchanger. A resonance peak is found in the scattering matrix of the flame, due to the intrinsic feedback mechanism. Both results from CFD-system identification and network model show that the presence of the heat exchanger downstream the flame amplifies the resonance around the same frequency. Comparison between CFD and network modeling shows that the peak in acoustic response of the system can be correcty captured by the network model for the case of d=$50\,\mathrm{mm}$, and in general, when the mean flow effects due to the short distance between the elements are negligible. When the distance between heat source and heat sink decreases, 2D mean flow effects on the heat exchanger scattering behaviour cannot be neglected anymore. CFD results for the case of d=$10\,\mathrm{mm}$ and d= $8\,\mathrm{mm}$ show that the resonance peak in the scattering matrix decreases considerably and that the predictions given by the network model are no longer accurate. The next step is to analyze the role of the heat exchanger on the system stability, and understand how the heat exchanger scattering behaviour changes in presence of non-uniform velocity profiles. Moreover, a study of the acoustic behaviour of the system in presence of realistic experimental boundary conditions (heat loss at combustor walls, conjugate heat transfer) is also needed.

6. Acknowledgements

The presented work is part of the Marie Curie Initial Training Network Thermo-acoustic and aero-acoustic nonlinearities in green combustors with orifice structures (TANGO). We gratefully acknowledge the financial support from the European Commission under call FP7-PEOPLE-ITN-2012.

REFERENCES

1. Polifke, W. System modelling and stability analysis, *Basics of Aero-Acoustics and Thermo-Acoustics*, Rhode-St-Genese, BE, Dec., VKI LS 2007-02, Von Karman Institute, (2007).
2. Hosseini, N., Kornilov, V., Teerling, O. J., Lopez Arteaga, I. and de Goey, L. P. H. Transfer Function Calculations of Segregated Elements in a Simplified Slit Burner with Heat Exchanger, *The 22nd International Congress on Sound and Vibration*, (2015).
3. Hosseini, N., Kornilov, V., Teerling, O. J., Lopez Arteaga, I. and de Goey, L. P. H. Development of a Numerical Model for Obtaining Flame Transfer Function in a Simplified Slit Burner with Heat Exchanger, *The 21st International Congress on Sound and Vibration*, (2014).
4. Jaensch, S., Sovardi, C. and Polifke, W. Imposing frequency dependent reflection coefficients at the boundary of a compressible flow simulation by coupling state-space models via characteristics, *submitted to J. Comp. Phys.*, (2015).
5. Silva, C. F., Emmert, T., Jaensch, S. and Polifke, W. Numerical study on intrinsic thermoacoustic instability of a laminar premixed flame, *Combustion and Flame*, **162** (9), 3370 – 3378, (2015).
6. Ljung, L., *System identification*, Springer (1998).
7. Sovardi, C. and Polifke, W., (2015), CFD-Based Modelling of Sound Generation in Ducted Discontinuities. Schram, C. (Ed.), *Progress in simulation, control and reduction of ventilation noise*, VKI Lecture Series 2015, VKI.
8. Emmert, T., Meindl, M., Jaensch, S. and Polifke, W. Linear State Space Network Modeling of Acoustic Systems, *submitted to Acta Acustica united with Acustica*, (2016).
9. Bomberg, S., Emmert, T. and Polifke, W. Thermal Versus Acoustic Response of Velocity Sensitive Premixed Flames, *35th Symposium on Combustion*, San Francisco, CA, USA, vol. 35, The Combustion Institute, (2014).